

Electronic Thesis and Dissertation Repository

---

7-12-2022 9:30 AM

## Design and Synthesis of Nef:SFK Interaction Inhibitors for Application in an Immune-directed HIV-1 Cure

Antony Lurie, *The University of Western Ontario*

Supervisor: Dikeakos, Jimmy D, *The University of Western Ontario*

A thesis submitted in partial fulfillment of the requirements for the Master of Science degree in Microbiology and Immunology

© Antony Lurie 2022

Follow this and additional works at: <https://ir.lib.uwo.ca/etd>

 Part of the [Medicinal-Pharmaceutical Chemistry Commons](#)

---

### Recommended Citation

Lurie, Antony, "Design and Synthesis of Nef:SFK Interaction Inhibitors for Application in an Immune-directed HIV-1 Cure" (2022). *Electronic Thesis and Dissertation Repository*. 8637.  
<https://ir.lib.uwo.ca/etd/8637>

This Dissertation/Thesis is brought to you for free and open access by Scholarship@Western. It has been accepted for inclusion in Electronic Thesis and Dissertation Repository by an authorized administrator of Scholarship@Western. For more information, please contact [wlsadmin@uwo.ca](mailto:wlsadmin@uwo.ca).

## Abstract

The human immunodeficiency virus type 1 (HIV-1) protein, Nef, binds and activates Src family kinases (SFKs) to reduce cell surface levels of major histocompatibility complex class I (MHC-I), thereby facilitating cytotoxic T lymphocyte (CTL) evasion. Importantly, Nef-mediated CTL evasion compromises the success of immune-directed curative approaches, underscoring Nef:SFK interaction inhibitors as promising adjuvants in an immune-directed cure. Previously, our group identified a dipeptide derivative (H3-1) which inhibits the Nef:SFK interaction and MHC-I downregulation *in vitro*, but is unstable *in vivo*. I hypothesized that H3-1's instability is due to its proteolysis and have generated peptidomimetic analogues of H3-1 which are predicted to maintain improved proteolytic stabilities. Herein, I describe the design and synthesis of analogues incorporating carboxyl (methyl ester, amide, nitrile, and tetrazole) and amide (thioamide and methyleneamino) replacing groups. With future biological studies, we aim to identify an *in vivo* stable Nef:SFK inhibitor for application in an immune-directed HIV-1 cure.

## Keywords

Human immunodeficiency virus type 1 (HIV-1), Nef, Src family kinase (SFK), major histocompatibility complex class I (MHC-I), accessory proteins, cure, immune evasion, viral infection, organic synthesis, peptidomimetics

## Summary for Lay Audience

To-date, there is still no practical cure for human immunodeficiency virus type 1 (HIV-1) infection. Many curative approaches in development rely on specific immune cells, known as cytotoxic T lymphocytes (CTLs), to recognize and kill HIV-1-infected cells. However, HIV-1 maintains mechanisms to evade CTL recognition and killing, which compromises the success of these cures. One of the key mechanisms for HIV-1's evasion of CTL killing is mediated by the HIV-1 protein, Nef. Specifically, Nef enables HIV-1-infected cells to avoid CTL recognition by reducing cell surface levels of the antigen presenting molecule, major histocompatibility complex class I (MHC-I). Importantly, this process depends on Nef's interactions with a set of signaling molecules, termed Src family kinases (SFKs), which highlights the Nef:SFK interaction as a target for therapeutic intervention. We therefore predict that inhibitors of the Nef:SFK interaction could be applied as adjuvants in an immune-directed HIV-1 cure to boost the CTL-mediated killing of infected cells.

Previously, our group identified a dipeptide derivative, termed H3-1, which inhibits the Nef:SFK interaction and rescues cell surface levels of MHC-I *in vitro*. However, H3-1 was found to be unstable *in vivo*, thereby precluding its therapeutic application. Considering H3-1's peptidic structure, I hypothesized that H3-1's *in vivo* instability is due to its susceptibility to proteolysis. In this thesis, I used organic synthesis to generate a panel of H3-1 analogues which are predicted to maintain improved proteolytic stabilities and should thereby enable their continued study as supportive agents in an HIV-1 cure. Specifically, I synthesized and isolated four peptidomimetic analogues incorporating replacements of H3-1's carboxylic acid group (methyl ester, amide, nitrile, and tetrazole). Attempts to synthesize analogues incorporating replacements of H3-1's amide group (thioamide and methyleneamino) were also made and are described herein. With this panel of H3-1 analogues, future studies will focus on characterizing these compounds biologically on measures of toxicity, potency, and biostability. By integrating each of these parameters, we aim to identify a next-generation *in vivo* stable Nef:SFK interaction inhibitor for application in an immune-directed HIV-1 cure.

## Co-Authorship Statement

Unless otherwise noted, all experiments were completed by Antony Lurie. Jimmy Dikeakos contributed to the genesis, design, implementation, and interpretation of all experiments. Robert Hudson contributed to the design, implementation, and interpretation of compound syntheses and isolation procedures.

Portions of Chapter 1 have been published as a review article in *Virologie*:

Lurie A, Fink C, Gosselin G, Dekaban GA, Dikeakos JD. Inhibitors of HIV-1 Nef: applications and developments for a practical cure. *Virologie (Montrouge)*. 2022;26(1):17-33. doi: 10.1684/vir.2022.0940

Antony Lurie wrote the entirety of the manuscript and assembled all figures and tables. All co-authors assisted in writing and editing the manuscript.



## Acknowledgments

First and foremost, I thank my supervisor, Jimmy Dikeakos, for his incredible support and guidance, from the completion of my undergraduate studies, through to my Master's. Most importantly, Jimmy pointed me “the right way” and helped me realize my own potential as a scientist. Even after dozens of failed co-immunoprecipitations or reaction attempts, his support has never wavered, but instead I have always been offered everything from experimental advice to writing suggestions and career advice – these are discussions and lessons I will always carry closely as I move forward. I certainly could not have asked for a better supervisor and mentor, and I truly consider myself lucky to have been welcomed with open arms into the group.

The chemistry work presented in this thesis was also closely guided with the help of Robert Hudson. In fact, it was as part of the Hudson group that I took on my first true research project, and I am especially grateful for the freedom I was always given in the lab. Of course, this was not without countless meetings filled with questions and discussions about chemistry, and life in general, and which I am also immensely thankful for.

The progress made in my research project was also aided by my advisory committee, Gregory Dekaban and Peter Stathopoulos, and I am indebted for their continued support, advice, and guidance. Many others have also directly contributed to this thesis, and while I cannot list them all here, I would like to especially thank James Wisner for assistance in interpreting NMR spectra, Mathew Willans for managing the NMR facility, and Haidy Metwally and Chathu Pulukkody for collecting mass spectra. Additionally, this work was only made possible with the generous support of our funding sources: the University of Western Ontario, the Government of Ontario, the Natural Science and Engineering Research Council of Canada, and the Canadian Institutes of Health Research.

Of course, our community is a great part of what makes research enjoyable and worth doing, and I can happily say that my fellow lab mates have only bettered and enriched my time at Western. In the Dikeakos lab, I especially thank Corby Fink for his direct help and involvement with studies relating to this project, Mitch Mumby for orienting me as a

newcomer to the Dikeakos lab and for turning me into a cloning master, Steven Trothen for showing me the way of the western blot (the ten commandments were key to this), Cassie Edgar for sharing her microscopy pro-tips, Geneviève Gosselin for supporting virtually every aspect of our lab operations, and Roy Zang for being my right-hand man through this whole experience. In the Hudson lab, I thank David Park and Ali Heidari for helping welcome me into the chemistry lab and teaching me the basics of organic synthesis, Filip Wojciechowski for his reprecipitation wisdom, and a special thank you to Mohammed Attaelmanan, Mria Chowdhury, Paul Winiarz, and Johanna de Jong, for their companionship, technical assistance, and patience, especially during my rantings about imidazoles and tetrazoles. To everyone in the Dikeakos and Hudson labs, listed here or not, thank you for your friendship and support – none of this would be possible without it all.

Finally, thank you to my family, especially Mom and Dad, for inspiring me, and helping make this, and what is to come, a reality. To my partner, Kyra, I am certain you deserve this degree equally as I do. Thank you for listening to every one of my practice talks, encouraging me when times get tough, and for making these past years the best I could ever ask for.

# Table of Contents

Abstract.....	ii
Summary for Lay Audience.....	iii
Co-Authorship Statement.....	iv
Acknowledgments.....	v
Table of Contents.....	vii
List of Tables .....	x
List of Figures.....	xi
List of Appendices .....	xiii
List of Abbreviations .....	xvi
Chapter 1.....	1
1 Introduction.....	1
1.1 The case for a practical HIV-1 cure.....	1
1.2 Approaches to cure HIV-1 .....	1
1.3 Biology of the HIV-1 Nef protein.....	2
1.4 Implications of Nef in an HIV-1 cure.....	5
1.4.1 Implications of Nef in latency reversal.....	5
1.4.2 Implications of Nef in infected cell clearance .....	6
1.5 Past developments towards inhibitors of HIV-1 Nef.....	8
1.5.1 Small molecule inhibitors of Nef-mediated kinase activation.....	11
1.5.2 Alternative small molecule inhibitors of Nef-mediated MHC-I downregulation .....	19
1.5.3 Small molecule inhibitors of additional Nef functions.....	21
1.5.4 Peptide and protein inhibitors of Nef.....	24
1.6 Goals of this thesis .....	25

Chapter 2.....	28
2 Experimental procedures.....	28
2.1 General.....	28
2.1.1 Synthetic materials and methods .....	28
2.1.2 Nuclear magnetic resonance .....	29
2.1.3 Mass spectrometry .....	29
2.1.4 High-performance liquid chromatography .....	30
2.2 Synthesis of <i>Z-L</i> -histidyl- <i>L</i> -tyrosine methyl ester (H3-1 methyl ester, H3-1M)..	30
2.3 Synthesis of <i>Z-D</i> -histidyl- <i>L</i> -tyrosine methyl ester ( <i>D,L</i> -H3-1 methyl ester, <i>D,L</i> -H3-1M).....	32
2.4 Synthesis of <i>Z-L</i> -histidyl- <i>L</i> -tyrosinamide (H3-1 C-terminal amide, H3-1A).....	33
2.5 Synthesis of <i>Z-L</i> -histidyl- <i>L</i> -tyrosine nitrile (H3-1 nitrile, H3-1N).....	34
2.6 Synthesis of <i>Z-L</i> -histidyl- <i>L</i> -tyrosine tetrazole hydrochloride (H3-1 tetrazole HCl, H3-1T•HCl).....	35
Chapter 3.....	37
3 Synthesis and characterization of H3-1 analogues.....	37
3.1 Design of H3-1 analogues.....	37
3.1.1 The thioamide group.....	39
3.1.2 The methyleneamino group .....	40
3.1.3 The methyl ester group .....	40
3.1.4 The C-terminal amide group.....	41
3.1.5 The nitrile group .....	41
3.1.6 The tetrazole group .....	42
3.1.7 General synthetic approach.....	42
3.2 Synthesis of H3-1 methyl ester (H3-1M).....	43
3.3 Synthesis of H3-1 C-terminal amide (H3-1A).....	47

3.4 Synthesis of H3-1 nitrile (H3-1N) .....	48
3.5 Synthesis of H3-1 tetrazole (H3-1T).....	49
3.6 Attempted synthesis of thioamide H3-1 methyl ester (TH3-1M).....	53
3.7 Attempted synthesis of methyleneamino H3-1 methyl ester (MH3-1M).....	54
Chapter 4.....	56
4 Discussion and conclusions .....	56
4.1 General summary .....	56
4.2 Synthesis of carboxyl replacing H3-1 analogues.....	57
4.2.1 H3-1M.....	57
4.2.2 H3-1A .....	57
4.2.3 H3-1N .....	58
4.2.4 H3-1T.....	58
4.3 Synthesis of amide replacing H3-1 analogues .....	59
4.3.1 TH3-1M .....	60
4.3.2 MH3-1M.....	61
4.4 Future directions .....	62
4.4.1 Synthesis of additional H3-1 analogues.....	62
4.4.2 Biological study of H3-1 analogues.....	62
4.5 Conclusions.....	63
References.....	65
Appendices.....	85
Curriculum Vitae .....	120

## List of Tables

Table 1.1 Summary of Nef inhibitors identified to-date.....	9
---	---

## List of Figures

Figure 1.1 Overview of key HIV-1 Nef activities. ....	4
Figure 1.2 Summary of selected Nef activities relevant to a practical HIV-1 cure. ....	8
Figure 1.3 Overview of the interaction between Nef and an SFK SH3 domain. ....	11
Figure 1.4 Structural representations of D1, DLC27, and DLC27-14. ....	13
Figure 1.5 Overview of the Nef homodimerization inhibitor, B9. ....	14
Figure 1.6 Structural representations of selected B9 analogues. ....	16
Figure 1.7 Structural representations of SRI-35879 and selected analogues. ....	17
Figure 1.8 Structural representations of DQBS and E11. ....	18
Figure 1.9 Overview of the Nef:SFK interaction inhibitor, 2c. ....	19
Figure 1.10 Overview of alternative small molecule inhibitors of Nef-mediated MHC-I downregulation. ....	21
Figure 1.11 Structural representations of the guanidine alkaloid analogues, compounds 14, 17, and 22. ....	22
Figure 1.12 Structural representations of NSC13987 and its analogue, AMS-55. ....	23
Figure 1.13 Structural representation of H3-1. ....	26
Figure 3.1 Structural representation of H3-1. ....	37
Figure 3.2 Overview of H3-1 peptidomimetic design. ....	39
Figure 3.3 Schematic of proposed chemical transformations for generating peptidomimetic analogues of H3-1. ....	43
Figure 3.4 Synthesis of crude H3-1M by solution-phase peptide coupling. ....	44

Figure 3.5 Proposed mechanism for histidine-promoted epimerization during peptide coupling.....	45
Figure 3.6 Synthesis of <i>D,L</i> -H3-1M by solution-phase peptide coupling. ....	45
Figure 3.7 <sup>1</sup> H NMR permits quantification of <i>L,L</i> and <i>D,L</i> diastereomer abundances in H3-1M.....	46
Figure 3.8 Final synthesis of H3-1M. ....	47
Figure 3.9 Synthesis of H3-1A by the ammonolysis of H3-1M. ....	48
Figure 3.10 Synthesis of H3-1N by the dehydration of H3-1A.....	49
Figure 3.11 Trial synthesis of H3-1T by reaction of H3-1N with NaN <sub>3</sub> and ZnBr <sub>2</sub> .....	50
Figure 3.12 Trial synthesis of H3-1T by reaction of H3-1N with NaN <sub>3</sub> and NH <sub>4</sub> Cl.....	52
Figure 3.13 Synthesis of H3-1T•HCl by reaction of H3-1N with NaN <sub>3</sub> and Et <sub>3</sub> N•HCl...	53
Figure 3.14 Trial synthesis of TH3-1M by the thionation of H3-1M. ....	54
Figure 3.15 Trial synthesis of MH3-1M by the reduction of TH3-1M. ....	55
Figure 4.1 Proposed synthesis of H3-1T by coupling <i>Z-L</i> -His-OH and <i>L</i> -tyrosine tetrazole.....	59
Figure 4.2 Examples of <i>N,N</i> -chelated phosphorus complexes derived from P <sub>4</sub> S <sub>10</sub> :pyridine. ....	61
Figure 4.3 Proposed approach to generate MH3-1M by reductive amination.....	61



## List of Appendices

Appendix 1. Baseline RP-HPLC chromatograms.....	85
Appendix 2. $^1\text{H}$ NMR spectrum of H3-1 methyl ester (H3-1M) in DMSO- $d_6$ .....	86
Appendix 3. $^1\text{H}$ NMR spectrum of H3-1 methyl ester (H3-1M) in DMSO- $d_6$ with the addition of D $_2$ O. ....	87
Appendix 4. $^{13}\text{C}\{^1\text{H}\}$ NMR spectrum of H3-1 methyl ester (H3-1M) in DMSO- $d_6$ .....	88
Appendix 5. ESI-TOF MS of H3-1 methyl ester (H3-1M). ....	89
Appendix 6. RP-HPLC chromatograms of H3-1 methyl ester (H3-1M).....	90
Appendix 7. $^1\text{H}$ NMR spectrum of <i>D,L</i> -H3-1 methyl ester ( <i>D,L</i> -H3-1M) in DMSO- $d_6$ ..	91
Appendix 8. $^1\text{H}$ NMR spectrum of <i>D,L</i> -H3-1 methyl ester ( <i>D,L</i> -H3-1M) in DMSO- $d_6$ with the addition of D $_2$ O. ....	92
Appendix 9. $^{13}\text{C}\{^1\text{H}\}$ NMR spectrum of <i>D,L</i> -H3-1 methyl ester ( <i>D,L</i> -H3-1M) in DMSO- $d_6$ . ....	93
Appendix 10. ESI-TOF MS of <i>D,L</i> -H3-1 methyl ester ( <i>D,L</i> -H3-1M).....	94
Appendix 11. RP-HPLC chromatograms of <i>D,L</i> -H3-1 methyl ester ( <i>D,L</i> -H3-1M). ....	95
Appendix 12. $^1\text{H}$ NMR spectrum of H3-1 C-terminal amide (H3-1A) in DMSO- $d_6$ . ....	96
Appendix 13. $^1\text{H}$ NMR spectrum of H3-1 C-terminal amide (H3-1A) in DMSO- $d_6$ with the addition of D $_2$ O. ....	97
Appendix 14. $^{13}\text{C}\{^1\text{H}\}$ NMR spectrum of H3-1 C-terminal amide (H3-1A) in DMSO- $d_6$ . ....	98
Appendix 15. ESI-TOF MS of H3-1 C-terminal amide (H3-1A).....	99
Appendix 16. RP-HPLC chromatograms of H3-1 C-terminal amide (H3-1A). ....	100

Appendix 17. $^{19}\text{F}$ NMR spectrum of H3-1 nitrile (H3-1N) in $\text{DMSO-}d_6$ without treatment with base. ....	101
Appendix 18. $^{19}\text{F}$ NMR spectrum of H3-1 nitrile (H3-1N) in $\text{DMSO-}d_6$ following treatment with base. ....	102
Appendix 19. $^1\text{H}$ NMR spectrum of H3-1 nitrile (H3-1N) in $\text{DMSO-}d_6$ .....	103
Appendix 20. $^1\text{H}$ NMR spectrum of H3-1 nitrile (H3-1N) in $\text{DMSO-}d_6$ with the addition of $\text{D}_2\text{O}$ . ....	104
Appendix 21. $^{13}\text{C}\{^1\text{H}\}$ NMR spectrum of H3-1 nitrile (H3-1N) in $\text{DMSO-}d_6$ . ....	105
Appendix 22. ESI-TOF MS of H3-1 nitrile (H3-1N). ....	106
Appendix 23. RP-HPLC chromatograms of H3-1 nitrile (H3-1N).....	107
Appendix 24. $^1\text{H}$ NMR spectrum of the complex between H3-1 tetrazole and zinc (H3-1T:Zn) in $\text{DMSO-}d_6$ .....	108
Appendix 25. $^1\text{H}$ NMR spectrum of H3-1 tetrazole hydrochloride (H3-1T•HCl) in $\text{DMSO-}d_6$ . ....	109
Appendix 26. $^1\text{H}$ NMR spectrum of H3-1 tetrazole hydrochloride (H3-1T•HCl) in $\text{DMSO-}d_6$ with the addition of $\text{D}_2\text{O}$ .....	110
Appendix 27. $^1\text{H}$ NMR spectrum of H3-1 tetrazole hydrochloride (H3-1T•HCl) in $\text{MeOH-}d_4$ .....	111
Appendix 28. $^{13}\text{C}\{^1\text{H}\}$ NMR spectrum of H3-1 tetrazole hydrochloride (H3-1T•HCl) in $\text{DMSO-}d_6$ . ....	112
Appendix 29. ESI-TOF MS of H3-1 tetrazole hydrochloride (H3-1T•HCl). ....	113
Appendix 30. RP-HPLC chromatograms of H3-1 tetrazole hydrochloride (H3-1T•HCl). ....	114

Appendix 31. $^1\text{H}$ NMR spectrum of crude thioamide H3-1 methyl ester (TH3-1M) in DMSO- $d_6$ . .....	115
Appendix 32. $^{13}\text{C}\{^1\text{H}\}$ NMR spectrum of crude thioamide H3-1 methyl ester (TH3-1M) in DMSO- $d_6$ . .....	116
Appendix 33. ESI-TOF MS of crude thioamide H3-1 methyl ester (TH3-1M). .....	117
Appendix 34. $^1\text{H}$ NMR spectrum of crude methyleneamino H3-1 methyl ester (MH3-1M) in DMSO- $d_6$ . .....	118
Appendix 35. ESI-TOF MS of crude methyleneamino H3-1 methyl ester (MH3-1M). .....	119

## List of Abbreviations

ABCA1	ATP-binding cassette A1
ACS	American Chemical Society
ADCC	antibody-dependant cellular cytotoxicity
AICD	activation-induced cell death
AIDS	acquired immunodeficiency syndrome
AP	adaptor protein
ARF	ADP-ribosylation factor
ASK1	apoptosis signal-regulating kinase 1
AU	absorbance units
BiFC	bimolecular fluorescence complementation
br	broad
Btk	Bruton's tyrosine kinase
c-Src	proto-oncogene tyrosine-protein kinase Src
calc	calculated
CAR	chimeric antigen receptor
cART	combination antiretroviral therapy
CCR5	C-C chemokine receptor type 5
CD	cluster of differentiation
CTL	cytotoxic T lymphocyte

CXCR4	C-X-C chemokine receptor type 4
$^{13}\text{C}\{\text{H}\}$ NMR	proton-decoupled carbon-13 nuclear magnetic resonance
d	doublet
dr	diastereomeric ratio
D <sub>2</sub> O	deuterium oxide
DCM	dichloromethane
DFP	diphenylfuopyrimidines
DIPEA	<i>N,N</i> -diisopropylethylamine
DMF	<i>N,N</i> -dimethylformamide
DMSO	dimethyl sulfoxide
DMSO- <i>d</i> <sub>6</sub>	deuterated dimethyl sulfoxide
EDC•HCl	<i>N</i> -(3-dimethylaminopropyl)- <i>N</i> '-ethylcarbodiimide hydrochloride
EDTA	ethylenediaminetetraacetic acid
ELISA	enzyme-linked immunosorbent assay
eq.	equivalents
ESI-TOF	electrospray ionization time-of-flight
Et <sub>3</sub> N	triethylamine
Et <sub>3</sub> N•HCl	triethylammonium chloride
EtOAc	ethyl acetate
EtOH	ethanol

ex	exchangeable
FRET	Förster resonance energy transfer
<sup>19</sup> F NMR	fluorine-19 nuclear magnetic resonance
Gag	group-specific antigen
h	hours
H3-1A	H3-1 C-terminal amide
H3-1M	H3-1 methyl ester
H3-1N	H3-1 nitrile
H3-1T	H3-1 tetrazole
Hck	haematopoietic cell kinase
HCl	hydrochloric acid
His	histidine
HIV-1	human immunodeficiency virus type 1
HLA	human leukocyte antigen
HMDSO	hexamethyldisiloxane
HMG-CoA	3-hydroxy-3-methylglutaryl-coenzyme A
HN <sub>3</sub>	hydrazoic acid
HRMS	high-resolution mass spectrometry
H <sub>2</sub> S	hydrogen sulfide
Hz	hertz

$^1\text{H}$ NMR	proton nuclear magnetic resonance
<i>i</i> -PrOH	isopropanol
ICP-MS	inductively coupled plasma mass spectrometry
Itk	interleukin-2-inducible T-cell kinase
<i>J</i>	coupling constant
LC-MS	liquid chromatography-mass spectrometry
Lck	lymphocyte-specific protein tyrosine kinase
LOPAC	library of pharmacologically active compounds
Lyn	Lck/Yes-related novel protein tyrosine kinase
m	multiplet
M	molar
MeCN	acetonitrile
MEK	methyl ethyl ketone
MeOH	methanol
MeOH- <i>d</i> <sub>4</sub>	deuterated methanol
MH3-1M	methyleneamino H3-1 methyl ester
MHC-I	major histocompatibility complex class I
min	minute
M <sup>pro</sup>	main protease
MST	microscale thermophoresis

MTT	3-(4,5-dimethylthiazol-2-yl)-2,5-diphenyltetrazolium bromide
N	number of experimental replicates
NaHS	sodium hydrosulfide
N.R.	not reported
Na <sub>2</sub> CO <sub>3</sub>	sodium carbonate
NaBH <sub>4</sub>	sodium borohydride
NaN <sub>3</sub>	sodium azide
NanoBiT	NanoLuc binary technology
NanoLuc	Nanoluciferase
NaOH	sodium hydroxide
Nef	negative factor
NH <sub>3</sub>	ammonia
NH <sub>4</sub> Cl	ammonium chloride
NiCl <sub>2</sub> •6H <sub>2</sub> O	nickel chloride hexahydrate
NMR	nuclear magnetic resonance
obs	observed
P <sub>4</sub> S <sub>10</sub>	phosphorus decasulfide
PACS	phosphofurin acidic cluster sorting protein
PAK2	p21-activated kinase 2
PCl <sub>5</sub>	phosphorus pentachloride



PI3K	phosphoinositide 3-kinase
PKC	protein kinase C
PLK1	polo-like kinase 1
PLWH	people living with HIV
PMA	phosphomolybdic acid
ppm	parts per million
q	quartet
RP-HPLC	reversed-phase high-performance liquid chromatography
rt	room temperature
s	singlet
SERINC5	serine incorporator 5
SFK	Src family kinase
SH	Src homology
SIV	simian immunodeficiency virus
SPR	surface plasmon resonance
Syk	spleen tyrosine kinase
t	triplet
TFA	trifluoroacetic acid
TFAA	trifluoroacetic anhydride
TFK	Tec family kinase

TH3-1M	thioamide H3-1 methyl ester
THF	tetrahydrofuran
Tim-3	T cell immunoglobulin and mucin domain-containing protein 3
TLC	thin layer chromatography
TNF- $\alpha$	tumor necrosis factor alpha
Tyr	tyrosine
UV	ultraviolet
v	volume
V-ATPase	vacuolar-type ATPase
Vif	viral infectivity factor
Vpr	viral protein R
Vpu	viral protein U
Z	benzyloxycarbonyl
ZAP-70	zeta-chain-associated protein kinase 70
Zn	zinc
ZnBr <sub>2</sub>	zinc bromide
ZnS	zinc sulfide
$\beta$ -COP	coatamer subunit $\beta$
$\delta$	chemical shift

# Chapter 1

## 1 Introduction

### 1.1 The case for a practical HIV-1 cure

Since the identification of human immunodeficiency virus type 1 (HIV-1) as the cause of acquired immunodeficiency syndrome (AIDS), significant progress has been made in treating and controlling HIV-1 infection<sup>1-3</sup>. Today, dozens of antiretroviral drugs are available, and their use in combination antiretroviral therapy (cART) effectively prevents AIDS onset in people living with HIV (PLWH)<sup>1</sup>. However, cART is not curative, and reservoirs of HIV-1 infected cells continue to persist within cART-treated individuals. PLWH must therefore be on life-long and continuous cART, which carries obstacles in treatment adherence and access, as well as risks for treatment failure<sup>4-6</sup>. Further, cART-treated PLWH can experience a multitude of chronic health conditions at an elevated rate, especially those associated with accelerated aging, in addition to severe stigma<sup>7-10</sup>. A practical cure for HIV-1 has therefore remained an urgent and top priority to improve the health outcomes for PLWH, especially as the 90-90-90 target rates for global HIV status testing, cART coverage, and viral suppression were not met with the end of 2020<sup>11</sup>.

### 1.2 Approaches to cure HIV-1

Only one HIV-1 curative strategy has shown success *in vivo*, namely, allogeneic haematopoietic stem cell transplantation from a donor maintaining the CCR5 $\Delta$ 32/ $\Delta$ 32 mutation<sup>12-15</sup>. To-date, only a handful of individuals have been successfully cured with this approach, displaying durable virological control following cART discontinuation. However, this approach is no silver bullet, with multiple cases undergoing transplantation without curation<sup>16-18</sup>. More importantly, this approach is impractical due to cost and donor availability, as well as being surgically extremely high-risk.

Alternatively, there is still an unmet need for a practical cure which is efficacious for the majority of PLWH, while maintaining a lessened burden and a greater margin of safety

than cART alone<sup>19,20</sup>. Efforts to develop such a practical cure for HIV-1 have largely focused on strategies such as shock and kill<sup>21,22</sup>, block and lock<sup>23</sup>, therapeutic vaccination<sup>24</sup>, chimeric antigen receptor (CAR) T cell therapy<sup>25</sup>, and treatment with cytokines, immune checkpoint inhibitors, and/or neutralizing antibodies<sup>26,27</sup>. Unfortunately, whether administered alone or in combination, none of these strategies have yet shown success in clinical trials. Although the reasons for their lack of success are multifaceted, several HIV-1-related barriers play an important role in undermining the efficacy of these curative approaches<sup>28</sup>. Indeed, as many curative approaches are immune-directed, including shock and kill, therapeutic vaccination, CAR T cell therapy, and antibody therapies, HIV-1-mediated immune evasion is likely to stifle cure efficacy *in vivo*<sup>29-31</sup>. Virus-driven defects in other cellular processes, including T cell receptor signaling, apoptosis, and autophagy, may also hinder cure activity, such as by restraining latency reversal or cytotoxic T lymphocyte (CTL) activity<sup>28</sup>. Importantly, the HIV-1 accessory protein, Nef, has been implicated in many of these processes, suggesting Nef to be a central mediator of cure success and thus a prime target for pharmacological inhibition<sup>32-39</sup>.

### 1.3 Biology of the HIV-1 Nef protein

Nef is one of four accessory proteins (Nef, Vif, Vpu, and Vpr) encoded by HIV-1. As an accessory protein, Nef is not strictly required for the viral replication cycle *in vitro*, but instead acts to optimize viral replication *in vivo* by boosting virion infectivity and production, as well as inhibiting antiviral immunity<sup>33,34,40,41</sup>. Indeed, numerous animal models and human cohorts have demonstrated an important role for Nef in replication enhancement and HIV-1 pathogenesis. Notably, infection of rhesus macaques with *nef*-deficient simian immunodeficiency virus (SIV) strains resulted in reduced viral replication and aborted pathogenesis<sup>42</sup>. In numerous transgenic mouse models, Nef expression was sufficient to induce CD4<sup>+</sup> T cell depletion<sup>43-46</sup>, and in one model, Nef expression was both necessary and sufficient for the development of a severe AIDS-like phenotype characterized by wasting, thymic atrophy, and CD4<sup>+</sup> T cell loss<sup>46</sup>. Studies in humanized mouse models have also affirmed a crucial role for Nef in enhancing HIV-1 replication *in vivo* and in mediating disease pathogenesis<sup>47-49</sup>. Most importantly, several human cohort

studies have described individuals infected with HIV-1 isolates encoding a dysfunctional Nef protein, and this has correlated with reduced viral replication and slower to non-progression to disease<sup>50-53</sup>.

At the molecular level, Nef forms numerous protein-protein interactions with host factors to hijack cellular signaling and trafficking pathways. Through these mechanisms, Nef predominantly acts to modulate the cell surface levels of proteins including CD4<sup>54,55</sup>, SERINC5<sup>56-58</sup>, and MHC-I<sup>59-61</sup> (**Figure 1.1**). For instance, Nef facilitates the downregulation of cell surface CD4 by binding and linking the CD4 cytoplasmic tail to adaptor protein 2 (AP-2)-dependent trafficking machinery, thus driving its endocytosis and subsequent lysosomal degradation<sup>62,63</sup>. CD4 downregulation in turn limits viral superinfection<sup>64</sup> and antibody-dependent cellular cytotoxicity (ADCC)<sup>65</sup>. In a similar AP-2-dependent manner, Nef downregulates the restriction factor, SERINC5, to promote virion infectivity<sup>56-58,66</sup>. Additionally, Nef downregulates cell surface MHC-I through two discrete modes, termed the signaling and stoichiometric modes. In the signaling mode, Nef binds and activates a suite of Src family kinases (SFKs), namely, Hck, Lyn, and c-Src, to assemble an SFK:ZAP-70/Syk:PI3K multi-kinase complex<sup>67-70</sup>. PI3K signaling from this Nef-associated kinase complex increases the endocytosis of cell surface MHC-I. Subsequently, Nef delays the recycling of MHC-I back to the cell surface by trafficking MHC-I from early endosomes to the *trans*-Golgi network for sequestration<sup>60</sup>. Alternately, in the stoichiometric mode, Nef hijacks nascent MHC-I molecules early in the secretory pathway for their subsequent degradation within the lysosome<sup>71,72</sup>. Numerous trafficking machinery have been implicated in these processes, including but not limited to, the trafficking regulators PACS-1/2, adaptor protein 1 (AP-1), ARF1/6, clathrin, and  $\beta$ -COP. Collectively, these two modes of downregulation result in reduced cell surface levels of levels of MHC-I, which abrogates viral antigen presentation from infected cells and thereby enables infected cells to elude their CTL-mediated killing<sup>32</sup>.

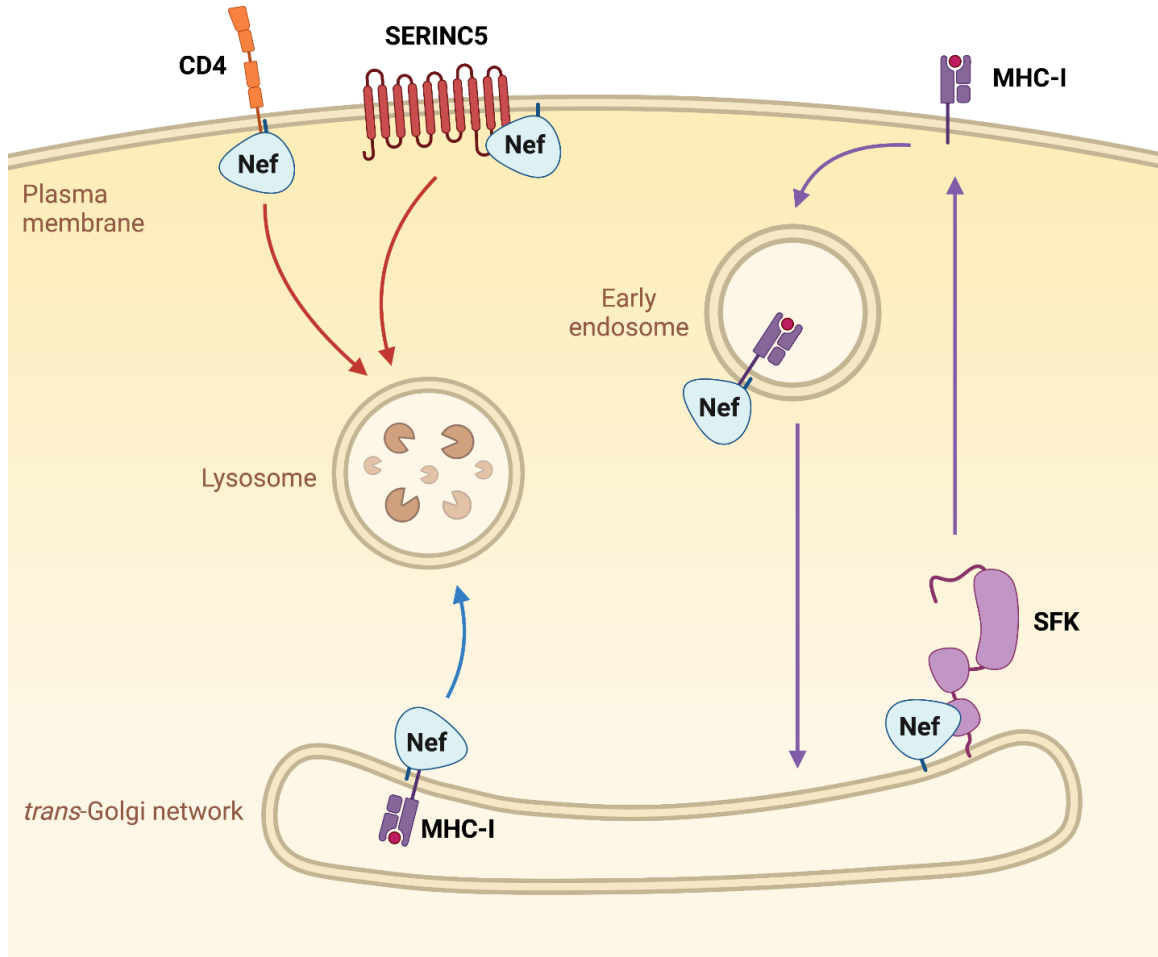


**Figure 1.1 Overview of key HIV-1 Nef activities.** In infected cells, Nef binds CD4 and SERINC5 to facilitate their endocytosis and trafficking to the lysosome for degradation (red arrows). Alternatively, Nef localized to the *trans*-Golgi network binds and activates a suite of SFKs to initiate the signaling mode of MHC-I downregulation, beginning with the endocytosis of cell surface MHC-I, followed by its trafficking from early endosomes to the *trans*-Golgi network for sequestration (purple arrows). Additionally, in the stoichiometric mode, Nef hijacks nascent MHC-I early in the secretory pathway for trafficking to the lysosome for degradation (blue arrow). Created with Biorender.com.

Numerous other cell surface receptors have been reported to be modulated by Nef, including the co-stimulatory molecules, CD28, CD80, and CD86<sup>73-75</sup>, the HIV-1 co-receptors, CCR5 and CXCR4<sup>76,77</sup>, and the immune checkpoint receptor, Tim-3<sup>78</sup>. Nef has also been implicated in binding and modulating many other signaling and trafficking factors, such as the Tec family kinases (TFKs)<sup>79,80</sup>, PAK2<sup>81</sup>, Lck<sup>82</sup>, PI3Ks<sup>35,67,69</sup>, ASK1<sup>36</sup>, and PKC<sup>83</sup>. Nef's numerous interactions with such host proteins are in turn essential for its many effects on infected and bystander cells, including alterations in T cell receptor signaling<sup>38,39</sup>, cellular activation<sup>38,39,41,84</sup>, lymphocyte chemotaxis<sup>84</sup>, extracellular vesicle release<sup>85</sup>, autophagy<sup>37</sup>, and apoptosis<sup>35,36,86</sup>. Altogether, these Nef effects ensure an optimal replicative environment for the virus, in addition to mediating disease pathogenesis.

## 1.4 Implications of Nef in an HIV-1 cure

HIV-1 maintains numerous mechanisms which act as barriers against a practical cure. Surprisingly, the paradigm of cure development has largely focused on the direct optimization of the curative agents themselves, while comparatively less attention has been devoted to inhibiting these barriers against a cure. Yet, developing mechanisms secondary to the curative agent which can boost cure efficacy is a promising and potentially necessary approach to functionalize a practical HIV-1 cure. Considering the crucial and multifactorial role Nef plays during HIV-1 infection, pharmacological inhibition of Nef may be an especially powerful strategy to boost efficacies in a broad panel of curative approaches, including shock and kill and HIV-1 immunotherapies.

### 1.4.1 Implications of Nef in latency reversal

HIV-1's maintenance within a reversibly non-productive state of infection, termed the latent reservoir, is a central mechanism for HIV-1's persistence in PLWH on cART<sup>87,88</sup>. As latently infected cells are not readily producing virions, mechanisms to clear these HIV-1-infected cells through immune killing or viral cytopathic effects are largely absent. Accordingly, it is thought that a reduction in latent reservoir size can be achieved by

reactivating latent proviruses, primarily by using a latency reversing agent (“shock”), followed by their clearance through immune-directed mechanisms and viral cytopathic effects (“kill”)<sup>21,22</sup>. This consequent reduction in latent reservoir size may then promote remission and long-term virological control independent of cART.

Despite the promise of a shock and kill approach, no derivative of this strategy has definitively shown success by considerably reducing latent reservoir size or delaying viral rebound following cART cessation. The reasons for this are numerous, with inefficient viral reactivation and differential latency reversal across immune cell subsets presented as central issues<sup>30</sup>. Notably, Nef may play a critical role in mediating latency reversal through its effects on host cell signaling. Indeed, several studies have affirmed Nef’s role in viral replication enhancement, especially through its effects on T cell receptor and general kinase signaling<sup>38,39,89,90</sup>, suggesting that Nef may act to promote latency reversal<sup>91–93</sup>. On the other hand, the signaling events associated with Nef’s enhancement of viral replication are aberrant, especially for T cell receptor signaling, in which Nef selectively dysregulates conventional signaling, likely to limit antiviral immunity and activation-induced cell death (AICD), while a compensatory Nef-associated signaling pathway is established to promote viral replication<sup>39</sup>. In light of this duality, Nef may instead hinder latency reversal, which suggests that inhibitors capable of blocking Nef-induced signaling, and its associated defects in immune function, could promote latency reversal. However, Nef’s effects on latency reversal remain almost entirely unknown and are likely to vary according to each latency reversing agent.

#### 1.4.2 Implications of Nef in infected cell clearance

The potent elimination of HIV-1-infected cells is central to many curative approaches; however, none have been successful in this aspect *in vivo*. Indeed, although shock and kill has achieved some successes in viral reactivation, this has not been associated with a reduction in reservoir size<sup>30,31</sup>. Similar deficiencies have also been identified for therapeutic vaccination approaches<sup>24</sup>. Importantly, these approaches’ ineffectiveness stems primarily from an inability for the adaptive immune response to clear HIV-1-infected cells



*in vivo*, and accumulating evidence suggests that a robust and broad anti-HIV-1 CTL response is necessary for infected cell clearance in a shock and kill or immunotherapy approach<sup>29,94</sup>. However, HIV-1-infected cells containing intact proviruses are intrinsically resistant to CTL-mediated killing, even in the absence of escape mutations, poor latency reversal, compartmentalization, or CTL dysfunction, highlighting a need to boost anti-HIV-1 CTL-mediated killing for a successful cure to be realized<sup>95</sup>. Notably, HIV-1 Nef downregulates cell surface MHC-I, specifically HLA-A and -B, which abrogates antigen presentation from HIV-1 infected cells to anti-HIV-1 CTLs, and may thus promote the persistence of infected cells *in vivo*<sup>32,59,96</sup>. Inhibition of Nef-mediated MHC-I downregulation could therefore serve a broad purpose in supporting any curative approach reliant on CTL activity by promoting infected cell killing.

In addition to MHC-I downregulation, HIV-1-infected cells may resist clearance through additional Nef effects, including blockade of Fas- and TNF- $\alpha$ -associated cell death signaling through ASK1 inhibition<sup>36</sup>, evasion of ADCC by CD4 downregulation<sup>65</sup>, or as suggested more recently, inhibition of viral cytopathic effects through PLK1 upregulation<sup>97</sup>. Nef additionally induces severe and broad defects in adaptive immunity, including dysregulation of T cell receptor signaling<sup>38,39</sup>, downregulation of the co-stimulatory receptors CD28, CD80, and CD86<sup>73-75</sup>, upregulation of the immune checkpoint receptor Tim-3<sup>78</sup>, induction of bystander T cell apoptosis<sup>98</sup>, and inhibition of B cell affinity maturation<sup>99</sup>. Together, these disparate effects of Nef highlight its role in preventing HIV-1-infected cell clearance and thus underscore the supportive role Nef inhibitors can play in a variety of curative approaches including shock and kill and HIV-1 immunotherapies such as therapeutic vaccination and CAR T cell therapies (summarized in **Figure 1.2**).

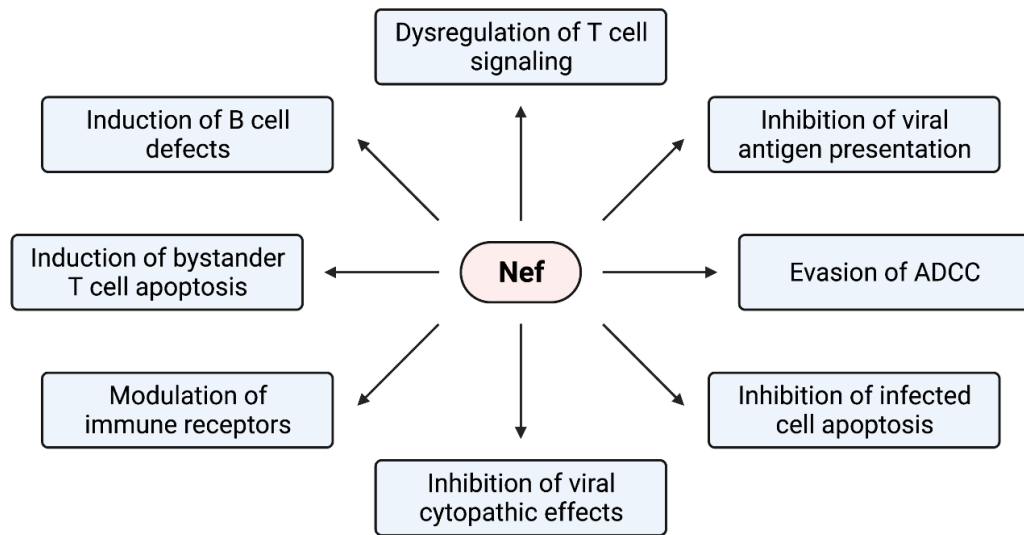


**Figure 1.2 Summary of selected Nef activities relevant to a practical HIV-1 cure.**  
 Created with Biorender.com.

## 1.5 Past developments towards inhibitors of HIV-1 Nef

Spanning almost 20 years of development, numerous groups have reported on potential Nef inhibitors, including small molecule, peptide, and protein inhibitors (summarized in **Table 1.1**).

**Table 1.1 Summary of Nef inhibitors identified to-date.**

Inhibitor(s)	Primary proposed mechanism of action	MHC-I rescue	CTL killing	Replication inhibition	Infectivity inhibition	Additional key effects	References
<b>Small molecule inhibitors</b>							
Adriamycin	Inhibition of the Nef:Hck interaction by reducing Hck expression.	N.R.	N.R.	N.R.	N.R.		100
D1, DLC27, and DLC27-14	Orthosteric inhibition of Nef's interactions with SH3 domains, namely the Hck SH3 domain, by binding the RT loop binding pocket of Nef.	+	N.R.	+ <sup>a</sup>	- <sup>a</sup>	Destabilization of Nef's structure resulting in its accelerated cleavage by HIV-1 Protease.	101–103
DFP-4AP, DFP-4AB, and DFP-APF	Inhibition of Nef-bound Hck and Lyn kinase activity by binding the kinases' active site.	N.R.	N.R.	+	N.R.		104–107
B9 and analogues	Inhibition of Nef dimerization by binding Nef at the dimerization interface.	+	+	+	+	Restoration of cell surface CD4 and inhibition of Nef-mediated SFK and TFK activation.	80,108–113
SRI-35789 and analogues	Inhibition of Nef-mediated Hck activation and Nef:MHC-I:AP-1 $\mu$ 1 complex assembly by binding Nef.	+	N.R.	+	+		114
DQBS	Inhibition of Nef-mediated SFK activation, namely Hck, by binding Nef.	+	+	+	-		103,113
E11	Inhibition of Nef dimerization by an unknown mechanism.	N.R.	N.R.	N.R.	N.R.		115
2c	Allosteric and/or orthosteric inhibition of the Nef:SFK interaction by binding the polyproline helix, the RT loop binding pocket, and/or a C-terminal pocket of Nef.	+	N.R.	+ <sup>a</sup>	+ <sup>a</sup>		70,116
Lovastatin	Inhibition of the Nef:AP-1 interaction by binding a pocket of Nef at the Nef:AP-1 $\mu$ 1 interaction interface.	+	+	N.R.	+	Restoration of cell surface CD4 and SERINC5.	117,118

Concanamycin A	Inhibition of Nef:MHC-I:AP-1 complex assembly by an unknown mechanism.	+	+	N.R.	N.R.		118
Guanidine alkaloid analogues (compounds 14, 17, and 22)	Inhibition of Nef's interactions with p53, Lck and actin by binding Nef.	N.R.	N.R.	N.R.	N.R.		119
NSC13987 and analogues (AMS-55)	Inhibition of the Nef:calnexin interaction by binding Nef.	N.R.	N.R.	+	N.R.	ABCA1 rescue and restoration of cholesterol efflux.	120,121
Triciribine	Unknown, likely inhibition of Akt.	N.R.	N.R.	+	-		122
<b>Selected peptide and protein inhibitors</b>							
sdAb19	Broad Nef interaction inhibition by binding a C-terminal pocket of Nef.	-	N.R.	+	+	Restoration of cell surface CD4, inhibition of the Nef:PAK2 interaction and its downstream actin remodeling effects. Reversal of CD4 <sup>+</sup> T cell maturation and activation defects in a transgenic Nef mouse model.	123,124
Nef interacting proteins	Broad Nef interaction inhibition by binding the polyproline helix, the RT loop binding pocket, and a proximal CD4 binding pocket of Nef.	+	N.R.	N.R.	+	Restoration of cell surface CD4 and CCR5.	125
Neffins	Broad Nef interaction inhibition by binding the polyproline helix, the RT loop binding pocket, and a C-terminal pocket of Nef to form a 2:2 Neffin:Nef complex.	+	N.R.	N.R.	+	Restoration of cell surface CD4, inhibition of Nef-mediated Hck activation, Lck relocalization, and macrophage defects.	124,126,127

N.R.: not reported.

*a* Only assessed in a follow-up study by a different group.

### 1.5.1 Small molecule inhibitors of Nef-mediated kinase activation

Inhibition of the interaction between Nef and its associated kinases, most importantly, the SFKs, Hck, Lyn, and c-Src, has been a central focus of Nef inhibitor development, holding promise to abrogate Nef-mediated MHC-I downregulation, as well as to impair Nef-mediated enhancements to HIV-1 replication, infectivity, and pathogenesis<sup>69,70,116,128,129</sup>. To bind and activate the SFKs, Nef engages the SFK's SH3 domain using a polyproline helix and a hydrophobic binding pocket which binds the SH3 domain RT loop, hereafter referred to as the RT loop binding pocket of Nef (**Figure 1.3**)<sup>130</sup>. Nef binding releases the SH3 domain from the SFK's SH2-kinase regulatory linker to constitutively activate the SFK<sup>131</sup>. Importantly, the same surfaces with which Nef binds and activates the SFKs, are also thought to engage the SH3 domains of TFKs<sup>79</sup>. Thus, inhibitors targeting the Nef:SFK interaction may not only mediate their effects by reducing constitutive SFK activation, but also other Nef signaling effects.

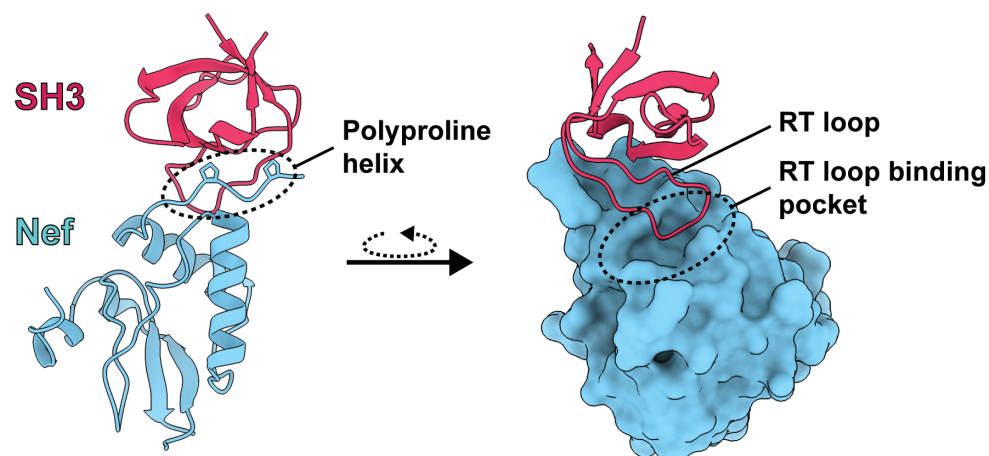


**Figure 1.3 Overview of the interaction between Nef and an SFK SH3 domain.** Binding of the SH3 domain (red) to the Nef (blue) polyproline helix is visualized on the left and binding of the SH3 domain RT loop to the Nef RT loop binding pocket is visualized on the right. Visualization was conducted with UCSF ChimeraX<sup>132</sup> using the X-ray crystal structure of NL4-3 Nef T71R in complex with Fyn SH3 R96I (PDB: 1EFN)<sup>130</sup>.

The earliest report on small molecule inhibitors of Nef stems from a mammalian two-hybrid screen which aimed to identify inhibitors of the Nef:Hck interaction<sup>100</sup>. By screening a small library of 500 selected synthetic and natural products, adriamycin and four of its derivatives were identified as potential Nef:Hck interaction inhibitors. Unfortunately, it was also found that adriamycin mediated its effects on the Nef:Hck interaction by reducing intracellular levels of Hck and was not explored further.

Subsequently, Collette and coworkers adapted a similar mammalian two-hybrid approach to screen for Nef:Hck interaction inhibitors<sup>101</sup>. A virtual docking screen targeting the RT loop binding pocket of Nef, followed by a mammalian two-hybrid assay, identified the compound, D1 (also referred to as D14) (**Figure 1.4**), which inhibited the interaction between Nef and the Hck SH3 domain (Hck-SH3) and bound Nef *in vitro* with micromolar affinity. In Nef-expressing cells, D1 partially restored cell surface MHC-I levels but had little to no effect on cell surface CD4 levels, consistent with its proposed mechanism of action. A secondary screen of D1 analogues identified the Nef:Hck-SH3 interaction inhibitor, DLC27 (**Figure 1.4**), which was validated to bind the RT loop binding pocket of Nef, further confirming these compounds' proposed mechanism of action as orthosteric inhibitors of the Nef:Hck-SH3 interaction. A subsequent follow-up study aimed to improve on DLC27's affinity for Nef by extending its nonpolar *tert*-butyl phenyl moiety<sup>102</sup>. Using this strategy, the DLC27 analogue, DLC27-14, was identified (**Figure 1.4**), which inhibited the Nef:Hck-SH3 interaction *in vitro* with improved potency. Interestingly, it was also observed that DLC27 and DLC27-14 binding destabilized Nef's tertiary structure and increased its processing by HIV-1 Protease *in vitro*, suggesting that these inhibitors can function as targeted Nef degraders. In a separate study, DLC27-14 was applied in cell culture, where it was found to inhibit Nef-mediated viral replication enhancement but not infectivity enhancement<sup>103</sup>.

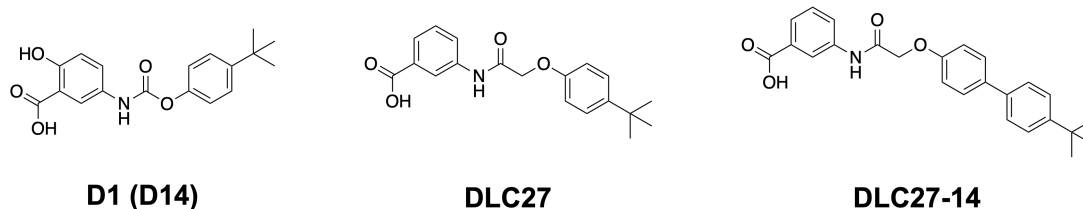


**Figure 1.4 Structural representations of D1, DLC27, and DLC27-14.**

Subsequent efforts to identify an improved Nef:SFK interaction inhibitor were spearheaded by Smithgall and coworkers who have developed a variety of Nef:SFK interaction assays for screening large libraries of small molecule inhibitors. Initially, an *in vitro* Förster resonance energy transfer (FRET)-based kinase assay, termed Z'-LYTE, was adapted to identify compounds which interfered with Nef's activation of Hck<sup>104</sup>. The Z'-LYTE screen was first applied to a library of approximately 10,000 compounds to identify a series of 4-amino substituted diphenylfuopyrimidines (DFPs), termed DFP-4AB, DFP-4AP, and DFP-4APF, which were found to inhibit Nef-mediated Hck and Lyn activation, as well as Nef-mediated enhancements to HIV-1 replication, with micromolar potency. A follow-up study further confirmed inhibition of Nef-mediated Hck and endogenous SFK activation, as well as replication enhancement, for a broad panel of group M Nef subtypes<sup>105</sup>. Notably, the DFP compounds were identified to be structurally similar to a series of previously described protein tyrosine kinase inhibitors which bound directly to the Lck active site, suggesting that the DFP inhibitors were functioning similarly to inhibit the SFK directly. Interestingly, although the authors observed the DFP compounds to mildly inhibit Hck and Lyn kinase activity in the absence of Nef, the presence of Nef resulted in a drastic increase in kinase inhibition. Follow-up studies further identified Nef:Hck binding to alter the kinases' active site conformation, which may promote DFP binding to the active site<sup>106,107</sup>.

In another report, the Nef:Hck Z'-LYTE assay was reapplied to screen a much larger and more diverse library of more than 220,000 compounds in an effort to identify compounds which bound to Nef instead of the SFK<sup>108</sup>. These screens identified the hydroxypyrazole, B9 (**Figure 1.5A**), which inhibited Nef-mediated Hck and endogenous SFK activation, as well as Nef-mediated replication enhancement, across all tested group M subtypes of Nef

with high nanomolar to low micromolar potencies. B9 additionally attenuated HIV-1 infectivity in cell culture at micromolar concentrations, but some impairment of SFK activity for Hck, Lyn, and c-Src in the absence of Nef was noted. Surface plasmon resonance (SPR) experiments identified B9 to bind Nef with nanomolar affinity and docking studies suggested that B9 may bind a pocket formed at the Nef dimerization interface (**Figure 1.5B**), in addition to other Nef pockets. A dimerization-associated binding pocket for B9 was supported by bimolecular fluorescence complementation (BiFC) experiments, with B9 inhibiting Nef homodimer BiFC at micromolar concentrations. Subsequent studies reported B9 to additionally restore cell surface CD4 and to inhibit Nef-mediated activation of the TFKs, Itk and Btk<sup>80,109,112</sup>.

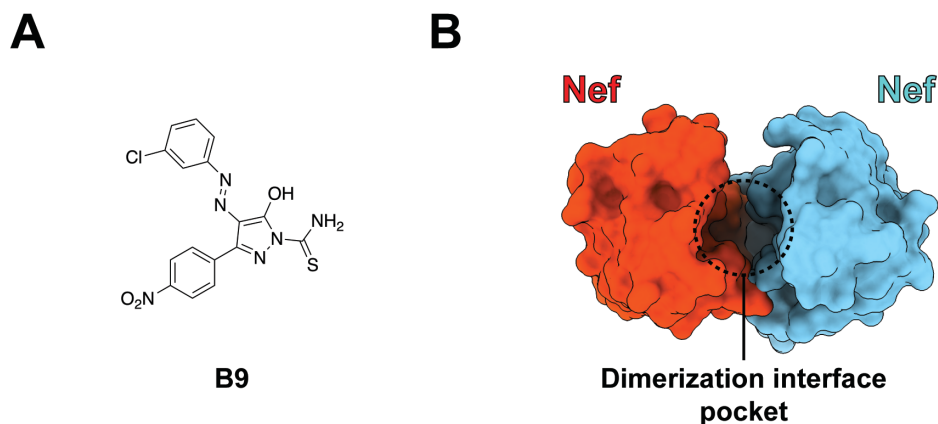


**Figure 1.5 Overview of the Nef homodimerization inhibitor, B9.** **A)** Structural representation of B9. **B)** Overview of a Nef dimer derived from an X-ray crystal structure of the Nef:Fyn-SH3 complex with a binding pocket formed at the Nef dimerization interface highlighted. Visualization was conducted with UCSF ChimeraX<sup>132</sup> using the X-ray crystal structure of NL4-3 Nef T71R in complex with Fyn SH3 R96I (PDB: 1EFN)<sup>130</sup>.

Follow-up studies have identified a variety of B9 analogues, with the goal of improving B9's potency and pharmacokinetic profile, as well as to replace troublesome groups within the hydroxypyrazole scaffold; namely, the azo, nitro, and thioamide groups<sup>110,111</sup>. Although



compounds which replaced each of the three groups were synthesized<sup>110</sup>, two B9 analogues which replaced the azo linker with ethylene or methylene bridges, but which maintained the nitro and thioamide groups, were found to be most promising<sup>111</sup>. These B9 analogues, referred to as compounds 2 and 4 (**Figure 1.6**), and in a later study, JZ-96-21 and JZ-97-21, respectively, maintained high nanomolar affinities for Nef, low micromolar inhibition of Nef-mediated HIV-1 infectivity and replication enhancement, reduced cytotoxicity, and improved oral bioavailability in mice compared to B9. A later report also identified that JZ-96-21 can inhibit Nef-mediated activation of the TFKs, Itk and Btk<sup>80</sup>.

Subsequently, an extensive synthetic effort was undertaken to improve on B9 with the generation of a 216 compound suite of B9 analogues maintaining numerous substitutions surrounding the hydroxypyrazole core<sup>112</sup>. By combining results for inhibitor binding to Nef and inhibition of Nef-mediated HIV-1 infectivity enhancement, the authors identified six top-scoring compounds (FC-7902, FC-7943, FC-7976, FC-8052, FC-8517, FC-8698; **Figure 1.6**) which bound Nef with picomolar to low nanomolar affinities, reduced HIV-1 infectivity at micromolar concentrations, inhibited HIV-1 replication with nanomolar potencies, and were of modest cytotoxicity at the high nanomolar to micromolar levels. Several inhibitors were also found to inhibit Nef-mediated Itk and Hck activation (FC-7902, FC-7943, FC-8052, FC-8517, FC-8698), as well as Nef-mediated MHC-I downregulation with a substantially improved potency compared to B9 (FC-7902, FC-7943, FC-7976, FC-8007, FC-8052, FC-8517, FC-8698, FC-8700).

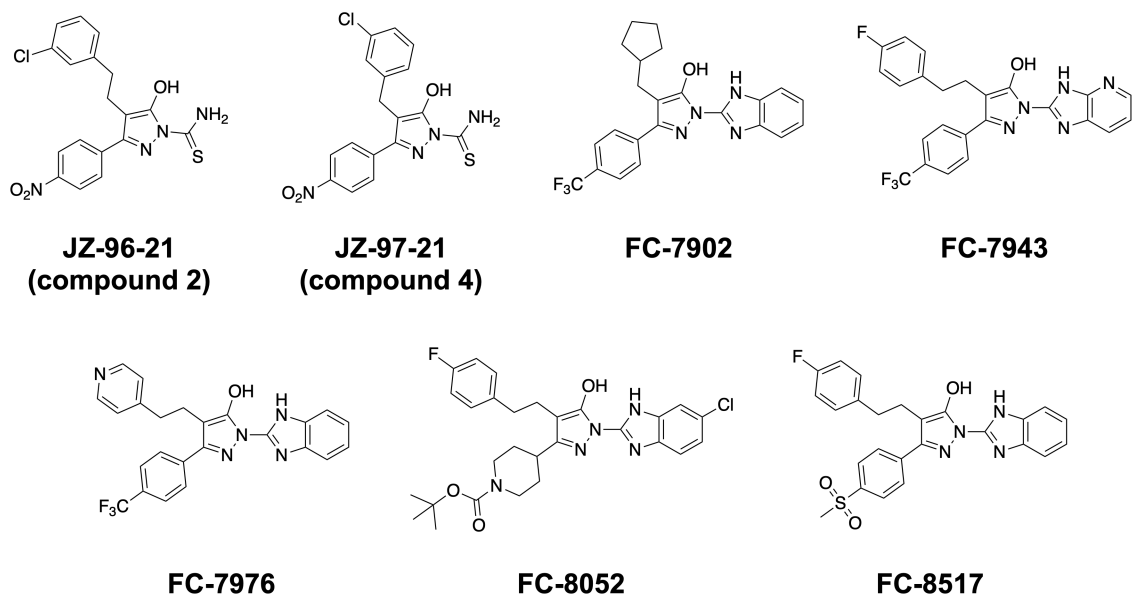


**Figure 1.6** Structural representations of selected B9 analogues.

More recently, the Nef:Hck Z'-LYTE assay was reapplied to screen a large library of more than 730,000 compounds, identifying the isothiazolone, SRI-35789, as a potential Nef inhibitor (**Figure 1.7**)<sup>114</sup>. Validation studies established SRI-35789 to inhibit Nef-mediated Hck activation, viral replication, and virion infectivity, as well as to bind HIV-1 and SIV Nef proteins with low micromolar potencies and affinities. Encouraged with the positive results for SRI-35789, 84 analogues were synthesized and evaluated, identifying numerous additional compounds which inhibited HIV-1 infectivity and bound Nef with similar or improved potencies and affinities (**Figure 1.7**). SRI-35789 and its analogue, SRI-37264, were also found to rescue cell surface MHC-I in HIV-1-infected cells, and SRI-37264 disrupted assembly of the Nef:MHC-I:AP-1 $\mu$ 1 complex *in vitro*. The pharmacokinetic properties of seven isothiazolone Nef inhibitors were evaluated, with two (SRI-37264 and SRI-38731) maintaining encouraging half-lives of greater than two hours in mouse and human liver microsomes. Finally, SRI-37264 was evaluated for *in vivo* stability by monitoring plasma concentrations in mice, but unfortunately SRI-37264 was found to be rapidly eliminated, with an approximately 40-minute half-life.

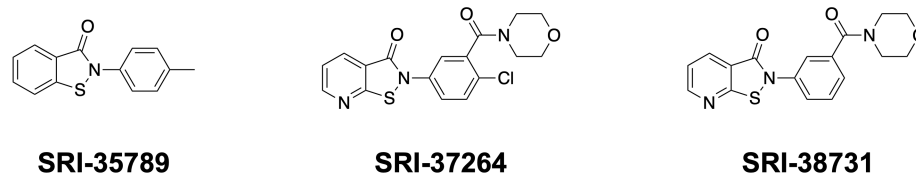


**Figure 1.7 Structural representations of SRI-35789 and selected analogues.**

Alternative screens for Nef inhibitors have also been piloted by the Smithgall group. Firstly, a yeast growth inhibition assay was developed for small molecule screening, where the co-expression of Nef and Hck in yeast results in constitutive Hck activation and a resulting inhibition of yeast growth<sup>103</sup>. Using this assay to screen a small library of nearly 2,500 compounds, followed by a secondary screen for inhibition of Nef-mediated HIV-1 replication enhancement, identified the compound, DQBS (**Figure 1.8**). DQBS was found to inhibit Nef-mediated Hck and endogenous SFK activation, as well as Nef:SFK:ZAP-70/Syk:PI3K complex assembly and MHC-I downregulation in cell culture with micromolar potency. Nef-mediated replication enhancement was also inhibited by DQBS across a panel of group M Nef subtypes. Importantly, DQBS was not observed to inhibit Hck or ZAP-70 kinase activity in the absence of Nef and bound to Nef *in vitro*, albeit at elevated concentrations. Docking studies of DQBS suggested it to bind a pocket of Nef formed at the dimerization interface, much like B9 and its analogues, in addition to other pockets, but this was not tested experimentally. Lastly, in a separate study, a Nef homodimer BiFC assay was used to screen a 1,597 compound library for Nef dimerization inhibitors<sup>115</sup>. This pilot screen identified the compound, E11 (**Figure 1.8**), which reduced Nef homodimer BiFC at low micromolar concentrations, but validation studies were not conducted.

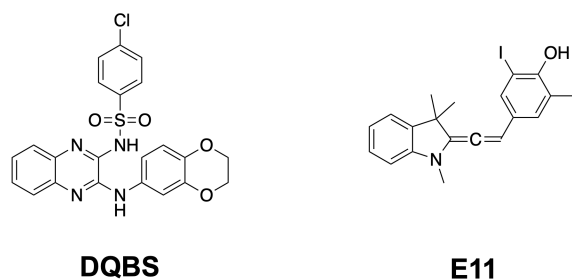


**Figure 1.8 Structural representations of DQBS and E11.**

Recently, several of the inhibitors described above have been applied as tool compounds to test if inhibition of Nef-mediated MHC-I downregulation can improve the CTL-mediated clearance of latently HIV-1-infected cells<sup>113</sup>. Specifically, DQBS, B9, and its derivatives, JZ-96-21 and JZ-97-21 (**Figures 1.5, 1.6, and 1.8**), were tested in a coculture assay of primary latently HIV-1-infected CD4<sup>+</sup> T cells and anti-HIV-1 CTLs derived from an HIV-1-infected donor. In this assay, application of each inhibitor at high nanomolar to low micromolar concentrations improved the CTL-mediated clearance of HIV-1-infected cells. Further, 23 of 26 tested donors responded to B9 treatment with increased infected cell killing, and when inhibitors were applied in two doses, HIV-1-infected cell clearance was greatly improved, with an 80-90% reduction in residual Gag<sup>+</sup> cells relative to vehicle-treated cells. Together, these results evidence inhibition of Nef-mediated MHC-I downregulation as a viable approach to boost infected cell clearance in an immune-directed HIV-1 cure.

Finally, Thomas and coworkers reported on a phenolic small molecule, 2c (**Figure 1.9A**), which inhibited Nef's interactions with Hck, Lyn, and c-Src, disrupted assembly of the Nef:SFK:ZAP-70/Syk:PI3K complex, and rescued cell surface MHC-I, but not CD4, in cell culture with a micromolar potency<sup>70</sup>. Compound 2c was identified from a previous study which characterized it as an inhibitor of multiple interactions between polyproline motifs and SH3 domains<sup>133</sup>. Interestingly, nuclear magnetic resonance (NMR) spectroscopy studies of the Nef:2c interaction primarily suggested 2c to bind a C-terminal pocket of Nef not typically associated with SFK activation or MHC-I downregulation, indicating 2c to be an allosteric inhibitor of the Nef:SFK interaction (**Figure 1.9B**).

Orthosteric inhibition of the Nef:SFK interaction by binding Nef's polyproline helix was also suggested (**Figure 1.3**). A follow-up report on 2c additionally observed inhibition of Nef-mediated enhancements to HIV-1 infectivity and replication at micromolar potencies, while their docking studies alternatively predicted 2c to bind the RT loop binding pocket of Nef<sup>116</sup>. Regardless, 2c has been successfully applied as a tool compound to study Nef-mediated MHC-I downregulation, but its development for therapeutic applications has stalled, primarily owing to its suboptimal potency and high toxicity.

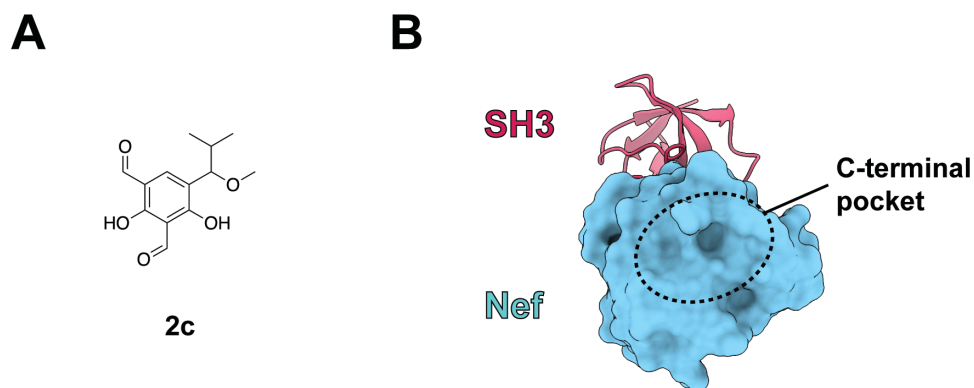


**Figure 1.9 Overview of the Nef:SFK interaction inhibitor, 2c.** **A)** Structural representation of 2c. **B)** Overview of the interaction between Nef (blue) and an SFK SH3 domain (red) with an allosteric C-terminal Nef pocket for 2c binding highlighted. Visualization was conducted with UCSF ChimeraX<sup>132</sup> using the X-ray crystal structure of NL4-3 Nef T71R in complex with Fyn SH3 R96I (PDB: 1EFN)<sup>130</sup>.

### 1.5.2 Alternative small molecule inhibitors of Nef-mediated MHC-I downregulation

Recently, two alternative inhibitors of Nef-mediated MHC-I downregulation have been reported which do not rely on inhibition of Nef-mediated SFK activation. Firstly, Li and coworkers used flow cytometry to screen a library of 1,600 FDA-approved compounds for cell surface MHC-I rescue in Nef-expressing cells<sup>117</sup>. This screen identified the statin drug,

lovastatin (**Figure 1.10A**), which broadly rescued cell surface MHC-I, CD4, and SERINC5 at micromolar potencies. As for other Nef inhibitors which rescued cell surface MHC-I, lovastatin inhibited Nef-mediated HIV-1 infectivity enhancement and enhanced the CTL-mediated killing of autologous HIV-1-infected CD4<sup>+</sup> T cells. Docking studies suggested that lovastatin, whether in its prodrug closed-ring form, or in the open-ring form, binds a pocket at the Nef:AP-1 $\mu$ 1 interface (**Figure 1.10B**). This was supported by SPR studies, which identified lovastatin to bind Nef with a high micromolar affinity, and that this affinity was reduced when Nef residues within the predicted binding pocket were mutated. Additionally, lovastatin inhibited the co-immunoprecipitation of AP-1 with Nef. However, lovastatin is principally an HMG-CoA reductase inhibitor<sup>134</sup>, which may complicate its application as a Nef inhibitor *in vivo*, especially in light of the micromolar concentrations required for Nef inhibition in cell culture.

More recently, Collins and coworkers also conducted a flow cytometry screen based on cell surface MHC-I rescue in Nef-expressing cells<sup>118</sup>. Although initial screening of a large library consisting of more than 200,000 small molecules was unable to identify any hits, subsequent screening of a natural product library of more than 20,000 extracts identified 11 microbial extracts which enhanced cell-surface MHC-I expression. From these extracts, it was found that the concanamycin and bafilomycin plecomacrolides were responsible for MHC-I rescue, with concanamycin A (**Figure 1.10C**) being the most potent. In Nef-expressing cells, concanamycin A rescued cell surface MHC-I, but not cell surface CD4, for a variety of group M Nef subtypes at picomolar to nanomolar concentrations and enhanced the elimination of HIV-1-infected CD4<sup>+</sup> T cells in an anti-HIV-1 CTL coculture assay. Studies into concanamycin A's mechanism of action suggested that concanamycin A was not functioning through its conventional biological mechanism, by inhibiting the V-ATPase to result in reduced lysosomal acidification<sup>135</sup>, since the concentrations required for MHC-I rescue were lower than at those where lysosomal acidification and degradation were affected. Instead, concanamycin A was found to reduce formation of the Nef:MHC-I:AP-1 complex implicated in mistrafficking intracellular MHC-I. However, concanamycin A did not bind any components of the Nef:MHC-I:AP-1 complex, nor did it limit MHC-I binding to AP-1 or Nef *in vitro*. Thus, concanamycin A may inhibit an

alternative factor at or upstream of Nef:MHC-I:AP-1 complex assembly, for example the Nef:SFK:ZAP-70/Syk:PI3K multi-kinase complex.

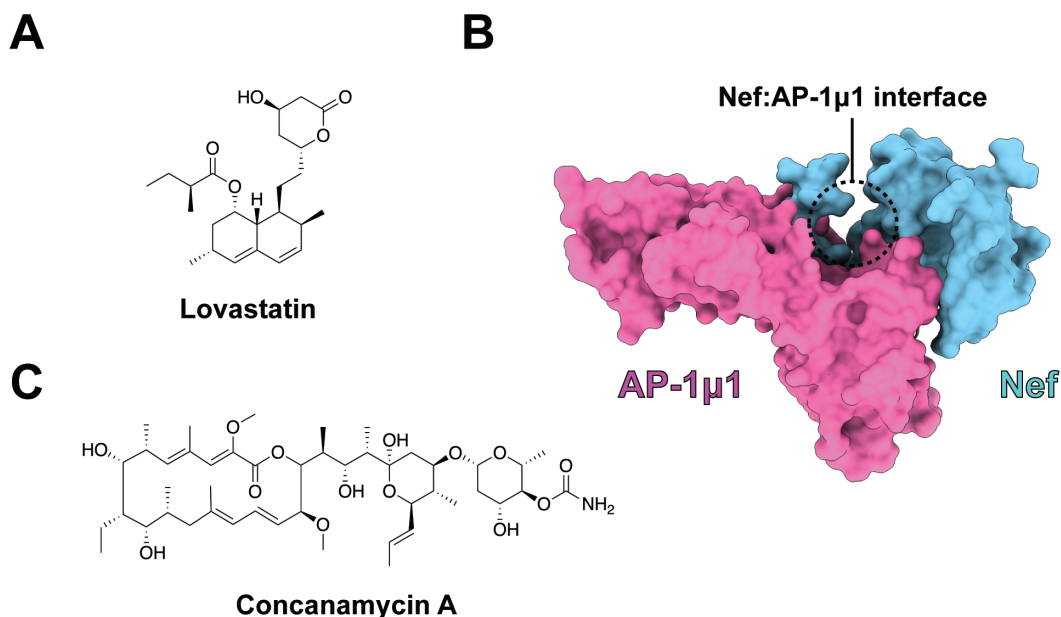


**Figure 1.10 Overview of alternative small molecule inhibitors of Nef-mediated MHC-I downregulation.** **A)** Structural representation of lovastatin in the closed ring form. **B)** Overview of the interaction between Nef (blue) and the AP-1 $\mu$ 1 subunit (pink) with the proposed binding pocket for lovastatin at the Nef:AP-1 $\mu$ 1 interface highlighted. Visualization was conducted with UCSF ChimeraX<sup>132</sup> using the X-ray crystal structure of NL4-3 Nef in complex with AP-1 $\mu$ 1 and the major histocompatibility complex class I (MHC-I) cytoplasmic domain (PDB: 4EMZ)<sup>136</sup>. **C)** Structural representation of concanamycin A.

### 1.5.3 Small molecule inhibitors of additional Nef functions

Among the earliest screens conducted for Nef inhibitors, a competition enzyme-linked immunosorbent assay (ELISA) was used to test the capacity for guanidine alkaloids to inhibit the interactions between phage-displayed Nef and p53, actin, and Lck<sup>119</sup>. Through

this approach, three guanidine alkaloid analogues from the batzelladine and crambescidin families, referred to as compounds 14, 17, and 22 (**Figure 1.11**), were identified which potently inhibited each tested Nef interaction at micromolar concentrations. However, further studies to test these compounds in cell culture were stifled due to their high toxicities.

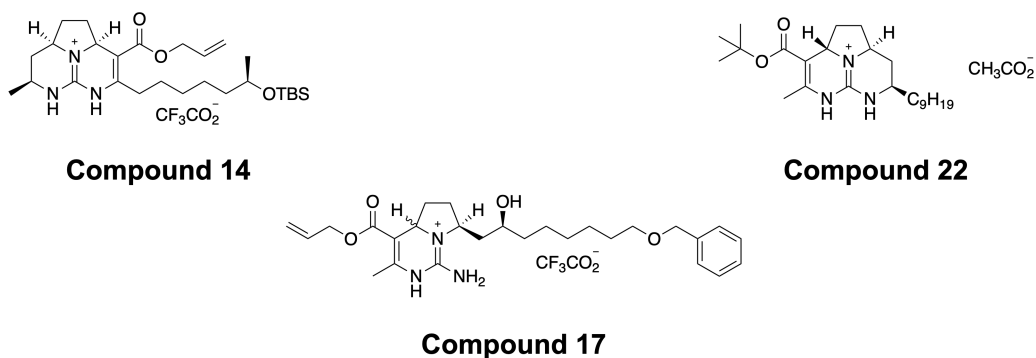


**Figure 1.11 Structural representations of the guanidine alkaloid analogues, compounds 14, 17, and 22.**

In a different vein, Bukrinsky and coworkers have focused on identifying inhibitors of Nef-mediated impairments to cholesterol efflux, a target which may find applications in treating chronic conditions associated with HIV-1 infection. Accumulating evidence suggests Nef to be in part responsible for the high risk of dyslipidemia and atherosclerosis seen among PLWH<sup>137</sup>. This is thought to be a consequence of Nef-mediated cholesterol efflux dysregulation established by its inhibition of the cholesterol efflux regulatory protein, ABCA1<sup>138</sup>. Importantly, the authors identified that one mechanism of Nef-mediated ABCA1 inhibition depends on Nef's interaction with the chaperone protein, calnexin<sup>139</sup>. By applying a virtual docking screen of over 130,000 compounds to a model of the Nef:calnexin interaction, the authors identified the small molecule, NSC13987 (also referred to as ZINC03953858 in later reports) (**Figure 1.12**), which blocked the Nef:calnexin interaction and Nef-mediated inhibition of cholesterol efflux with



micromolar potency, in addition to reducing viral replication in cell culture<sup>120</sup>. In a follow-up study, virtual docking was carried out on a refined model of the Nef:calnexin interaction to identify the NSC13987 analogue, AMS-55 (**Figure 1.12**), which rescued ABCA1 levels with micromolar potency and is purported to maintain improved solubility compared to NSC13987<sup>121</sup>. Docking screens have also been used to identify potential inhibitors of the interaction between Nef and ABCA1; however, these have not yet been tested outside of a virtual context<sup>140</sup>.

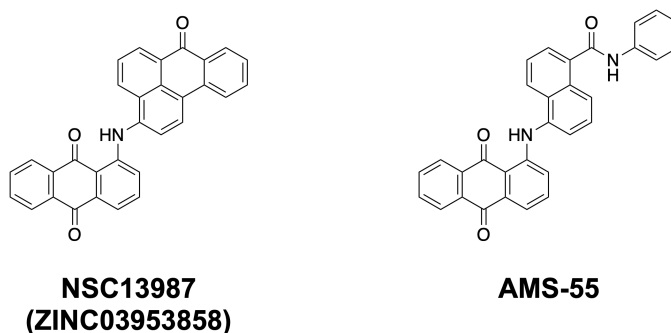


**Figure 1.12 Structural representations of NSC13987 and its analogue, AMS-55.**

Finally, the nucleoside analogue, tricyridine, has been noted to inhibit HIV-1 replication in cell culture, but this is not linked to inhibition of the HIV-1 reverse transcriptase, integrase or protease enzymes<sup>122,141</sup>. Instead, a follow-up study reported that resistance mutations to tricyridine primarily localized to the *nef* gene, implicating Nef in tricyridine's mechanism of action<sup>122</sup>. However, tricyridine binding to Nef was not tested, and it is more likely that tricyridine mediates its antiviral effects by inhibiting Akt kinase activity, as was previously shown in cancer cells<sup>142</sup>. Indeed, as Nef has been reported to activate Akt<sup>143,144</sup>, resistance mutations may accumulate in Nef to compensate for tricyridine's inhibitory effects on Akt, although this remains to be experimentally tested.

#### 1.5.4 Peptide and protein inhibitors of Nef

Several peptide and protein inhibitors of Nef have also been reported. Although such inhibitors are inherently limited for therapeutic application, they represent highly specific and potent tools for studying Nef's functions in cell culture and *in vivo*. Indeed, a variety of engineered peptides and SH3 domains have been developed and applied to study the Nef:SH3 interaction and the roles it plays in HIV-1 infection<sup>116,145-148</sup>. More excitingly, a series of antibody and fusion protein inhibitors of Nef have also been reported. Firstly, an  $\alpha$ -Nef camelid single-domain antibody, sdAb19, was developed which bound Nef with nanomolar potency and inhibited Nef-mediated CD4 downregulation for Nef alleles across M, N, O, and P groups, but which did not relieve MHC-I downregulation<sup>123</sup>. Nef-mediated enhancements to HIV-1 replication and infectivity in cell culture were also inhibited by sdAb19, as was the Nef:PAK2 interaction, reversing downstream effects on actin remodeling. Finally, in a mouse model expressing the Nef transgene, sdAb19 reversed Nef-induced defects to CD4<sup>+</sup> T cell maturation and activation. Concomitantly, a novel Nef inhibition approach was described whereby a series of Nef interacting proteins, namely engineered versions of the Hck SH3 domain and the CD4 cytoplasmic tail, were fused together to "wrap Nef" and block its activity<sup>125</sup>. These fusion proteins bound Nef with low- to high-nanomolar affinities and inhibited Nef-mediated downregulation of cell-surface CD4, MHC-I, and CCR5, as well as Nef-mediated infectivity enhancement in cell culture.

Combining the two strategies mentioned above identified Neffins, fusion proteins of sdAb19 and engineered high-affinity Hck SH3 domains<sup>126,127</sup>. Neffins were found to bind Nef remarkably well, with picomolar to low nanomolar affinities, as well as inhibiting a variety of Nef functions, including its interaction and activation of Hck, Nef-mediated CD4 and MHC-I downregulation, Lck relocalization, and infectivity enhancement in cell culture. Neffins also interfered with a variety of Nef-induced macrophage phenotypes, including phagocytosis defects, cell fusion induction, and podocyte rosette formation. A structural basis for Neffin action was later elucidated which identified the engineered Hck SH3 domain to bind Nef conventionally, engaging the Nef polyproline motif and RT loop binding pocket, whereas sdAb19 bound to a C-terminal Nef surface opposite of the SH3 binding surface<sup>124</sup>. Interestingly, *in vitro* experiments observed Neffin binding to form a

quaternary 2:2 Nef:Neffin complex, which may reflect an unanticipated intracellular binding mechanism for Neffins.

The interaction between Nef and sdAb19 has also been leveraged for small molecule inhibitor screening, where a homogenous time-resolved fluorescence assay was adapted to screen the library of pharmacologically active compounds (LOPAC) for inhibitors of the Nef:sdAb19 interaction<sup>149</sup>. This *in vitro* approach identified eight diverse compounds which inhibited the Nef:sdAb19 interaction and bound Nef; however, these compounds were not validated or assessed further. A similar time-resolved fluorescence energy transfer assay was applied in a pilot screen of the LOPAC library for inhibitors of the Nef:Hck-SH3 interaction, although hits were also not validated or tested further<sup>150</sup>.

## 1.6 Goals of this thesis

Following nearly twenty years of effort, there is still no ideal Nef inhibitor that exhibits favourable potency, specificity, toxicity, and pharmacokinetic properties. Although inhibition of Nef-mediated MHC-I downregulation has been a foremost goal in Nef inhibitor development, only a handful of scaffolds have been validated for use as tool compounds, and none have yet been tested *in vivo*. The central goal of this research is to develop a potent small molecule inhibitor of Nef-mediated MHC-I downregulation which can be applied *in vivo* to study the utility of this inhibitory approach towards an immune-directed HIV-1 cure.

Previous studies have elucidated two distinct pathways for Nef-mediated MHC-I downregulation, termed the signaling and stoichiometric modes (see Section 1.3)<sup>33,70</sup>. However, it is important to note that the signaling and stoichiometric modes are not mutually exclusive. In fact, it has been identified that the signaling mode predominates early in infection, while the stoichiometric mode predominates late in infection, suggesting a temporal link of regulation between the two modes<sup>70</sup>. More importantly, studies with the Nef:SFK interaction inhibitor, 2c, have identified that pharmacological blockade of the signaling mode also blocks onset of the stoichiometric mode<sup>70</sup>. Taken together, this

suggests that the Nef:SFK interaction is essential for initiating both modes of Nef-mediated MHC-I downregulation, and thus underscores the Nef:SFK interaction as an ideal target for inhibition, as opposed to inhibition of Nef's interactions with MHC-I or the adaptor protein complexes, which would only block the stoichiometric mode.

In pursuit of a Nef:SFK interaction inhibitor suitable for *in vivo* study, our group conducted an *in silico* docking screen for small molecule binders of Nef, identifying a dipeptide derivative (H3-1, **Figure 1.13**) as a candidate lead (unpublished data). Subsequent cell culture studies characterized the ability of H3-1 to inhibit the Nef:SFK interaction *in vitro* and to rescue cell surface MHC-I in HIV-1-infected cells in cell culture with micromolar potencies. However, preliminary pharmacokinetic studies in mice established H3-1 to be highly unstable *in vivo*, with an inability to detect the presence of H3-1 in mouse plasma within 60 minutes post-administration. Taken together, these preliminary studies demonstrated that H3-1 is a promising Nef:SFK inhibitor lead compound, but one which is unstable *in vivo* and is thus unsuitable for therapeutic application.

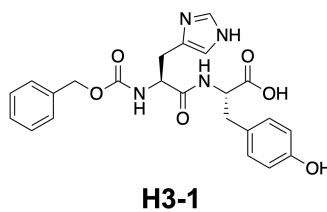


**Figure 1.13 Structural representation of H3-1.**

In light of H3-1's susceptibility to rapid clearance, we aimed to identify an improved *in vivo* stable Nef:SFK inhibitor. For our approach, we decided to use H3-1 as a chemical starting point to synthesize analogues which should maintain enhanced *in vivo* stabilities. Importantly, H3-1 is a dipeptide derivative, and more specifically, a histidyl-tyrosine dipeptide which maintains an N-terminal *N*<sup>α</sup>-benzyloxycarbonyl (*Z*) capping group. Peptide inhibitors such as H3-1 are well appreciated in medicinal chemistry as starting scaffolds owing to their generally favourable properties of low cytotoxicity, high

specificity, and the existence of robust protocols for their production<sup>151,152</sup>. However, translation of a peptide from an investigational agent towards a therapeutic often requires extensive modifications to the peptide's structure, usually due to issues with membrane permeability, oral bioavailability, and/or *in vivo* stability<sup>151,152</sup>. Indeed, rapid clearance is a common phenomenon observed with peptide inhibitors, which is primarily attributed to their susceptibility towards proteolysis<sup>153</sup>. Thus, considering these general properties of peptides, we hypothesized that H3-1's rapid clearance *in vivo* is a result of its proteolysis.

To test this hypothesis and to develop improved *in vivo* stable Nef:SFK inhibitors derived from H3-1, we used organic synthesis to generate a panel of peptidomimetic H3-1 analogues incorporating carboxyl and amide replacing groups. Detailed reporting on the methodologies for these syntheses and their associated chemical characterization studies is described in Chapter 2. A rationale for and summary of these synthetic efforts is provided in Chapter 3. Finally, Chapter 4 provides a discussion about the identified compounds and areas for future study which will be required to identify a potent Nef:SFK inhibitor for *in vivo* study.

## Chapter 2

### 2 Experimental procedures

#### 2.1 General

##### 2.1.1 Synthetic materials and methods

All common reagents and solvents were obtained from commercial sources, were of American Chemical Society (ACS) reagent grade or higher, and were used without further purification unless otherwise noted. For high-performance liquid chromatography (HPLC) and reaction solvents, peptide grade DMF was obtained from Caledon Laboratories (Georgetown, ON, Canada), Optima grade MeOH and MeCN were obtained from Fisher Chemical/Thermo Fisher Scientific (Waltham, MA, U.S.A.), HPLC grade DCM was obtained from Sigma-Aldrich/MilliporeSigma (Burlington, MA, U.S.A.), and anhydrous THF and dioxane were each prepared by passing through a column of activated alumina. Milli-Q-filtered water (18.2 M $\Omega$ •cm) (MilliporeSigma) was used in HPLC studies and to prepare all aqueous solutions. Amino acid monomers *N*<sup>α</sup>-benzyloxycarbonyl-*L*-histidine (*Z-L*-His-OH) and *L*-tyrosine methyl ester (*L*-Tyr-OMe) were obtained from AK Scientific (Union City, CA, U.S.A.), and *N*<sup>α</sup>-benzyloxycarbonyl-*D*-histidine (*Z-D*-His-OH) was obtained from TCI America (Portland, OR, U.S.A.).

All reactions were conducted in oven-dried glassware using Teflon-coated magnetic stir bars. Reactions performed at elevated temperatures were heated using a temperature-controlled oil bath, with temperatures measured externally using a mercury-in-glass thermometer. Unless otherwise noted, solvent was removed at reduced pressures using a rotary evaporator with a water bath temperature not exceeding 70 °C. Reactions were monitored using thin layer chromatography (TLC), which was performed on SiliCycle (Quebec City, QC, Canada) SiliaPlate aluminum-backed 200  $\mu$ m silica gel F254 TLC plates. TLC plates were visualized using ultraviolet illumination ( $\lambda = 254$  nm) and/or staining with 10% (w/v) phosphomolybdic acid (PMA) solution in anhydrous EtOH. Flash column chromatography was performed with SiliCycle SiliaFlash F60 40-63  $\mu$ m 230 – 400 mesh irregular silica gel.

### 2.1.2 Nuclear magnetic resonance

Nuclear magnetic resonance (NMR) spectra were collected at 25 °C on a Bruker (Billerica, MA, U.S.A.) Avance III HD 400 equipped with an H/FX Bruker SmartProbe or a Bruker Ascend 600 equipped with an H-FX 5 mm liquids probe. Deuterated solvents were purchased from Cambridge Isotope Laboratories (Tewksbury, MA, U.S.A.) or Sigma-Aldrich/MilliporeSigma. Chemical shifts ( $\delta$ ) are reported in parts per million (ppm) from tetramethylsilane (0 ppm) and are referenced to the residual solvent signal: DMSO- $d_6$  (2.50 ppm) or MeOH- $d_4$  (3.31 ppm) for  $^1\text{H}$  NMR, and DMSO- $d_6$  ( $\delta = 39.5$  ppm) for  $^{13}\text{C}$  NMR.  $^{19}\text{F}$  NMR spectra are presented uncorrected. Multiplicities are described as s (singlet), d (doublet), m (multiplet), and br s (broad singlet). Coupling constants ( $J$ ) are reported in hertz (Hz). Exchangeable protons are denoted as ex (exchangeable) and were qualitatively determined by acquiring spectra following the addition of  $\text{D}_2\text{O}$  to a sample dissolved in DMSO- $d_6$  and/or acquiring spectra in MeOH- $d_4$ . Spectral analysis was conducted using MestReNova software (version 12.0.03; Mestrelab Research, Santiago De Compostela, Galicia, Spain). Diastereomeric ratios (dr) were quantified by deconvolution of the peaks of interest.

### 2.1.3 Mass spectrometry

High-resolution mass spectra (HRMS) were collected on a Bruker micrOTOF II using electrospray ionization (ESI) with a time-of-flight (TOF) mass analyzer. Samples were dissolved in a suitable solvent (MeOH or 1:1 (v/v) MeOH and water) and introduced by direct infusion using a syringe pump. Spectral analysis was conducted using Bruker DataAnalysis (version 4.2.383.1). Reported values are in  $m/z$ . Inductively coupled plasma mass spectra (ICP-MS) were acquired and analyzed by the Biotron Analytical Services Laboratory (University of Western Ontario, London, Ontario, Canada).

#### 2.1.4 High-performance liquid chromatography

Analytical reversed-phase HPLC (RP-HPLC) spectra were obtained using a Varian/Agilent (Santa Clara, CA, U.S.A.) Microsorb-MV 100-5 C18 column (250 mm × 4.6 mm, 5 μm), Waters (Milford, MA, U.S.A.) Delta 600 pump, Waters 600 controller, Waters prep degasser, and a Waters 2996 photodiode array. Two mobile phases were used, 0.1% trifluoroacetic acid (TFA) in water (A) and 0.1% TFA in MeCN (B). For RP-HPLC, compounds were dissolved in A for injection and eluted at a flow rate of 1 mL per minute at room temperature using a gradient from 100% A to 100% B over 30 minutes, followed by a 10-minute hold of 100% B. The column was then washed with a 10-minute hold of 100% A and equilibrated for 15 minutes prior to the next injection. Chromatogram acquisition and analysis was conducted using Waters Empower (build number 1154), monitoring at a range of wavelengths ( $\lambda = 210 - 395$  nm).

## 2.2 Synthesis of Z-L-histidyl-L-tyrosine methyl ester (H3-1 methyl ester, H3-1M)

To a flask charged with EDC•HCl (3.84 g, 20.0 mmol, 1.0 eq), 120 mL of a 1:1 (v/v) solution of DCM and DMF was added at room temperature under a nitrogenous atmosphere. The mixture was stirred vigorously until dissolution (approximately 30 minutes), after which it was cooled to 0 °C. Immediately upon reaching 0 °C, Z-L-His-OH (5.79 g, 20.0 mmol, 1.0 eq) and Oxyma Pure (ethyl cyanohydroxyiminoacetate) (2.84 g, 20.0 mmol, 1.0 eq) were added to the flask. After two minutes, L-Tyr-OMe (3.90 g, 20.0 mmol, 1.0 eq) and DIPEA (3.50 mL, 20.1 mmol, 1.0 eq) were added. The reaction mixture was stirred at 0 °C for one hour, after which it was allowed to warm to room temperature and stirred overnight (approximately 22 hours). The reaction mixture was then evaporated to dryness to yield a crude oil (22 g) which was adsorbed onto silica gel (48 g) and purified by flash column chromatography, eluting over a gradient of 3 – 10% (v/v) MeOH in DCM. The resulting solids (7.10 g) were then dissolved in boiling MeCN (25 mL) and EtOAc (75 mL), the solution was cooled slightly, and ethyl ether was added gradually until the cloud point (30 mL). The solution was made clear again with gentle warming and dropwise



addition of MeCN and EtOAc, after which it was allowed to stand at 4 °C overnight. The precipitate was then collected by vacuum filtration and washed with cold EtOAc (100 mL) to yield H3-1M as a white powder (5.44 g, 11.7 mmol, 58%).

$^1\text{H}$  NMR (600 MHz, DMSO- $d_6$ )<sup>a</sup>:  $\delta$  11.80 (br s, 1H, ex), 9.24 (s, 1H, ex), 8.25 (d,  $J$  = 7.5 Hz, 1H, ex), 7.54 (s, 1H), 7.40–7.30 (m, 6H, 1H ex<sup>b</sup>), 6.98 (d,  $J$  = 8.3 Hz, 2H), 6.76 (s, 1H), 6.66 (d,  $J$  = 8.2 Hz, 2H), 5.01–4.96 (m, 2H), 4.40–4.37 (m, 1H), 4.29–4.25 (m, 1H), 3.57 (s, 3H)<sup>c</sup>, 2.90–2.70 (m, 4H).

$^{13}\text{C}\{^1\text{H}\}$  NMR (151 MHz, DMSO- $d_6$ )<sup>a,d</sup>:  $\delta$  171.9, 171.5, 156.0, 155.7, 137.0, 134.6, 130.1, 128.3, 127.8, 127.6, 127.0, 115.1, 65.4, 54.5, 53.9, 51.8, 35.9, 29.6.

HRMS (ESI-TOF): calculated for  $\text{C}_{24}\text{H}_{27}\text{N}_4\text{O}_6^+$  [ $\text{M} + \text{H}$ ]<sup>+</sup>, 467.1925; found, 467.1919.

dr ( $L,L$  :  $D,L$ ): 98.1 : 1.9.

- a* Minor peaks consistent with rotamers were observed. In such cases, major and minor rotamers were integrated as one, while chemical shifts ( $\delta$ ), multiplicities, and coupling constants ( $J$ ) are reported only for the major rotamer.
- b* One of six protons was exchangeable due to signal overlap.
- c* A minor peak ( $\delta$  3.60) corresponding to the methyl ester protons of the  $D,L$  diastereomer was observed. Deconvolution at  $\delta$  3.51–3.63 permitted integration of  $\delta$  3.60 and 3.57 to quantify relative abundances of the  $D,L$  and  $L,L$  diastereomers, respectively (dr, see above). Additionally, deconvolution identified a third peak at  $\delta$  3.56, which we attribute to be a rotamer of the parent methyl ester proton peak ( $\delta$  3.57); however, for simplicity, we have excluded this peak in our calculations.
- d* Two carbon peaks were not observed, which we attribute to chemical exchange/dynamics, signal overlap, and/or long relaxation times.

## 2.3 Synthesis of Z-D-histidyl-L-tyrosine methyl ester (*D,L*-H3-1 methyl ester, *D,L*-H3-1M)

To a flask charged with EDC•HCl (384 mg, 2.0 mmol, 1.0 eq), 12 mL of a 1:1 (v/v) solution of DCM and DMF was added at room temperature under a nitrogenous atmosphere. The mixture was stirred vigorously until dissolution (approximately 30 minutes), after which it was cooled to 0 °C. Immediately upon reaching 0 °C, Z-*L*-His-OH (580 mg, 2.0 mmol, 1.0 eq) and Oxyma Pure (287 mg, 2.0 mmol, 1.0 eq.) were added to the flask. After two minutes, *L*-Tyr-OMe (393 mg, 2.0 mmol, 1.0 eq) and DIPEA (0.35 mL, 2.0 mmol, 1.0 eq) were added. The reaction mixture was stirred at 0 °C for one hour, after which it was allowed to warm to room temperature and stirred overnight (approximately 20 hours). The reaction mixture was then evaporated to dryness to yield a crude oil (2.5 g) which was adsorbed onto silica gel (6.0 g) and purified by flash column chromatography, eluting over a gradient of 3 – 10% (v/v) MeOH in DCM to yield *D,L*-H3-1M as a beige off-white powder (735 mg, 1.6 mmol, 79%).

<sup>1</sup>H NMR (600 MHz, DMSO-*d*<sub>6</sub>)<sup>a</sup>: δ 11.74 (br s, 1H, ex), 9.23 (s, 1H, ex), 8.23 (d, *J* = 7.9 Hz, 1H, ex), 7.52 (s, 1H), 7.36–7.30 (m, 6H, 1H ex<sup>b</sup>), 6.96 (d, *J* = 8.4 Hz, 2H), 6.64 (d, *J* = 8.5 Hz, 3H)<sup>c</sup>, 5.01–4.96 (m, 2H), 4.40–4.37 (m, 1H), 4.28–4.24 (m, 1H), 3.60 (s, 3H)<sup>d</sup>, 2.90–2.61 (m, 4H).

<sup>13</sup>C {<sup>1</sup>H} NMR (151 MHz, DMSO-*d*<sub>6</sub>)<sup>a,e</sup>: δ 171.9, 171.3, 156.0, 155.7, 137.0, 134.7, 130.1, 128.3, 127.8, 127.6, 127.0, 115.0, 65.4, 54.6, 53.7, 51.8, 36.1, 29.7.

HRMS (ESI-TOF): calculated for C<sub>24</sub>H<sub>27</sub>N<sub>4</sub>O<sub>6</sub><sup>+</sup> [M + H]<sup>+</sup>, 467.1925; found, 467.1929.

dr (*D,L* : *L,L*): 90.2 : 9.8.

*a* Minor peaks consistent with rotamers were observed. In such cases, major and minor rotamers were integrated as one, while chemical shifts (δ), multiplicities, and coupling constants (*J*) are reported only for the major rotamer.

- b* One of six protons was exchangeable due to signal overlap.
- c* The doublet exhibited severe asymmetry due to signal overlap.
- d* A minor peak ( $\delta$  3.57) corresponding to the methyl ester protons of the *L,L* diastereomer was observed. Deconvolution at  $\delta$  3.51–3.63 permitted integration of  $\delta$  3.60 and 3.57 to quantify relative abundances of the *D,L* and *L,L* diastereomers, respectively (dr, see above). Additionally, deconvolution identified a third peak at  $\delta$  3.55, which we attribute to be a rotamer of the parent methyl ester proton peak ( $\delta$  3.60); however, for simplicity, we have excluded this peak in our calculations.
- e* Two carbon peaks were not observed, which we attribute to chemical exchange/dynamics, signal overlap, and/or long relaxation times.

## 2.4 Synthesis of Z-*L*-histidyl-*L*-tyrosinamide (H3-1 C-terminal amide, H3-1A)

A 7 M solution of NH<sub>3</sub> in MeOH (15 mL) was added to a cooled flask (0 °C) charged with H3-1M (466 mg, 1.0 mmol, 1.0 eq). The flask was sealed, and the solution was stirred gently at room temperature for 48 hours. The solution was then concentrated to dryness using a stream of air and the resulting solids were triturated with EtOAc (50 mL) at room temperature for one hour, collected by vacuum filtration, and washed with additional EtOAc (100 mL) to yield an off-white powder (428 mg). The precipitate was then dissolved in boiling MeOH (30 mL) and decolorized with activated charcoal, stirring for 5 minutes. The solution was vacuum filtered over Celite and evaporated to dryness to yield H3-1A as a white powder (378 mg, 0.8 mmol, 84%).

<sup>1</sup>H NMR (600 MHz, DMSO-*d*<sub>6</sub>)<sup>a</sup>:  $\delta$  11.79 (s, 1H, ex), 9.15 (s, 1H, ex), 7.85 (d, *J* = 7.8 Hz, 1H, ex), 7.56 (s, 1H, ex), 7.51 (s, 1H), 7.38–7.29 (m, 6H, 1H ex<sup>b</sup>), 7.08 (s, 1H, ex), 6.98 (d, *J* = 8.2 Hz, 2H), 6.76 (s, 1H), 6.63 (d, *J* = 8.3 Hz, 2H), 5.03–4.96 (m, 2H), 4.34–4.31 (m, 1H), 4.21–4.17 (m, 1H), 2.92–2.70 (m, 4H).

$^{13}\text{C}\{^1\text{H}\}$  NMR (151 MHz, DMSO- $d_6$ )<sup>a,c</sup>:  $\delta$  172.9, 170.9, 155.8, 155.7, 136.9, 134.7, 130.1, 128.4, 127.82, 127.76, 127.6, 126.9, 114.9, 65.5, 55.0, 54.0, 36.7, 29.7.

HRMS (ESI-TOF): calculated for  $\text{C}_{23}\text{H}_{26}\text{N}_5\text{O}_5^+$   $[\text{M} + \text{H}]^+$ , 452.1928; found, 452.1928.

- a* Minor peaks consistent with rotamers were observed. In such cases, major and minor rotamers were integrated as one, while chemical shifts ( $\delta$ ), multiplicities, and coupling constants ( $J$ ) are reported only for the major rotamer.
- b* One of six protons was exchangeable due to signal overlap.
- c* One carbon peak was not observed, which we attribute to chemical exchange/dynamics, signal overlap, and/or long relaxation times.

## 2.5 Synthesis of Z-L-histidyl-L-tyrosine nitrile (H3-1 nitrile, H3-1N)

Under a nitrogenous atmosphere,  $\text{Et}_3\text{N}$  (0.56 mL, 4.0 mmol, 4.0 eq) was added to a stirred suspension of H3-1A (452 mg, 1.0 mmol, 1.0 eq) in THF (25 mL) at room temperature. The mixture was cooled to 0 °C, after which trifluoroacetic anhydride (TFAA) (0.49 mL, 3.5 mmol, 3.5 eq) was slowly added over five minutes. The resulting solution was stirred for one hour, after which it was quenched with 20 mL of water. To eliminate any trifluoroacetylated byproducts, the solution was basified with 1 M NaOH to pH 9 (as determined by universal pH paper) and stirred at room temperature for two hours. The solution was subsequently neutralized with 1 M HCl and concentrated to remove volatile organics. The resulting precipitate was collected by vacuum filtration and washed with cold water (200 mL) to yield H3-1N as a white powder (387 mg, 0.9 mmol, 89%).

$^1\text{H}$  NMR (600 MHz, DMSO- $d_6$ )<sup>a</sup>:  $\delta$  11.80 (s, 1H, ex), 9.34 (s, 1H, ex), 8.82 (d,  $J = 7.5$  Hz, 1H, ex), 7.54 (s, 1H), 7.48 (d,  $J = 7.8$  Hz, 1H, ex), 7.37–7.31 (m, 5H), 7.08 (d,  $J = 7.8$  Hz, 2H), 6.77 (s, 1H), 6.70 (d,  $J = 7.8$  Hz, 2H), 5.04–4.97 (m, 2H), 4.80–4.76 (m, 1H), 4.25–4.21 (m, 1H), 2.95–2.73 (m, 4H).

$^{13}\text{C}\{^1\text{H}\}$  NMR (151 MHz, DMSO- $d_6$ )<sup>a,b</sup>:  $\delta$  171.5, 156.5, 155.7, 136.9, 134.8, 130.4, 128.4, 127.8, 127.7, 127.0, 125.5, 119.0, 115.2, 65.5, 54.7, 42.2, 36.6, 29.5.

HRMS (ESI-TOF): calculated for  $\text{C}_{23}\text{H}_{23}\text{N}_5\text{NaO}_4^+$   $[\text{M} + \text{Na}]^+$ , 456.1642; found, 456.1639.

- a* Minor peaks consistent with rotamers were observed. In such cases, major and minor rotamers were integrated as one, while chemical shifts ( $\delta$ ), multiplicities, and coupling constants ( $J$ ) are reported only for the major rotamer.
- b* One carbon peak was not observed, which we attribute to chemical exchange/dynamics, signal overlap, and/or long relaxation times.

## 2.6 Synthesis of Z-L-histidyl-L-tyrosine tetrazole hydrochloride (H3-1 tetrazole HCl, H3-1T•HCl)

H3-1N (521 mg, 1.2 mmol, 1.0 eq),  $\text{NaN}_3$  (156 mg, 2.4 mmol, 2.0 eq), and  $\text{Et}_3\text{N}\cdot\text{HCl}$  (496 mg, 3.6 mmol, 3.0 eq) were stirred in dioxane (10 mL) under a nitrogenous atmosphere and heated to 80 °C for 24 hours. The reaction mixture was then diluted with water, acidified with 1 M HCl to pH 2 (as determined by pH indicator paper), and evaporated to dryness. To remove any residual azide, the solution was resuspended in water, adjusted to pH 2, and evaporated again to dryness, after which this step was repeated once more. To precipitate H3-1T•HCl, the resulting solids were stirred with 1 M HCl (50 mL) at 0 °C for 30 minutes, vacuum filtered, and washed with cold 1 M HCl (25 mL), room temperature EtOAc (30 mL), and room temperature ethyl ether (30 mL). To remove residual  $\text{Et}_3\text{N}\cdot\text{HCl}$ , the collected precipitate was dissolved in 15 mL of water adjusted to pH 2, cooled to 0 °C, and 15 mL of 2 M HCl was added, stirring at 0 °C for 30 minutes. The resulting precipitate was vacuum filtered and washed with cold 1 M HCl (75 mL) and room temperature methyl ethyl ketone (MEK) (30 mL) to yield H3-1T•HCl as a white powder (233 mg, 0.5 mmol, 38%).

$^1\text{H}$  NMR (600 MHz, DMSO- $d_6$ )<sup>a</sup>:  $\delta$  14.32 (br s, 1–2H, ex), 9.27 (s, 1H, ex), 8.96 (s, 1H), 8.84 (d,  $J = 7.3$  Hz, 1H, ex<sup>b</sup>), 7.59 (d,  $J = 8.5$  Hz, 1H, ex), 7.38–7.23 (m, 6H), 6.95 (d,  $J = 7.8$  Hz, 2H), 6.62 (d,  $J = 7.7$  Hz, 2H), 5.28–5.24 (m, 1H), 5.04–4.97 (m, 2H), 4.42–4.39 (m, 1H), 3.15–2.85 (m, 4H).

$^{13}\text{C}\{^1\text{H}\}$  NMR (151 MHz, DMSO- $d_6$ )<sup>a,c</sup>:  $\delta$  170.2, 156.1, 155.8, 136.8, 133.6, 130.1, 129.5, 128.4, 127.8, 127.6, 126.7, 116.6, 115.1, 65.6, 53.6, 46.2, 38.0, 26.9.

HRMS (ESI-TOF): calculated for  $\text{C}_{23}\text{H}_{25}\text{N}_8\text{O}_4^+$  [ $\text{M} + \text{H}$ ]<sup>+</sup>, 477.1993; found, 477.2006.

- a* Minor peaks consistent with rotamers were observed. In such cases, major and minor rotamers were integrated as one, while chemical shifts ( $\delta$ ), multiplicities, and coupling constants ( $J$ ) are reported only for the major rotamer.
- b* Upon the addition of  $\text{D}_2\text{O}$ , the peak was not appreciably reduced; however, the peak was not observed in a  $^1\text{H}$  NMR spectrum obtained in MeOH- $d_4$ .
- c* One carbon peak was not observed, which we attribute to chemical exchange/dynamics, signal overlap, and/or long relaxation times.

## Chapter 3

### 3 Synthesis and characterization of H3-1 analogues

#### 3.1 Design of H3-1 analogues

Structurally, H3-1 is a modified dipeptide consisting of *L*-histidine (*L*-His) as the N-terminal residue and *L*-tyrosine (*L*-Tyr) as the C-terminal residue, as well as incorporating an N-terminal cap, the *N*<sup>α</sup>-benzyloxycarbonyl group (Z) (**Figure 3.1**). Peptide inhibitors such as H3-1 are well-known for generally maintaining favourable attributes, such as high specificity, high potency, and low toxicity; however, they can be difficult to translate into therapeutic agents primarily owing to their propensity for rapid elimination by proteolysis<sup>151–153</sup>. Thus, considering H3-1's peptidic structure and the minute time-scale half-life observed in mouse experiments, we hypothesized that proteolysis was the primary mechanism for its elimination *in vivo*.

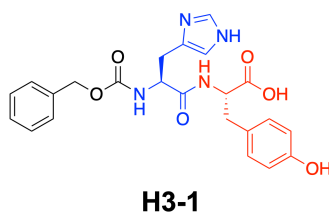


**Figure 3.1 Structural representation of H3-1.** The N-terminal *N*<sup>α</sup>-benzyloxycarbonyl group (Z) is coloured black, the *L*-histidine residue is coloured blue, and the *L*-tyrosine residue is coloured red.

To improve the pharmacological properties of a peptide, medicinal chemists often employ a synthetic strategy known as peptidomimetics<sup>154,155</sup>. In this approach, the peptide is structurally modified to generate closely related derivatives which should exhibit improved properties, such as reduced proteolysis, while limiting any negative impacts to target affinity or specificity. Frequently used modifications for developing proteolytically stable peptidomimetics include the addition of N-terminal and C-terminal capping groups,

modifications to the peptide backbone, substitution of natural *L* amino acids for synthetic ones or their *D* isomers, as well as more global alterations such as peptide stapling or cyclization. In fact, usually one approach is not sufficient, but a combination of the above strategies is required to stabilize the peptide against proteolysis, as well as to improve other properties such as potency, permeability, hepatic metabolism, and renal excretion.

In selecting which peptidomimetic modifications to pursue for generating H3-1 analogues, it is important to consider several restricting factors. First, we do not yet have a structural or pharmacophoric model for H3-1 binding to its target. Additionally, considering the intrinsic flexibility of H3-1, and the intrinsically disordered and structurally heterogeneous nature of Nef, the proposed but unconfirmed binding target of H3-1, we decided not to inform our design approach with computational predictions of inhibitor binding. Thus, for feasibility, we only considered subtle structural modifications, as blindly introducing drastic changes to the H3-1 scaffold would be more likely to inhibit target binding. Second, as H3-1 is only a dipeptide derivative, we judged more global modification strategies, such as peptide stapling or cyclization, to be unsuitable, as these strategies are applied primarily in longer peptides. Lastly, it is important to point out the synthetically challenging scaffold that H3-1 presents. H3-1 maintains several reactive groups which can complicate syntheses, including the imidazole ring of histidine, the phenol ring of tyrosine, and the C-terminal carboxylic acid. Thus, for many synthetic transformations, these moieties would require the use of protecting groups, which can themselves provide challenges in installation and removal, or in ensuring that these protecting groups are not labile under reaction conditions or in purification procedures. H3-1 also maintains two chiral centers at the  $\alpha$  carbons of each amino acid residue which can be epimerized in many transformations. Finally, the high polarity of the H3-1 scaffold presents issues for organic solvent solubility, as well as barriers to compound isolation and purification procedures.

With these factors in mind, to synthesize peptidomimetic analogues of H3-1, we used a conservative design approach, focusing on producing synthetically feasible compounds with only local modifications to the parent scaffold. Specifically, we decided to modify H3-1's amide and carboxyl groups (**Figure 3.2A**; highlighted in blue and red, respectively), two sites which are frequently modified to generate peptidomimetics of improved



proteolytic stability<sup>154-156</sup>. Of note, we did not pursue modifications to H3-1's N-terminus, due to the presence of the N-terminal Z group. To replace H3-1's amide bond, we proposed to synthesize analogues incorporating the thioamide and methyleneamino groups (**Figure 3.2B**), and to replace H3-1's carboxyl group, we proposed to synthesize analogues incorporating the methyl ester, amide, nitrile, and tetrazole groups (**Figure 3.2C**).

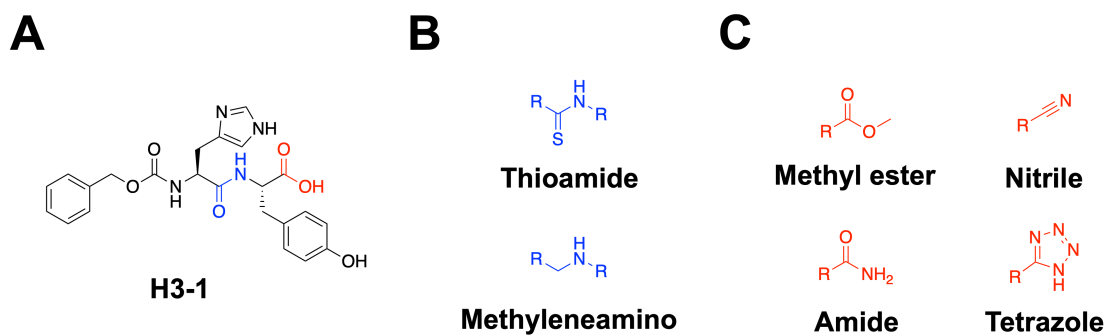


**Figure 3.2 Overview of H3-1 peptidomimetic design.** A) Structural representation of H3-1 with the amide bond highlighted in blue and the carboxyl group highlighted in red. B) Summary of proposed amide replacing groups. C) Summary of proposed carboxyl replacing groups.

### 3.1.1 The thioamide group

Thioamides (**Figure 3.2B**), with the simple substitution of an oxygen atom for a sulfur atom, are true amide isosteres<sup>157,158</sup>. Both amides and thioamides are planar, exhibit cis-trans isomerism, and have similar steric and electronic properties. Of note, the sulfur atom is significantly larger than the oxygen atom, the thioamide C=S bond is longer than the C=O bond (i.e. more single bond character), and the C-N bond is shorter in thioamides compared to amides (i.e. more double bond character)<sup>157-160</sup>. As well, thioamides are weaker hydrogen bond acceptors and stronger hydrogen bond donors<sup>161,162</sup>. Lastly, it is important to note that the C-N bond in thioamides maintains a greater energy barrier to rotation compared to amides<sup>163</sup>.

Many cases exist in the literature where thioamides have been applied to stabilize peptides against proteolysis<sup>164–170</sup>. Interestingly, incorporation of a thioamide only near a peptide's scissile bond has also been noted to be stabilizing<sup>170</sup>. Although still unclear, it has been purported that the higher barrier to rotation about the C–N bond in thioamides is the key driver for their reduced proteolysis; however, diminished proteolytic recognition has also been noted<sup>170–172</sup>. Yet, despite the promising nature of thioamides as minimal peptide stabilizing units, they are known to be more reactive compared to their amide counterparts<sup>173</sup>, leading to concerns of toxicity.

### 3.1.2 The methyleneamino group

The methyleneamino group (or, the reduced amide group) (**Figure 3.2B**) removes the carbonyl (C=O) component of the amide bond to eliminate its potential for hydrolysis by proteases. In fact, methyleneamino-containing peptidomimetics have been widely applied as transition state mimetics for developing inhibitors of proteases such as renin,  $\beta$ -secretase 1, and HIV-1 Protease<sup>174–177</sup>. On a physicochemical level, introduction of the methyleneamino group removes the planar and cis-trans character of the amide bond, imparting a greater degree of flexibility, as well as inducing a positive charge on the amine at physiological pH<sup>177</sup>. Thus, while introduction of a methyleneamino group is one of the most direct approaches to stabilize H3-1 against proteolysis, it is possibly the most drastic replacing group proposed, and may have severe impacts to target affinity and specificity.

### 3.1.3 The methyl ester group

In designing carboxyl replacing groups, the methyl ester group (**Figure 3.2C**) was selected primarily because the H3-1 methyl ester analogue can serve as a convenient starting material to generate all other H3-1 analogues (see Section 3.1.7). Indeed, esters are generally well known for being unstable *in vivo* due to their rapid hydrolysis. However, the methyl ester is still an interesting group for studying the structure-activity-relationship of H3-1-type inhibitors *in vitro*, as the methyl ester maintains altered electronic and steric

properties, being bulkier and of neutral charge. As well, by removing the negative charge of H3-1's carboxyl group, the methyl ester group may confer improved permeability properties. It is also tempting to speculate that the methyl ester analogue may serve as a pro-drug to H3-1, a strategy which can be exploited with other H3-1 analogues, such as the central amide replacing analogues, and developed further by testing other C-terminal esters<sup>178</sup>.

### 3.1.4 The C-terminal amide group

Replacement of a carboxylic acid with a C-terminal amide group (**Figure 3.2C**) is a popular modification in peptidomimetics, and has been reported to reduce proteolytic degradation<sup>156,179</sup>. Importantly, the C-terminal amide group removes the negative charge of the carboxyl without introducing significant bulkiness, and may thus also serve to improve permeability despite its highly polar character.

### 3.1.5 The nitrile group

Although a less conventional replacing group for conferring proteolytic stability, C-terminal nitriles (**Figure 3.2C**) can be found among reversible covalent peptidomimetic inhibitors<sup>180</sup>, most notably, the SARS-CoV-2 main protease (M<sup>Pro</sup>) inhibitor, nirmatrelvir (PF-07321332), the principal antiviral component of Paxlovid<sup>181</sup>. Of course, considering this propensity for nitrile inhibitors to be covalent inhibitors, alongside the possibility of their metabolism to cyanide, toxicity is a leading concern. Yet, many nitrile-containing pharmacological agents are approved for therapeutic uses, and not all nitrile-containing inhibitors are recognized to proceed by covalent inhibition, which merits their study as H3-1 analogues<sup>180</sup>. Indeed, the nitrile group is a highly condensed polarized group, and is suggestive of a carboxyl isostere. Finally, it is important to note that nitriles are useful starting materials for synthesizing tetrazoles (see Section 3.1.7).

### 3.1.6 The tetrazole group

The tetrazole group (**Figure 3.2C**) is a well-known isostere of the carboxyl group, with both groups being planar and maintaining similar  $pK_a$  values to result in their ionization at physiological pH<sup>182,183</sup>. Moreover, tetrazoles are purported to be metabolically robust, often not being subject to the same biotransformation reactions as their carboxyl counterparts, and sometimes even being excreted unchanged<sup>183–185</sup>. Of course, tetrazoles are also significantly bulkier, more lipophilic, and delocalize the negative charge along the ring, which together results in significantly altered steric and electronic properties. In line with these differences, C-terminal tetrazoles have been reported to confer improved proteolytic stability and permeability properties in peptidomimetics<sup>186,187</sup>.

### 3.1.7 General synthetic approach

For our initial studies on H3-1 peptidomimetics, we intended to synthesize at least one analogue for each replacing group. A general schematic for compound synthesis is outlined below (**Figure 3.3**). Briefly, H3-1 methyl ester (H3-1M) can be synthesized by coupling the monomers *Z*-*L*-His-OH and *L*-Tyr-OMe (**A**). Subsequently, H3-1M can be used as a starting material for producing the H3-1 C-terminal amide (H3-1A) (**B**) analogue, and which can in turn be used to generate the H3-1 nitrile (H3-1N) (**C**) and H3-1 tetrazole (H3-1T) (**D**) analogues. In parallel, H3-1M can also be used as a starting material for generating thioamide H3-1 methyl ester (TH3-1M) (**E**), and which can in turn be used to generate methyleneamino H3-1 methyl ester (MH3-1M) (**F**).

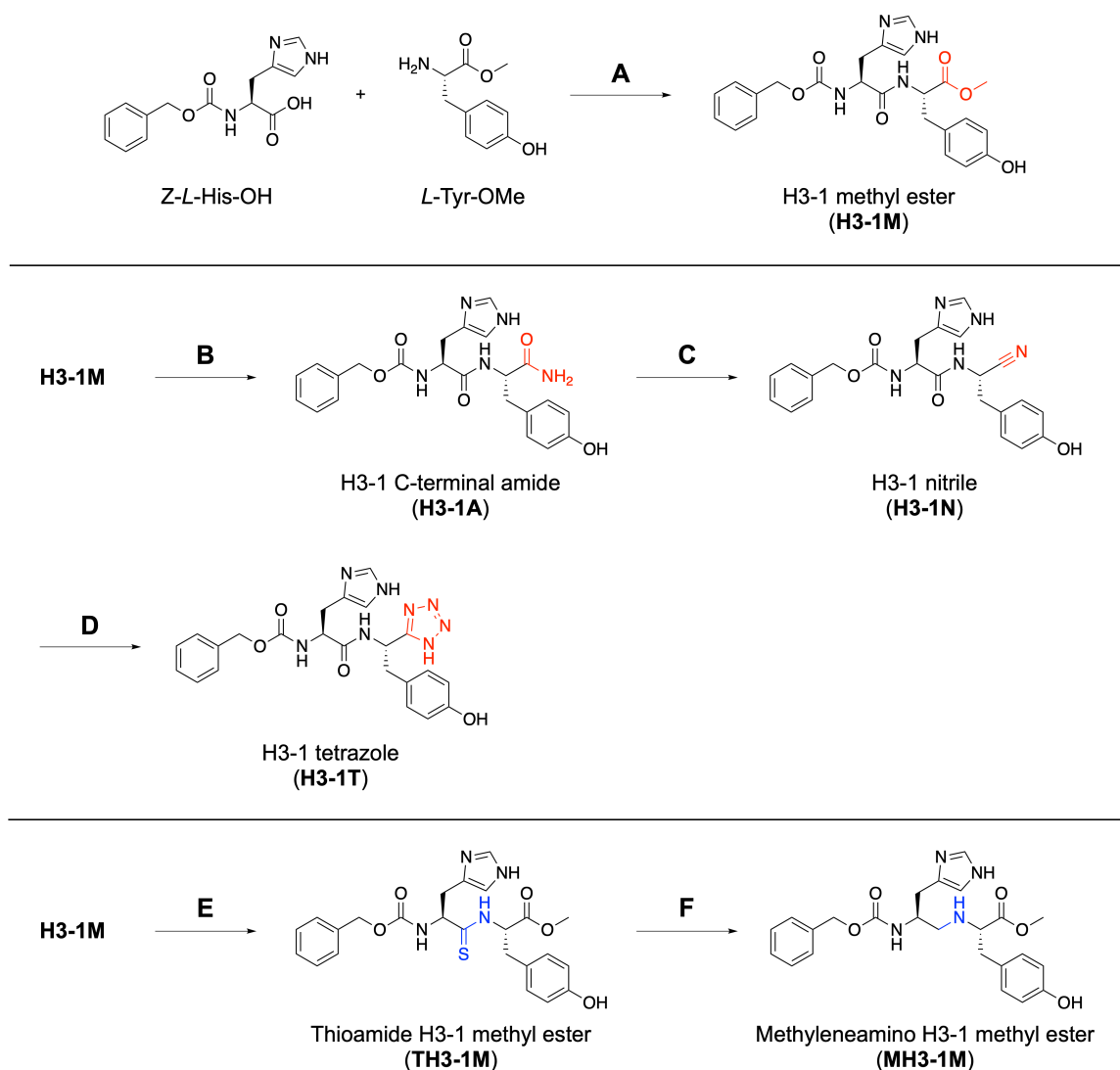


**Figure 3.3** Schematic of proposed chemical transformations for generating peptidomimetic analogues of H3-1.

### 3.2 Synthesis of H3-1 methyl ester (H3-1M)

To generate H3-1 methyl ester (H3-1M), we employed solution-phase peptide coupling to couple the amino acid monomers *Z*-L-His-OH and *L*-Tyr-OMe using a reagent combination of EDC•HCl, Oxyma Pure, and DIPEA in a solvent system of 1:1 DCM and DMF (**Figure 3.4**). These reagents and conditions were selected specifically as they have been demonstrated to produce dipeptides in good yields and with minimal side reactions

and risks for epimerization<sup>188,189</sup>. By allowing the reaction mixture to stir at room temperature overnight, followed by evaporation of the solvent, crude H3-1M could be isolated at 72 – 85% yields (7.93 – 10.12 g, 17.0 – 21.7 mmol) using flash column chromatography. Unfortunately, though we did attempt to implement an extractive work-up step prior to column chromatography, H3-1M was only weakly soluble in EtOAc, hence necessitating column chromatography of the entire reaction mixture.

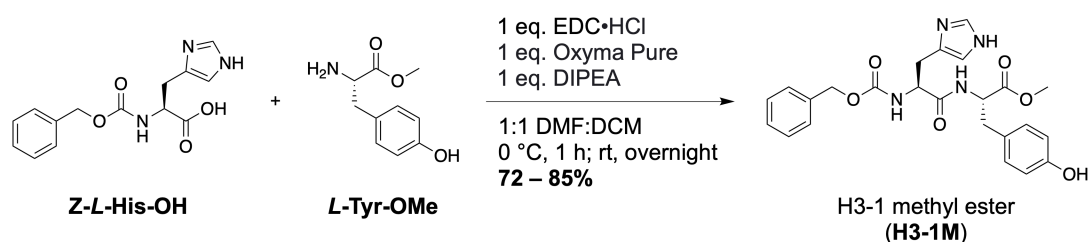


**Figure 3.4** Synthesis of crude H3-1M by solution-phase peptide coupling.

Importantly, a key limitation of synthetic peptide coupling is the potential for epimerization at the  $\alpha$  carbon of each amino acid. Although the conditions used were chosen specifically for their low epimerization potential, peptide couplings with histidine as the N-terminal residue are uniquely prone to epimerization. This is because the histidine imidazole group can act as an intramolecular base to deprotonate the  $\alpha$  carbon and drive enolization of the residue once the histidine active ester is formed (**Figure 3.5**). Epimerization is especially evident when the imidazole moiety is unprotected, as it is in our case, and thus we required a method to assess the isomeric purity of H3-1M by resolving and quantifying the relative abundances of its *L,L* and *D,L* diastereomers.

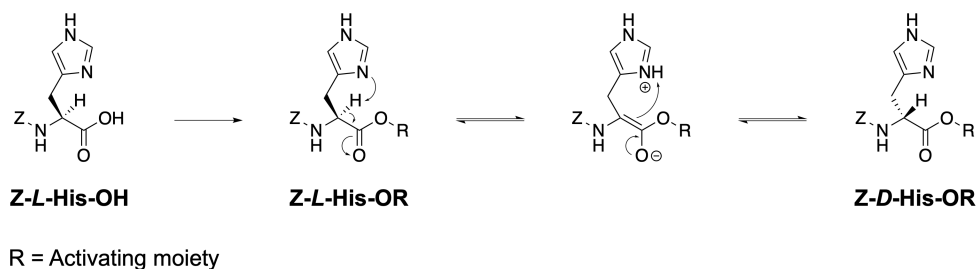


**Figure 3.5 Proposed mechanism for histidine-promoted epimerization during peptide coupling.**

To this end, we synthesized the *D,L* diastereomer of H3-1M (*D,L*-H3-1M) at a 79% yield (735 mg, 1.6 mmol) by using the approach outlined above, but substituting *Z-L*-His-OH with *Z-D*-His-OH (Figure 3.6). While we were unable to separate *L,L*- and *D,L*-H3-1M by RP-HPLC (Figure 3.7A), we identified that the two diastereomers exhibited a  $^1\text{H}$  NMR chemical shift inequivalence for the peak corresponding to the C-terminal methyl ester protons ( $\delta_{L,L} = 3.57$  ppm,  $\delta_{D,L} = 3.60$  ppm), and which therefore enables quantification of their relative abundances (Figure 3.7B). A similar methyl ester  $^1\text{H}$  NMR peak inequivalence has also been identified for dipeptides incorporating the phenylglycine residue<sup>190,191</sup>. By deconvolving the two peaks, we identified that H3-1M obtained directly following column chromatography maintains approximately ~10% of the *D,L* isomer.

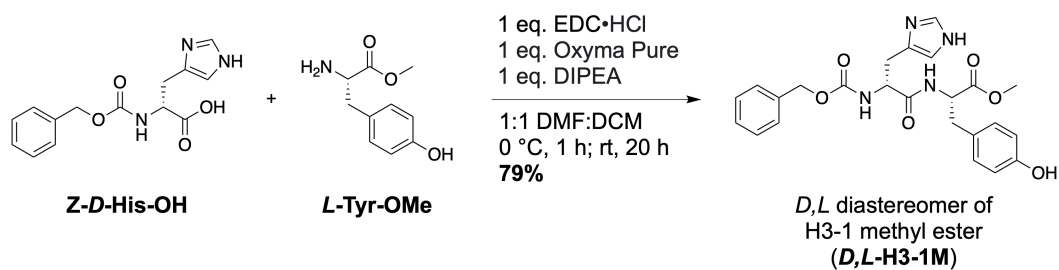


**Figure 3.6 Synthesis of *D,L*-H3-1M by solution-phase peptide coupling.**

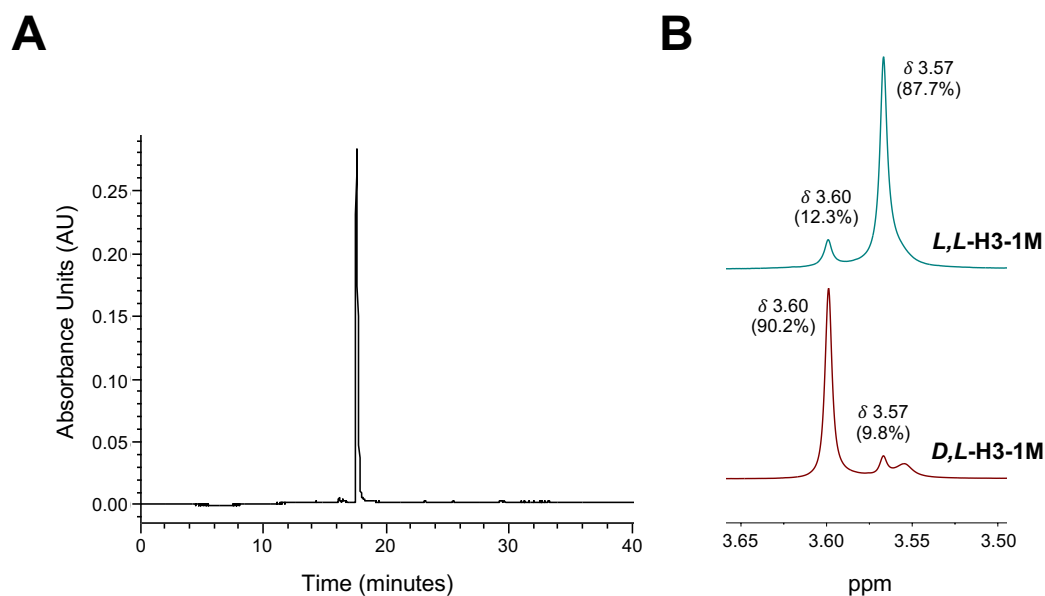


**Figure 3.7**  $^1\text{H}$  NMR permits quantification of *L,L* and *D,L* diastereomer abundances in H3-1M. **A**) Partial RP-HPLC chromatogram ( $\lambda = 275$  nm) of a 1:1 mixture of *L,L*- and *D,L*-H3-1M, indicating an inability to separate the two diastereomers. The presented chromatogram is representative of three independent injections ( $N = 3$ ). **B**) Partial  $^1\text{H}$  NMR spectra for crude *L,L*-H3-1M (top) and *D,L*-H3-1M (bottom) in  $\text{DMSO-}d_6$ , highlighting the methyl ester  $^1\text{H}$  NMR chemical shift inequivalence ( $\delta_{L,L} = 3.57$  ppm,  $\delta_{D,L} = 3.60$  ppm).

In order to reduce the abundance of the contaminating *D,L* diastereomer, we developed an additional purification step, whereby H3-1M was reprecipitated from a solvent mixture of MeCN, EtOAc, and ethyl ether. On smaller scales, this step was able to consistently reduce the presence of the *D,L* diastereomer to just 1 – 2%, with approximately 50 – 60% recovery.

With the above methodologies in place, we synthesized H3-1M on a multi-gram scale at an overall 58% yield (5.44 g, 11.7 mmol) (**Figure 3.8**).  $^1\text{H}$  and  $^{13}\text{C}\{^1\text{H}\}$  NMR studies demonstrated the product to be of consistent identity with H3-1M, and which was further supported with HRMS ( $[\text{M} + \text{H}]^+_{\text{calc}} = 467.1925$ ,  $[\text{M} + \text{H}]^+_{\text{obs}} = 467.1919$ ) (**Appendices 2 – 5**). Finally, purity assessment by RP-HPLC (monitoring at wavelengths  $\lambda = 220$  and 275



nm) identified the material to be homogenous (**Appendix 6**) and  $^1\text{H}$  NMR studies quantified an abundance of 1.9% for the *D,L* diastereomer.

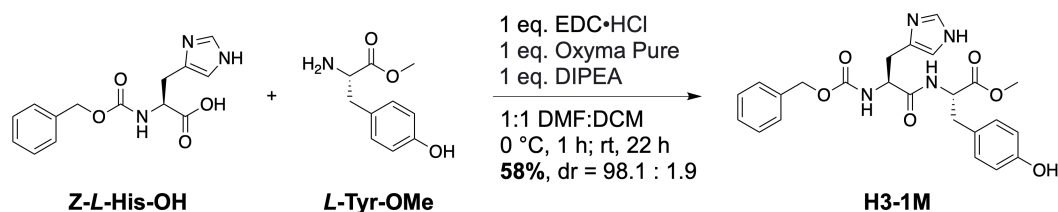


**Figure 3.8** Final synthesis of H3-1M.

### 3.3 Synthesis of H3-1 C-terminal amide (H3-1A)

To generate the H3-1 C-terminal amide analogue (H3-1A), we used H3-1M as the starting material to afford H3-1A by ammonolysis (**Figure 3.9**). By dissolving H3-1M in an appropriate volume of 7 M  $\text{NH}_3$  in MeOH solution, H3-1M was typically consumed within 48 hours at room temperature. At this point, the solvent was evaporated, most conveniently using a stream of air, and the resulting solids were triturated with EtOAc to remove trace non-polar impurities. Vacuum filtration and additional EtOAc washes afforded a crude product at a 95% yield (0.43 g, 1.0 mmol). Of note, this crude product visibly maintained faint coloured impurities, but which were not detectable by NMR. However, out of an abundance of caution, crude H3-1A was purified further by treatment with activated charcoal, followed by filtration over celite, which provided H3-1A at an overall 84% yield (378 mg, 0.8 mmol). In initial syntheses, a slightly altered approach was also trialed, whereby H3-1M was suspended in a 1:1 (v/v) solution of MeOH and concentrated ammonia water, which following partial evaporation to remove volatiles, precipitated H3-1A at a 75% yield (0.37 g, 0.8 mmol). Although this method exhibited a lower yield and was less convenient owing to the requirement for rotary evaporation of the ammonia solution, the aqueous method was found to proceed much quicker, usually being complete within 6 – 8 hours, as compared to ammonolysis with  $\text{NH}_3$  in MeOH, which was complete within 48 hours.

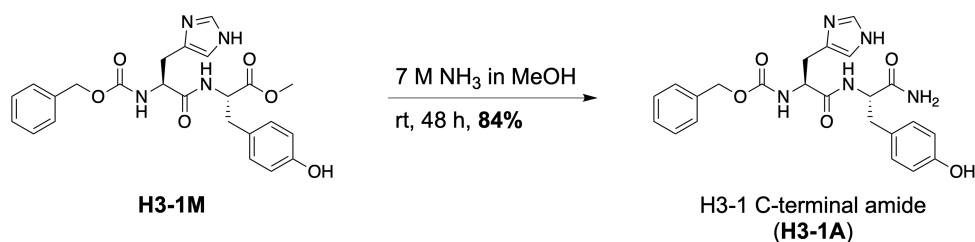


**Figure 3.9 Synthesis of H3-1A by the ammonolysis of H3-1M.**

$^1\text{H}$  and  $^{13}\text{C}\{^1\text{H}\}$  NMR studies were consistent with the identity of H3-1A, most notably, with the disappearance of the methyl ester proton peak in  $^1\text{H}$  NMR spectra (**Appendices 12 – 14**). The identity of H3-1A was further confirmed by HRMS ( $[\text{M} + \text{H}]^+_{\text{calc}} = 452.1928$ ,  $[\text{M} + \text{H}]^+_{\text{obs}} = 452.1928$ ), and purity assessment by RP-HPLC (monitoring at wavelengths  $\lambda = 220$  and  $275$  nm) identified the material to be homogenous (**Appendices 15 – 16**).

### 3.4 Synthesis of H3-1 nitrile (H3-1N)

H3-1 nitrile (H3-1N) was generated by the dehydration of H3-1A (**Figure 3.10**)<sup>192,193</sup>. By suspending H3-1A in THF, followed by the addition of  $\text{Et}_3\text{N}$  and TFAA, H3-1A was smoothly converted to H3-1N over one hour, after which the reaction was quenched with the addition of water. Of note, H3-1A and H3-1N's other nucleophilic groups can react with TFAA, for example, to result in trifluoroacetylation on the imidazole ring of histidine or the phenol ring of tyrosine, and which would eventually yield a trifluoroacetylated H3-1N derivative. In support of this side reaction, TLC analysis displayed abundant impurities, and products obtained directly from the reaction revealed pronounced peaks in  $^{19}\text{F}$  NMR spectra (**Appendix 17**). However, basification of the reaction mixture to pH 9 and stirring at room temperature for two hours was sufficient to ensure near-complete consumption of any trifluoroacetylated byproducts, as indicated by the presence of only trace peaks in  $^{19}\text{F}$  NMR spectra (**Appendix 18**). Following quenching and basification, the reaction was neutralized, volatiles were removed by evaporation, and the resulting white precipitate was

collected by vacuum filtration, washing with cold water, to provide H3-1N at an 89% yield (387 mg, 0.9 mmol).

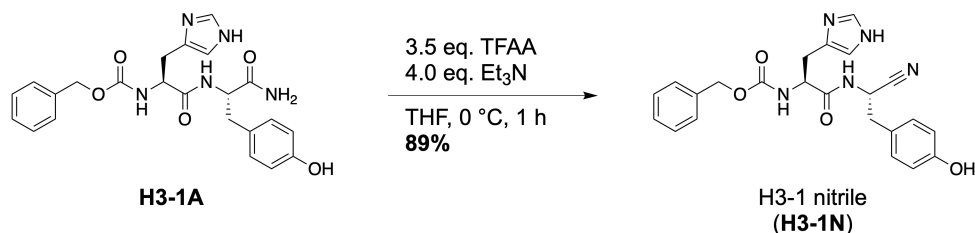


**Figure 3.10** Synthesis of H3-1N by the dehydration of H3-1A.

As for other analogues, <sup>1</sup>H and <sup>13</sup>C {<sup>1</sup>H} NMR studies were consistent with the identity of H3-1N, and which was further confirmed by HRMS ([M + Na]<sup>+</sup><sub>calc</sub> = 456.1642, [M + Na]<sup>+</sup><sub>obs</sub> = 456.1639) (**Appendices 19 – 22**). To our surprise, despite the minimal work-up, H3-1N obtained from this procedure was identified to be a homogenous material by RP-HPLC (monitoring at wavelengths λ = 220 and 275 nm) (**Appendix 23**).

### 3.5 Synthesis of H3-1 tetrazole (H3-1T)

The primary method for synthesizing 5-substituted 1*H*-tetrazoles is by cycloaddition of a nitrile derivative with azide<sup>183,194</sup>. In this manner, the most straightforward method to produce H3-1T is by cycloaddition of H3-1N with azide. Several approaches exist for this transformation, although most are marked with a necessity for harsh conditions or strong Lewis acids, in addition to posing serious combustion and toxicity risks. In light of these issues, we determined to generate H3-1T by reaction of H3-1N with sodium azide and zinc bromide, a method which is reported to occur in mild conditions, with wide applicability, and with generally high yields and simple workups<sup>195</sup>. As well, this approach has been applied to generate amino acid tetrazoles and was noted to typically proceed with low levels of racemization<sup>196</sup>.

To this end, refluxing H3-1N, NaN<sub>3</sub>, and ZnBr<sub>2</sub> in a solvent system of water and isopropanol was found to reliably consume H3-1N within 20 – 24 hours (**Figure 3.11**). Concentration of the reaction mixture to remove isopropanol readily precipitated off-white solids which were anticipated to be crude H3-1T. Interestingly, these solids were insoluble in many solvents which dissolved other H3-1 analogues, most notably, methanol, and <sup>1</sup>H NMR studies of these solids revealed spectra to be exclusively comprised of broad peaks with a lack of splitting; however, the chemical shifts of these peaks agreed with what would be expected for H3-1T (**Appendix 24**). Considering these surprising properties, the use of zinc bromide as a catalyst in this reaction, and the well-known propensity for imidazoles and tetrazoles to chelate transition metals, we hypothesized that over the course of the reaction and during workup, H3-1T coordinates Zn<sup>2+</sup> ions to form an organometallic complex, hereafter denoted as H3-1T:Zn.

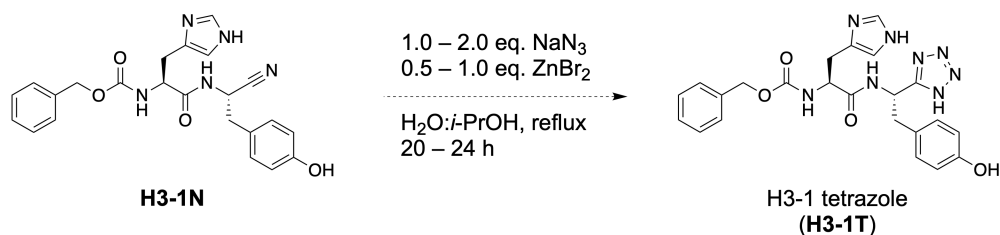


**Figure 3.11** Trial synthesis of H3-1T by reaction of H3-1N with NaN<sub>3</sub> and ZnBr<sub>2</sub>.

To test the idea that the isolated solids consist of an H3-1T:Zn complex, we used ICP-MS to quantify the abundance of zinc in the crude product. In line with our hypothesis, ICP-MS quantified approximately 8% of the crude product to be zinc by mass (79187.50 μg/g), evidencing that the immediate reaction product is an H3-1T:Zn complex, and is likely even a mixture of complexes with varied stoichiometries (i.e. 1:1 to 1:4 H3-1T:Zn).

In an attempt to isolate H3-1T from the H3-1T:Zn complex, we trialed a number of purification strategies, primarily focusing on the selective precipitation of zinc as zinc sulfide. Specifically, we tested adding excess NaHS to acidic or basic solutions of H3-

1T:Zn, as well as bubbling H<sub>2</sub>S gas into an acidic solution of H3-1T:Zn. However, despite numerous attempts to optimize this approach, H3-1T recovered following sulfide treatment was noted to still maintain residual zinc as identified by poor sample solubility and the presence of broad peaks with a lack of splitting in <sup>1</sup>H NMR spectra. In addition, we piloted the use of metal scavenging resins to reduce zinc levels in sulfide-treated H3-1T samples; however, we again did not observe a substantial reduction in residual zinc.

Alternatively, we decided to test the use of EDTA, a uniquely potent chelator of transition metals, by adding excess EDTA to a basic solution of H3-1T:Zn. Interestingly, following treatment with EDTA, we were able to isolate solids with good solubility characteristics and sharp <sup>1</sup>H NMR spectra, suggesting that this method effectively frees H3-1T from the H3-1T:Zn complex. However, we also noted free H3-1T to be moderately water soluble, which complicated its isolation from EDTA, the EDTA:Zn complex, and other impurities. We additionally remained concerned that the procedure would not be sufficient to reduce zinc concentrations to a permissible level for biological study (i.e. < 100 ppm).

Thus, considering the difficulties encountered in purifying H3-1T from zinc, we aimed to instead generate H3-1T by a transition metal-free method. Importantly, prior to the use of zinc salts, ammonium salts were one of the primary catalysts used to generate 5-substituted 1*H*-tetrazoles by cycloaddition of nitriles and azide. Indeed, the original report by Lofquist and coworkers identified that heating substituted nitriles with sodium azide and ammonium chloride in DMF typically provides the appropriate tetrazoles in good yields<sup>197</sup>.

To test this approach, we heated 1.0 eq. H3-1N, 1.1 – 1.2 eq. NaN<sub>3</sub>, and 1.1 – 1.2 eq. NH<sub>4</sub>Cl in DMF to 90 °C for 24 hours or 110 – 120 °C for 48 hours (**Figure 3.12**). Unfortunately, only partial consumption of H3-1N could be achieved, and upon work-up, only a small portion of an impure product was obtained. We hypothesized that the imidazole of H3-1N may be competing for protonation by ammonium chloride, thereby resulting in the observed poor conversion of H3-1N to H3-1T. To this end, we repeated this reaction, heating 1.0 eq. H3-1N, 1.2 eq. NaN<sub>3</sub>, and 2.2 eq. NH<sub>4</sub>Cl in DMF to 90 °C for 24 hours (**Figure 3.12**). Although an increase in H3-1N consumption was noted, again only a small crop of an impure product was obtained.

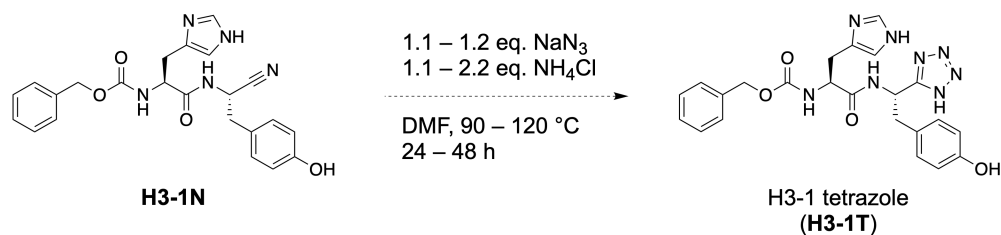


**Figure 3.12 Trial synthesis of H3-1T by reaction of H3-1N with NaN<sub>3</sub> and NH<sub>4</sub>Cl.**

Inspired by several reports which have reworked the original NaN<sub>3</sub> / NH<sub>4</sub>Cl / DMF method by changing the ammonium salt and solvent system of choice<sup>197–199</sup>, we decided to substitute DMF for dioxane and ammonium chloride for triethylammonium chloride. We chose to replace DMF with dioxane, as we suspected that the use of DMF was resulting in the abundant formation of impurities, as has been observed by others<sup>199</sup>. Meanwhile dioxane was predicted to be unreactive in the selected conditions, which alongside its favourable solubility characteristics and ideal boiling point, made it a prime candidate for evaluation. Consequently, we selected triethylammonium chloride as the ammonium salt catalyst due to its improved solubility profile and past reports noting a similar reactivity to ammonium chloride.

Following this approach, 1.0 eq. of H3-1N, 2.0 eq. of NaN<sub>3</sub>, and 3.0 eq. of Et<sub>3</sub>N•HCl were heated in dioxane to 80 °C for 24 hours (**Figure 3.13**). TLC analysis identified near complete consumption of H3-1N, and the reaction was worked up by serial evaporation from acidic water to remove residual azide as HN<sub>3</sub>. As part of our studies, we serendipitously identified that H3-1T precipitates from 1 M HCl, presumably as the hydrochloride salt. Thus, following acidic evaporation steps, H3-1T was precipitated by stirring in 1 M HCl, and reprecipitated once more to remove residual triethylammonium chloride, providing the hydrochloride salt of H3-1T (H3-1T•HCl) at a 38% yield (233 mg, 0.5 mmol).

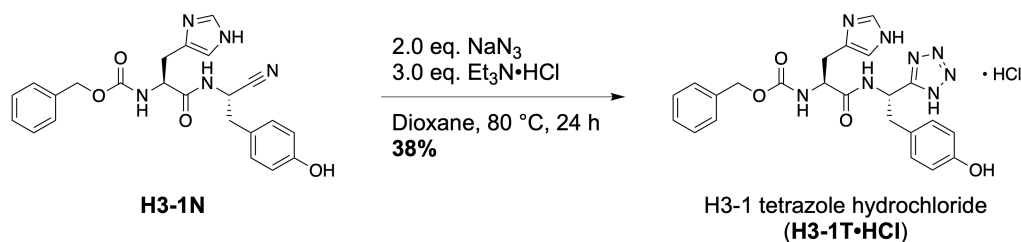


**Figure 3.13** Synthesis of H3-1T•HCl by reaction of H3-1N with NaN<sub>3</sub> and Et<sub>3</sub>N•HCl.

As for other analogues, <sup>1</sup>H and <sup>13</sup>C{<sup>1</sup>H} NMR studies were consistent with H3-1T•HCl, and the product's identity was further supported with HRMS ([M + H]<sup>+</sup><sub>calc</sub> = 477.1993, [M + H]<sup>+</sup><sub>obs</sub> = 477.2006) (**Appendix 25 – 29**). As well, RP-HPLC studies (monitoring at wavelengths λ = 220 and 275 nm) identified the product to be homogenous (**Appendix 30**).

### 3.6 Attempted synthesis of thioamide H3-1 methyl ester (TH3-1M)

To produce thioamide H3-1 methyl ester (TH3-1M), we decided to directly thionate H3-1M, as several reports exist in the literature describing the direct thionation of orthogonally protected dipeptides<sup>169,200,201</sup>.

Notably, thionation using a reagent combination of P<sub>4</sub>S<sub>10</sub> and hexamethyldisiloxane (HMDSO) has been successfully applied to orthogonally protected dipeptides and was noted to be superior to Lawesson's reagent or P<sub>4</sub>S<sub>10</sub> alone, the most widely used thionating reagents<sup>200,202</sup>. Using this approach, 1.0 eq. of H3-1M was refluxed at 55 – 60 °C with 1.0 – 1.3 eq. of P<sub>4</sub>S<sub>10</sub> and 5.0 – 5.5 eq. of HMDSO in a solvent system of 9:1 DCM and MeCN for five hours, followed by a second addition of 1.0 eq. of P<sub>4</sub>S<sub>10</sub> and 5.0 eq. of HMDSO and continued reflux overnight (**Figure 3.14**). Following evaporation of the solvent, one to two rounds of column chromatography, and an extractive work-up, a yellow solid was obtained (111 – 390 mg product from 0.47 – 3.97 g (1.0 – 8.5 mmol) H3-1M), which was consistent with TH3-1M, as indicated by <sup>1</sup>H and <sup>13</sup>C{<sup>1</sup>H} NMR studies and HRMS ([M + H]<sup>+</sup><sub>calc</sub> = 483.1697, [M + H]<sup>+</sup><sub>obs</sub> = 483.1707) (**Appendices 31 – 33**). However, the product

was noticeably impure by NMR, and the method additionally suffered from being low yielding, highly laborious, difficult to replicate, and extremely odorous.

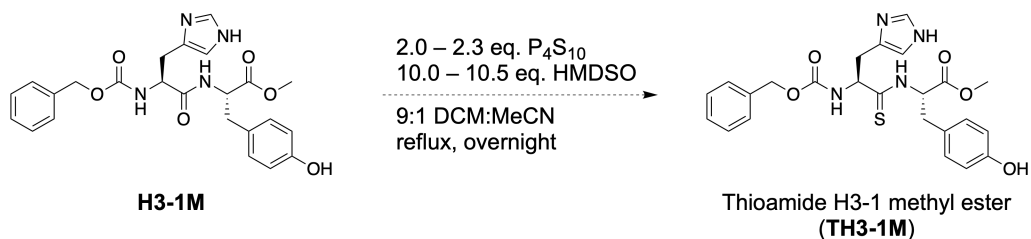


**Figure 3.14** Trial synthesis of TH3-1M by the thionation of H3-1M.

Attempts to optimize the above method by altering stoichiometry, order of addition, solvents, and work-up strategies were trialed but to no success, with most adjustments lowering the obtained yield or increasing tediousness. Several alternative thionating procedures were also tested, including lone  $P_4S_{10}$ <sup>203</sup>, Lawesson's reagent<sup>204</sup>,  $P_4S_{10}$ /pyridine<sup>205</sup>,  $P_4S_{10}/Na_2CO_3$ <sup>206</sup>, and the reagent combination of  $PCl_5$ , thiourea, and DMF<sup>201</sup>. However, these methods were similarly unsuccessful in providing a higher-yielding, less tedious, and cleaner procedure for generating TH3-1M. Considering the issues associated with producing TH3-1M, further attempts to optimize its synthesis were not pursued.

### 3.7 Attempted synthesis of methyleneamino H3-1 methyl ester (MH3-1M)

Attempts to synthesize MH3-1M were conducted by reducing the thioamide of TH3-1M to a methyleneamino group with nickel boride. Notably, a past report characterized this method as effective for the reduction of thioamide-containing dipeptides maintaining N-terminal Z and C-terminal methyl ester protecting groups, and to be more effective than the use of Raney nickel or diborane<sup>207</sup>.



Following this approach, 1.0 eq. of crude TH3-1M and 8.0 eq. of  $\text{NiCl}_2 \cdot 6\text{H}_2\text{O}$  were dissolved in a 1:3 solvent system of THF and MeOH, after which 24 eq. of  $\text{NaBH}_4$  were added in portions to generate an excess of the reducing agent, nickel boride, *in situ* (**Figure 3.15**). The reaction was stirred for 15 minutes at 0 °C, after which it was quenched by filtration over celite, and evaporated to dryness. The crude grey mass was taken up in acidic water (pH  $\approx$  1) and washed twice with EtOAc. The aqueous fraction was then basified (pH  $\approx$  11) and extracted a total of eight times with EtOAc, after which the organic fractions were combined and evaporated to yield a crude white solid (40 mg product from 145 mg crude TH3-1M).

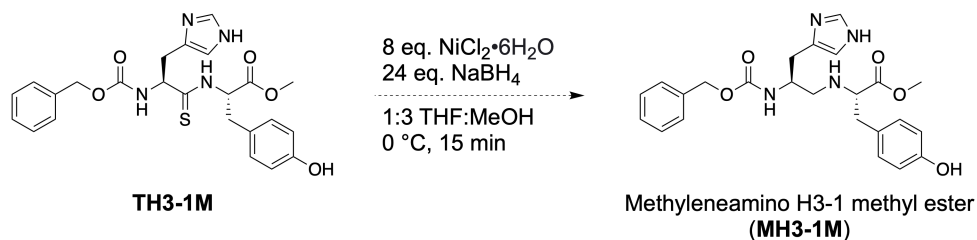


**Figure 3.15** Trial synthesis of MH3-1M by the reduction of TH3-1M.

Although  $^1\text{H}$  NMR spectra were only modestly suggestive for the formation of MH3-1M, MS studies better supported that the crude product contained MH3-1M ( $[\text{M} + \text{H}]^+_{\text{calc}} = 453.2132$ ,  $[\text{M} + \text{H}]^+_{\text{obs}} = 453.2156$ ) (**Appendices 34 – 35**). However, only a small crop of a highly impure product was obtained, making further studies difficult. As well, considering the propensity for H3-1-like compounds to chelate transition metals, as was found for H3-1T and zinc, it is anticipated that MH3-1M could be a nickel chelator, and which may be complicating its isolation. Regardless, owing to issues with generating TH3-1M, we were unable to further pursue this transformation, especially to optimize its isolation and purification procedures.

## Chapter 4

### 4 Discussion and conclusions

#### 4.1 General summary

By reducing cell surface levels of MHC-I, Nef facilitates efficient evasion of CTL killing for HIV-1-infected cells, which compromises the efficacy of several immune-directed HIV-1 cure approaches<sup>32,59,96,113,118</sup>. Inhibition of Nef-mediated MHC-I downregulation is therefore an attractive pharmacological target to functionalize an immune-directed HIV-1 cure strategy; however, no such inhibitor exists to-date that is suitable for *in vivo* study.

Herein, we described our attempts to synthesize *in vivo* stable inhibitors of Nef's interactions with the SFKs, an upstream step in Nef-mediated MHC-I downregulation. These inhibitors were derived from a previously identified lead compound, termed H3-1, which was characterized to inhibit the Nef:SFK interaction *in vitro* and to rescue cell surface MHC-I in HIV-1-infected cells in cell culture, but which is rapidly cleared *in vivo*. Considering that H3-1 is a dipeptide derivative, we hypothesized that its observed *in vivo* instability arises from a high susceptibility to proteolysis.

In this thesis, we prepared a panel of peptidomimetic H3-1 analogues, with the goal of developing compounds of improved proteolytic stabilities. Specifically, four analogues (H3-1M, H3-1A, H3-1N, and H3-1T) which maintained functional group replacements of H3-1's carboxyl group were synthesized, isolated, and chemically characterized. As well, synthetic efforts were made towards two analogues (TH3-1M and MH3-1M) incorporating functional group replacements of the amide group. Through future biological studies to characterize these compounds on measures of potency, toxicity, and biostability, as well as additional rounds of chemical optimization, we aim to identify an *in vivo* stable Nef inhibitor for evaluation as part of an immune-directed HIV-1 cure.

## 4.2 Synthesis of carboxyl replacing H3-1 analogues

Four H3-1 analogues incorporating carboxyl replacing groups were generated, namely, H3-1M, H3-1A, H3-1N, and H3-1T, which maintain C-terminal methyl ester, amide, nitrile, or tetrazole groups, respectively. Importantly, the syntheses described in this thesis were not optimized for yields, and multiple alternative methods can be used to reach each analogue to improve final compound yields and/or simplify the workflow. Finally, as is discussed below, isomeric purity was not assessed for each carboxyl replacing analogue besides H3-1M; however, carboxyl transformations can result in side reactions, leading to peptide epimerization at the C-terminal residue. Thus, it will be imperative for future studies to replicate and quantify the extent of epimerization for each synthesis, such as by chiral chromatography.

### 4.2.1 H3-1M

The synthesis of H3-1M was accomplished using solution-phase peptide coupling between *Z*-*L*-His-OH and *L*-Tyr-OMe<sup>188,189</sup>. Our approach used a histidine monomer with an unprotected side chain, which while more direct and simpler in theory, complicated the synthesis of H3-1M due to solubility issues and abundant formation of the *D,L* diastereomer, at approximately 10%. An additional purification step was therefore required, which lowered the overall yield appreciably and was ultimately unable to fully eliminate the *D,L* diastereomer. In the future, coupling using a protected histidine monomer would be preferable to avoid these issues. On the other hand, the tyrosine monomer does not require protecting, as it maintains good solubility in organic solvents, and more importantly, is not known to contribute to epimerization.

### 4.2.2 H3-1A

The synthesis of H3-1A was accomplished by the ammonolysis of H3-1M. Although we used ammonia in methanol solution for our approach, which yielded H3-1A following 48 hours of reaction, we also noted that the use of aqueous ammonia and methanol yielded

H3-1A in a shorter timeframe of 6 – 8 hours. It is also important to note that ammonolysis necessitates strongly basic conditions, which can result in epimerization at the C-terminal residue for H3-1M, and can in turn, produce a mixture of *L,L* and *L,D* diastereomers for H3-1A. However, in this thesis we did not quantify the extent of epimerization during ammonolysis. It is also unknown which procedure for generating H3-1A would result in higher rates of epimerization: a longer reaction time in anhydrous conditions (ammonia in methanol solution), or a shorter reaction time in aqueous conditions.

#### 4.2.3 H3-1N

H3-1N was generated by the dehydration of H3-1A with TFAA and Et<sub>3</sub>N<sup>192,193</sup>. To our surprise, this synthesis proceeded cleanly and in high yield with only minimal work-up. However, a large excess of TFAA and Et<sub>3</sub>N was required to ensure completion of the reaction, most likely due to trifluoroacetylation of the histidine and tyrosine sidechains. Basification of the reaction to pH 9 was therefore necessary to remove any trifluoroacetylated byproducts. Of note, this basic work-up step may introduce some risks of epimerization at the C-terminal residue, especially considering the polarized nature of the nitrile group.

#### 4.2.4 H3-1T

H3-1T was ultimately prepared by heating H3-1N with sodium azide and triethylammonium chloride in dioxane. However, the reaction presents serious toxicity and explosivity risks, as well as providing only suboptimal yields. In future syntheses, yields for the current method can likely be improved by simplifying the work-up, such as by directly acidifying the reaction mixture to precipitate H3-1T•HCl. Additionally, triethylammonium chloride can be substituted for another ammonium salt, such as benzylamine hydrochloride, which has been associated with improved reactivity and safety in a past report<sup>198</sup>.

Additionally, we identified the reagent combination of sodium azide and zinc bromide to efficiently convert H3-1N to H3-1T, but this method was hampered by the formation of H3-1T:Zn complexes and an inability to effectively isolate H3-1T free from any residual zinc. This is a critical issue, as residual transition metals, including zinc, are well known to cause false-positive readouts in biological studies<sup>208-210</sup>. Yet, the identification that 1 M HCl precipitates H3-1T•HCl suggests that it may be possible to isolate zinc-free H3-1T following reaction with sodium azide and zinc bromide. Another alternative to generate H3-1T would be to first install the C-terminal tetrazole moiety on *L*-tyrosine, similarly as has been reported before<sup>196,211</sup>, followed by peptide coupling of this tyrosine tetrazole monomer with *Z*-*L*-His-OH to generate H3-1T (**Figure 4.1**). Indeed, it will be imperative to evaluate which of the above synthetic approaches is most favourable, especially when considering safety, simplicity, cleanliness, yields, and epimerization rates.

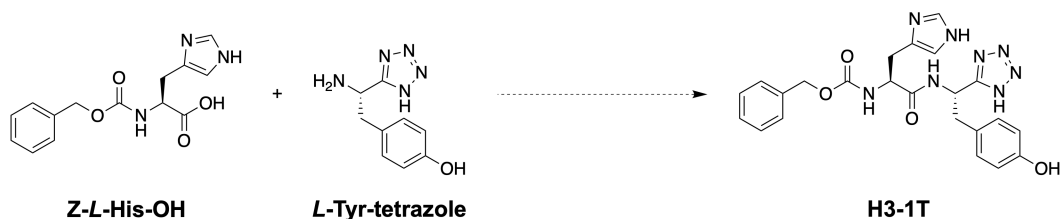


**Figure 4.1 Proposed synthesis of H3-1T by coupling *Z*-*L*-His-OH and *L*-tyrosine tetrazole.**

### 4.3 Synthesis of amide replacing H3-1 analogues

The synthesis of two central amide replacing analogues was attempted, TH3-1M and MH3-1M, which incorporate the thioamide and methyleneamino replacing groups, respectively. Although both TH3-1M and MH3-1M were successfully formed, we were unable to isolate the analogues in good purity, nor were they generated on-scale with acceptable yields.

### 4.3.1 TH3-1M

For the synthesis of TH3-1M, thionation of H3-1M using P<sub>4</sub>S<sub>10</sub> and HMDSO was found to be most successful<sup>200,202</sup>; however, the method is still prohibitive owing to its low yields, tediousness, and stench. Future studies should focus on the development of a higher yielding and more feasible approach. Although several alternative thionating agents were trialed, including P<sub>4</sub>S<sub>10</sub><sup>203</sup>, Lawesson's reagent<sup>204</sup>, P<sub>4</sub>S<sub>10</sub>/pyridine<sup>205</sup>, P<sub>4</sub>S<sub>10</sub>/Na<sub>2</sub>CO<sub>3</sub><sup>206</sup>, and the reagent combination of PCl<sub>5</sub>, thiourea, and DMF<sup>201</sup>, we were unable to identify a more suitable method for producing TH3-1M. However, each of these methods can be explored further by optimizing on stoichiometry, scale, solvents, temperature, and other variables. Many more thionating agents exist which can also be tested including elemental sulfur<sup>212</sup>, P<sub>4</sub>S<sub>10</sub>/Al<sub>2</sub>O<sub>3</sub><sup>213</sup>, or Belleau's reagent<sup>214</sup>, as well as thioacylation approaches<sup>168,215,216</sup>.

Although it is not entirely clear where the issues in generating TH3-1M stem from, it is likely due to the reactivity of the histidine imidazole group towards P<sub>4</sub>S<sub>10</sub> and its related thionating reagents. Indeed, in the original report on the P<sub>4</sub>S<sub>10</sub>/HMDSO method, when reactants maintained a basic nitrogen, or pyridine was used as the solvent, low yields and the abundant formation of insoluble solids was noted<sup>202</sup>; both of which were observed in our case. In line with this reasoning, P<sub>4</sub>S<sub>10</sub> in pyridine is known to generate a P<sub>4</sub>S<sub>10</sub>:pyridine complex, highlighting the reactivity of basic nitrogens towards P<sub>4</sub>S<sub>10</sub><sup>205</sup>. Additionally, *N,N*-chelated phosphorus complexes derived from P<sub>4</sub>S<sub>10</sub>:pyridine have been described, and from which the desired compound was isolated only after basic hydrolysis (**Figure 4.2**)<sup>217</sup>. It is tempting to speculate that H3-1M and/or TH3-1M may be forming a similar complex in the presence of P<sub>4</sub>S<sub>10</sub> or its related thionating reagents, yet this remains to be demonstrated. If confirmed, it may therefore be possible to isolate TH3-1M in good yields following its formation through P<sub>4</sub>S<sub>10</sub>:pyridine, or another thionating approach, followed by a basic work-up as previously described<sup>217</sup>. However, this approach may prove faulty, as thiopeptides can easily epimerize in basic conditions<sup>218,219</sup>. Alternatively, histidine side chain protecting groups can be trialed; however, these may also hamper the formation of TH3-1M by introducing steric barriers.

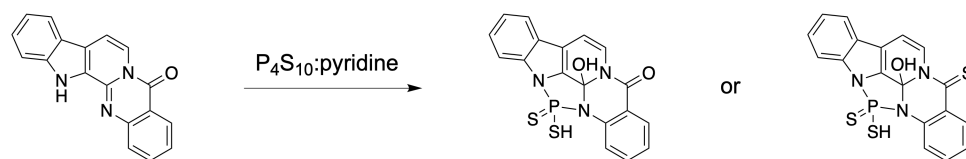


**Figure 4.2** Examples of *N,N*-chelated phosphorus complexes derived from  $P_4S_{10}$ :pyridine.

### 4.3.2 MH3-1M

To generate MH3-1M, we pursued the reduction of TH3-1M by nickel boride<sup>207</sup>. Unfortunately, issues in producing TH3-1M on larger scales stalled the development and optimization of this method. As well, pilot syntheses using this approach were noted for the formation of numerous by-products, difficulties in work-up, and the potential for nickel chelation by MH3-1M. Future studies to generate MH3-1M from the reduction of TH3-1M should focus on optimizing isolation procedures for the nickel boride method, and to test if nickel complexation is an issue. Otherwise, alternative reduction approaches can be applied such as Raney nickel<sup>220</sup> or borane<sup>221</sup>, although selectivity is likely to be an issue. More promisingly, reductive amination can be used to generate MH3-1M by coupling an aldehyde derivative of *Z*-*L*-histidine (*Z*-*L*-His-CHO) with *L*-Tyr-OMe (**Figure 4.3**).

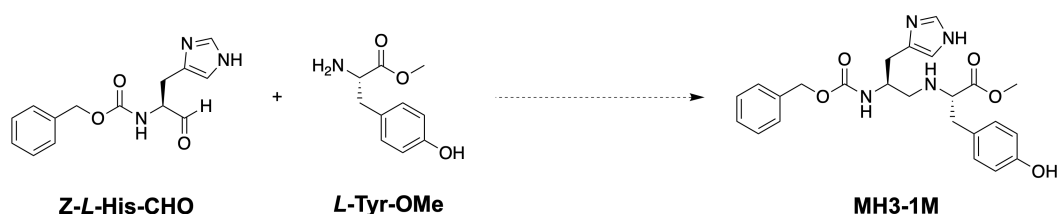


**Figure 4.3** Proposed approach to generate MH3-1M by reductive amination. Of note, for simplicity, the unprotected aldehyde derivative *Z*-*L*-His-CHO is shown; however, protection of the histidine sidechain is anticipated to be necessary.

## 4.4 Future directions

### 4.4.1 Synthesis of additional H3-1 analogues

Although this thesis focused on generating proteolytically stable H3-1 analogues by substituting its amide and carboxyl groups, numerous other sites on H3-1's scaffold merit potential modification. Indeed, if the analogues described herein do not maintain reduced proteolysis, additional substitutions can be introduced, including replacement of the histidine and tyrosine residues for synthetic amino acids or their *D* isomer counterparts, *N*-methylation of the amide bond, or even installation of alternative amide and carboxyl replacing groups<sup>154–156,222</sup>. The carbamate linker which connects the N-terminal Z group and the histidine residue may also be prone to hydrolysis, and may therefore require substitution<sup>223</sup>.

Future studies should also evaluate H3-1 analogues on other pharmacokinetic parameters, including hepatic metabolism, permeability, and renal excretion, each of which may necessitate chemical modification. Indeed, the polar and ionizable nature of H3-1 and its analogues may result in their rapid renal excretion and poor permeability<sup>224,225</sup>. Numerous sites on the H3-1 scaffold are also prone to hepatic metabolism, such as the phenyl ring of the Z group<sup>226</sup>. Finally, it is important to note that H3-1 is a highly flexible molecule, and rigidification of the scaffold may improve compound affinity and specificity<sup>227</sup>.

### 4.4.2 Biological study of H3-1 analogues

In the immediate future, we intend to biologically characterize our synthesized H3-1 analogues, and have identified a set of preliminary studies to evaluate each compound on measures of cytotoxicity, potency, and proteolytic stability. To quantify cytotoxicity, we propose to use the CellTiter-Glo assay (Promega, Madison, WI, U.S.A.), which is a luminescent cell viability assay. Alternative approaches, such as the MTT assay, can be used as well. To quantify potency, we propose to use the split luciferase NanoBiT assay (Promega)<sup>228</sup>. In the NanoBiT approach, Nef and Hck proteins are fused in frame with one half of a split luciferase, NanoLuc. Transfection of these fusion protein constructs should



reconstitute the luciferase protein upon interaction of Nef and Hck, thereby providing a convenient method to quantify Nef:SFK interaction inhibition. Of note, the NanoBiT assay is conducted in live cells and the reconstitution of NanoLuc is reversible, making the assay particularly amenable to small molecule inhibition studies. We also propose to test each inhibitor in HIV-1-infected cells to quantify cell surface MHC-I rescue by flow cytometry, a method which our group has applied extensively to study H3-1. Finally, to evaluate the proteolytic stability of each H3-1 analogue, we propose to use a plasma LC-MS assay, a standard approach for evaluating peptide proteolytic stability<sup>229</sup>. In this experiment, the inhibitor of interest is incubated at a set concentration in plasma, and compound concentrations are monitored over time by LC-MS to derive a correlative readout of proteolytic stability.

Beyond these initial studies, H3-1 and its analogues should be studied further to better understand their mechanism of action. Using techniques such as surface plasmon resonance (SPR), microscale thermophoresis (MST), or other protein binding studies, the binding target of H3-1-type inhibitors can be identified, especially to test whether it is Nef, the SFKs, the Nef:SFK complex, or an entirely alternative target. By identifying the binding target, it is then feasible to derive the binding pocket for these inhibitors, such as by using protein NMR or X-ray crystallography studies, which can then inform the synthesis of additional H3-1 analogues. Finally, to evaluate their suitability for *in vivo* study, it will be critical to characterize the pharmacokinetics of each H3-1 analogue more completely, including their permeability, metabolism, and excretion profiles.

## 4.5 Conclusions

Despite significant progress in treating and controlling HIV-1 infection in PLWH, there is still no practical cure for HIV-1 infection. The HIV-1 Nef protein plays a major role in inhibiting several leading curative approaches dependant on CTL action, primarily by downregulating cell surface levels of MHC-I in infected cells<sup>32,59,96,113,118</sup>. Nef's interactions with the SFKs have been established as an essential step in Nef-mediated

MHC-I downregulation<sup>67-70</sup>, identifying Nef:SFK interaction inhibitors as promising adjuvants for an immune-directed HIV-1 cure.

In this thesis, we developed a peptidomimetic series of potential Nef:SFK inhibitors derived from a previously identified lead compound (H3-1), and which are predicted to maintain improved *in vivo* stabilities. Four inhibitors incorporating replacements of the parent molecule's carboxyl group were isolated on-scale and are prepared for immediate biological characterization. With future studies to evaluate these compounds on potency, toxicity, and pharmacokinetic parameters, we aim to identify a Nef:SFK inhibitor suitable for *in vivo* study. We anticipate that application of a potent and *in vivo* stable Nef:SFK inhibitor will be crucial for the success of an immune-directed HIV-1 cure.

## References

1. Deeks SG, Overbaugh J, Phillips A, Buchbinder S. HIV infection. *Nat Rev Dis Primer*. 2015;1(1):15035. doi:10.1038/nrdp.2015.35
2. Simon V, Ho DD, Abdool Karim Q. HIV/AIDS epidemiology, pathogenesis, prevention, and treatment. *Lancet*. 2006;368(9534):489-504. doi:10.1016/S0140-6736(06)69157-5
3. Arts EJ, Hazuda DJ. HIV-1 Antiretroviral Drug Therapy. *Cold Spring Harb Perspect Med*. 2012;2(4):a007161-a007161. doi:10.1101/cshperspect.a007161
4. Chun TW, Davey RT, Engel D, Lane HC, Fauci AS. Re-emergence of HIV after stopping therapy. *Nature*. 1999;401(6756):874-875. doi:10.1038/44755
5. Davey RT, Bhat N, Yoder C, et al. HIV-1 and T cell dynamics after interruption of highly active antiretroviral therapy (HAART) in patients with a history of sustained viral suppression. *Proc Natl Acad Sci U S A*. 1999;96(26):15109-15114. doi:10.1073/pnas.96.26.15109
6. Mills EJ, Nachega JB, Buchan I, et al. Adherence to antiretroviral therapy in sub-Saharan Africa and North America: a meta-analysis. *JAMA*. 2006;296(6):679-690. doi:10.1001/jama.296.6.679
7. Deeks SG. HIV infection, inflammation, immunosenescence, and aging. *Annu Rev Med*. 2011;62(1):141-155. doi:10.1146/annurev-med-042909-093756
8. Deeks SG, Lewin SR, Havlir DV. The end of AIDS: HIV infection as a chronic disease. *Lancet*. 2013;382(9903):1525-1533. doi:10.1016/S0140-6736(13)61809-7
9. Herek GM, Capitano JP, Widaman KF. HIV-related stigma and knowledge in the United States: prevalence and trends, 1991–1999. *Am J Public Health*. 2002;92(3):371-377. doi:10.2105/AJPH.92.3.371
10. Rueda S, Mitra S, Chen S, et al. Examining the associations between HIV-related stigma and health outcomes in people living with HIV/AIDS: a series of meta-analyses. *BMJ Open*. 2016;6(7):e011453. doi:10.1136/bmjopen-2016-011453
11. Joint United Nations Programme on HIV/AIDS (UNAIDS). *2020 Global AIDS Update — Seizing the Moment — Tackling Entrenched Inequalities to End Epidemics.*; 2020. Accessed October 28, 2021. [https://www.unaids.org/sites/default/files/media\\_asset/2020\\_global-aids-report\\_en.pdf](https://www.unaids.org/sites/default/files/media_asset/2020_global-aids-report_en.pdf)
12. Allers K, Hütter G, Hofmann J, et al. Evidence for the cure of HIV infection by CCR5 $\Delta$ 32/ $\Delta$ 32 stem cell transplantation. *Blood*. 2011;117(10):2791-2799. doi:10.1182/blood-2010-09-309591

13. Hütter G, Nowak D, Mossner M, et al. Long-Term Control of HIV by *CCR5* Delta32/Delta32 Stem-Cell Transplantation. *N Engl J Med.* 2009;360(7):692-698. doi:10.1056/NEJMoa0802905
14. Gupta RK, Abdul-Jawad S, McCoy LE, et al. HIV-1 remission following *CCR5*Δ32/Δ32 haematopoietic stem-cell transplantation. *Nature.* 2019;568(7751):244-248. doi:10.1038/s41586-019-1027-4
15. Gupta RK, Peppas D, Hill AL, et al. Evidence for HIV-1 cure after *CCR5*Δ32/Δ32 allogeneic haematopoietic stem-cell transplantation 30 months post analytical treatment interruption: a case report. *Lancet HIV.* 2020;7(5):e340-e347. doi:10.1016/S2352-3018(20)30069-2
16. Henrich TJ, Hanhauser E, Marty FM, et al. Antiretroviral-Free HIV-1 Remission and Viral Rebound After Allogeneic Stem Cell Transplantation: Report of 2 Cases. *Ann Intern Med.* 2014;161(5):319. doi:10.7326/M14-1027
17. Kordelas L, Verheyen J, Esser S. Shift of HIV Tropism in Stem-Cell Transplantation with *CCR5* Delta32 Mutation. *N Engl J Med.* 2014;371(9):880-882. doi:10.1056/NEJMc1405805
18. Hütter G. More on Shift of HIV Tropism in Stem-Cell Transplantation with *CCR5* Delta32/Delta32 Mutation. *N Engl J Med.* 2014;371(25):2437-2438. doi:10.1056/NEJMc1412279
19. International AIDS Society Towards a Cure Working Group, Deeks SG, Lewin SR, et al. International AIDS Society global scientific strategy: towards an HIV cure 2016. *Nat Med.* 2016;22(8):839-850. doi:10.1038/nm.4108
20. Ndung'u T, McCune JM, Deeks SG. Why and where an HIV cure is needed and how it might be achieved. *Nature.* 2019;576(7787):397-405. doi:10.1038/s41586-019-1841-8
21. Choudhary SK, Margolis DM. Curing HIV: pharmacologic approaches to target HIV-1 latency. *Annu Rev Pharmacol Toxicol.* 2011;51(1):397-418. doi:10.1146/annurev-pharmtox-010510-100237
22. Deeks SG. Shock and kill. *Nature.* 2012;487(7408):439-440. doi:10.1038/487439a
23. Vansant G, Bruggemans A, Janssens J, Debyser Z. Block-and-lock strategies to cure HIV infection. *Viruses.* 2020;12(1):84. doi:10.3390/v12010084
24. Stephenson KE. Therapeutic vaccination for HIV: hopes and challenges. *Curr Opin HIV AIDS.* 2018;13(5):408-415. doi:10.1097/COH.0000000000000491
25. Qi J, Ding C, Jiang X, Gao Y. Advances in developing CAR T-cell therapy for HIV cure. *Front Immunol.* 2020;11:361. doi:10.3389/fimmu.2020.00361

26. Margolis DM, Koup RA, Ferrari G. HIV antibodies for treatment of HIV infection. *Immunol Rev.* 2017;275(1):313-323. doi:10.1111/imr.12506
27. Hoang TN, Paiardini M. Role of cytokine agonists and immune checkpoint inhibitors toward HIV remission. *Curr Opin HIV AIDS.* 2019;14(2):121-128. doi:10.1097/COH.0000000000000528
28. Delannoy A, Poirier M, Bell B. Cat and mouse: HIV transcription in latency, immune evasion and cure/remission strategies. *Viruses.* 2019;11(3):269. doi:10.3390/v11030269
29. Collins DR, Gaiha GD, Walker BD. CD8<sup>+</sup> T cells in HIV control, cure and prevention. *Nat Rev Immunol.* 2020;20(8):471-482. doi:10.1038/s41577-020-0274-9
30. Abner E, Jordan A. HIV “shock and kill” therapy: in need of revision. *Antiviral Res.* 2019;166:19-34. doi:10.1016/j.antiviral.2019.03.008
31. Kim Y, Anderson JL, Lewin SR. Getting the “kill” into “shock and kill”: strategies to eliminate latent HIV. *Cell Host Microbe.* 2018;23(1):14-26. doi:10.1016/j.chom.2017.12.004
32. Collins KL, Chen BK, Kalams SA, Walker BD, Baltimore D. HIV-1 Nef protein protects infected primary cells against killing by cytotoxic T lymphocytes. *Nature.* 1998;391(6665):397-401. doi:10.1038/34929
33. Pawlak EN, Dikeakos JD. HIV-1 Nef: a master manipulator of the membrane trafficking machinery mediating immune evasion. *Biochim Biophys Acta Gen Subj.* 2015;1850(4):733-741. doi:10.1016/j.bbagen.2015.01.003
34. Fackler OT, Baur AS. Live and let die: Nef functions beyond HIV replication. *Immunity.* 2002;16(4):493-497. doi:10.1016/S1074-7613(02)00307-2
35. Wolf D, Witte V, Laffert B, et al. HIV-1 Nef associated PAK and PI3-Kinases stimulate Akt-independent Bad-phosphorylation to induce anti-apoptotic signals. *Nat Med.* 2001;7(11):1217-1224. doi:10.1038/nm1101-1217
36. Geleziunas R, Xu W, Takeda K, Ichijo H, Greene WC. HIV-1 Nef inhibits ASK1-dependent death signalling providing a potential mechanism for protecting the infected host cell. *Nature.* 2001;410(6830):834-838. doi:10.1038/35071111
37. Castro-Gonzalez S, Shi Y, Colomer-Lluch M, et al. HIV-1 Nef counteracts autophagy restriction by enhancing the association between BECN1 and its inhibitor BCL2 in a PRKN-dependent manner. *Autophagy.* 2021;17(2):553-577. doi:10.1080/15548627.2020.1725401
38. Markle TJ, Mwimanzi P, Brockman MA. HIV-1 Nef and T-cell activation: a history of contradictions. *Future Virol.* 2013;8(4):391-404. doi:10.2217/fvl.13.20

39. Abraham L, Fackler OT. HIV-1 Nef: a multifaceted modulator of T cell receptor signaling. *Cell Commun Signal*. 2012;10(1):39. doi:10.1186/1478-811X-10-39
40. Kirchhoff F. Immune evasion and counteraction of restriction factors by HIV-1 and other primate lentiviruses. *Cell Host Microbe*. 2010;8(1):55-67. doi:10.1016/j.chom.2010.06.004
41. Foster JL, Garcia JV. HIV-1 Nef: at the crossroads. *Retrovirology*. 2008;5(1):84. doi:10.1186/1742-4690-5-84
42. Kestler HW, Ringler DJ, Mori K, et al. Importance of the nef gene for maintenance of high virus loads and for development of AIDS. *Cell*. 1991;65(4):651-662. doi:10.1016/0092-8674(91)90097-I
43. Skowronski J, Parks D, Mariani R. Altered T cell activation and development in transgenic mice expressing the HIV-1 nef gene. *EMBO J*. 1993;12(2):703-713.
44. Brady HJ, Pennington DJ, Miles CG, Dzierzak EA. CD4 cell surface downregulation in HIV-1 Nef transgenic mice is a consequence of intracellular sequestration. *EMBO J*. 1993;12(13):4923-4932. doi:10.1002/j.1460-2075.1993.tb06186.x
45. Lindemann D, Wilhelm R, Renard P, Althage A, Zinkernagel R, Mous J. Severe immunodeficiency associated with a human immunodeficiency virus 1 NEF/3'-long terminal repeat transgene. *J Exp Med*. 1994;179(3):797-807. doi:10.1084/jem.179.3.797
46. Hanna Z, Kay DG, Rebai N, Guimond A, Jothy S, Jolicoeur P. Nef harbors a major determinant of pathogenicity for an AIDS-like disease induced by HIV-1 in transgenic mice. *Cell*. 1998;95(2):163-175. doi:10.1016/S0092-8674(00)81748-1
47. Jamieson BD, Aldrovandi GM, Planelles V, et al. Requirement of human immunodeficiency virus type 1 nef for in vivo replication and pathogenicity. *J Virol*. 1994;68(6):3478-3485. doi:10.1128/jvi.68.6.3478-3485.1994
48. Zou W, Denton PW, Watkins RL, et al. Nef functions in BLT mice to enhance HIV-1 replication and deplete CD4<sup>+</sup>CD8<sup>+</sup> thymocytes. *Retrovirology*. 2012;9(1):44. doi:10.1186/1742-4690-9-44
49. Watkins RL, Foster JL, Garcia JV. In vivo analysis of Nef's role in HIV-1 replication, systemic T cell activation and CD4<sup>+</sup> T cell loss. *Retrovirology*. 2015;12(1):61. doi:10.1186/s12977-015-0187-z
50. Deacon NJ, Tsykin A, Solomon A, et al. Genomic structure of an attenuated quasi species of HIV-1 from a blood transfusion donor and recipients. *Science*. 1995;270(5238):988-991. doi:10.1126/science.270.5238.988

51. Learmont JC, Geczy AF, Mills J, et al. Immunologic and virologic status after 14 to 18 years of infection with an attenuated strain of HIV-1 — a report from the Sydney Blood Bank Cohort. *N Engl J Med.* 1999;340(22):1715-1722. doi:10.1056/NEJM199906033402203
52. Zaunders J, Dyer WB, Churchill M, et al. Possible clearance of transfusion-acquired nef/LTR-deleted attenuated HIV-1 infection by an elite controller with CCR5  $\Delta$ 32 heterozygous and HLA-B57 genotype. *J Virus Erad.* 2019;5(2):73-83.
53. Kirchhoff F, Greenough TC, Brettler DB, Sullivan JL, Desrosiers RC. Absence of intact nef sequences in a long-term survivor with nonprogressive HIV-1 infection. *N Engl J Med.* 1995;332(4):228-232. doi:10.1056/NEJM199501263320405
54. Garcia JV, Miller AD. Serine phosphorylation-independent downregulation of cell-surface CD4 by nef. *Nature.* 1991;350(6318):508-511. doi:10.1038/350508a0
55. Aiken C, Konner J, Landau NR, Lenburg ME, Trono D. Nef induces CD4 endocytosis: requirement for a critical dileucine motif in the membrane-proximal CD4 cytoplasmic domain. *Cell.* 1994;76(5):853-864. doi:10.1016/0092-8674(94)90360-3
56. Rosa A, Chande A, Ziglio S, et al. HIV-1 Nef promotes infection by excluding SERINC5 from virion incorporation. *Nature.* 2015;526(7572):212-217. doi:10.1038/nature15399
57. Usami Y, Wu Y, Göttlinger HG. SERINC3 and SERINC5 restrict HIV-1 infectivity and are counteracted by Nef. *Nature.* 2015;526(7572):218-223. doi:10.1038/nature15400
58. Mumby MJ, Johnson AL, Trothen SM, et al. An Amino Acid Polymorphism within the HIV-1 Nef Dileucine Motif Functionally Uncouples Cell Surface CD4 and SERINC5 Downregulation. *J Virol.* 2021;95(16). doi:10.1128/JVI.00588-21
59. Schwartz O, Maréchal V, Le Gall S, Lemonnier F, Heard JM. Endocytosis of major histocompatibility complex class I molecules is induced by the HIV-1 Nef protein. *Nat Med.* 1996;2(3):338-342. doi:10.1038/nm0396-338
60. Dirk BS, Pawlak EN, Johnson AL, et al. HIV-1 Nef sequesters MHC-I intracellularly by targeting early stages of endocytosis and recycling. *Sci Rep.* 2016;6:37021. doi:10.1038/srep37021
61. Johnson AL, Dirk BS, Coutu M, et al. A highly conserved residue in HIV-1 Nef alpha helix 2 modulates protein expression. *mSphere.* 2016;1(6). doi:10.1128/mSphere.00288-16
62. daSilva LLP, Sougrat R, Burgos PV, Janvier K, Mattera R, Bonifacino JS. Human immunodeficiency virus type 1 Nef protein targets CD4 to the multivesicular body pathway. *J Virol.* 2009;83(13):6578-6590. doi:10.1128/JVI.00548-09

63. Kwon Y, Kaake RM, Echeverria I, et al. Structural basis of CD4 downregulation by HIV-1 Nef. *Nat Struct Mol Biol.* 2020;27(9):822-828. doi:10.1038/s41594-020-0463-z
64. Wildum S, Schindler M, Münch J, Kirchhoff F. Contribution of Vpu, Env, and Nef to CD4 down-modulation and resistance of human immunodeficiency virus type 1-infected T cells to superinfection. *J Virol.* 2006;80(16):8047-8059. doi:10.1128/JVI.00252-06
65. Veillette M, Desormeaux A, Medjahed H, et al. Interaction with cellular CD4 exposes HIV-1 envelope epitopes targeted by antibody-dependent cell-mediated cytotoxicity. *J Virol.* 2014;88(5):2633-2644. doi:10.1128/JVI.03230-13
66. Staudt RP, Smithgall TE. Nef homodimers down-regulate SERINC5 by AP-2-mediated endocytosis to promote HIV-1 infectivity. *J Biol Chem.* 2020;295(46):15540-15552. doi:10.1074/jbc.RA120.014668
67. Blagoveshchenskaya AD, Thomas L, Feliciangeli SF, Hung CH, Thomas G. HIV-1 Nef downregulates MHC-I by a PACS-1- and PI3K-regulated ARF6 endocytic pathway. *Cell.* 2002;111(6):853-866. doi:10.1016/s0092-8674(02)01162-5
68. Atkins KM, Thomas L, Youker RT, et al. HIV-1 Nef binds PACS-2 to assemble a multikinase cascade that triggers major histocompatibility complex class I (MHC-I) down-regulation: analysis using short interfering RNA and knock-out mice. *J Biol Chem.* 2008;283(17):11772-11784. doi:10.1074/jbc.M707572200
69. Hung CH, Thomas L, Ruby CE, et al. HIV-1 Nef assembles a Src family kinase-ZAP-70/Syk-PI3K cascade to downregulate cell-surface MHC-I. *Cell Host Microbe.* 2007;1(2):121-133. doi:10.1016/j.chom.2007.03.004
70. Dikeakos JD, Atkins KM, Thomas L, et al. Small molecule inhibition of HIV-1-induced MHC-I down-regulation identifies a temporally regulated switch in Nef action. *Mol Biol Cell.* 2010;21(19):3279-3292. doi:10.1091/mbc.E10-05-0470
71. Kasper MR, Roeth JF, Williams M, Filzen TM, Fleis RI, Collins KL. HIV-1 Nef disrupts antigen presentation early in the secretory pathway. *J Biol Chem.* 2005;280(13):12840-12848. doi:10.1074/jbc.M413538200
72. Schaefer MR, Wonderlich ER, Roeth JF, Leonard JA, Collins KL. HIV-1 Nef targets MHC-I and CD4 for degradation via a final common  $\beta$ -COP-dependent pathway in T cells. *PLoS Pathog.* 2008;4(8):e1000131. doi:10.1371/journal.ppat.1000131
73. Swigut T. Mechanism for down-regulation of CD28 by Nef. *EMBO J.* 2001;20(7):1593-1604. doi:10.1093/emboj/20.7.1593



74. Pawlak EN, Dirk BS, Jacob RA, Johnson AL, Dikeakos JD. The HIV-1 accessory proteins Nef and Vpu downregulate total and cell surface CD28 in CD4<sup>+</sup> T cells. *Retrovirology*. 2018;15(1):6. doi:10.1186/s12977-018-0388-3
75. Chaudhry A, Das SR, Hussain A, et al. The Nef protein of HIV-1 induces loss of cell surface costimulatory molecules CD80 and CD86 in APCs. *J Immunol*. 2005;175(7):4566-4574. doi:10.4049/jimmunol.175.7.4566
76. Michel N, Allespach I, Venzke S, Fackler OT, Keppler OT. The Nef protein of human immunodeficiency virus establishes superinfection immunity by a dual strategy to downregulate cell-surface CCR5 and CD4. *Curr Biol*. 2005;15(8):714-723. doi:10.1016/j.cub.2005.02.058
77. Venzke S, Michel N, Allespach I, Fackler OT, Keppler OT. Expression of Nef downregulates CXCR4, the major coreceptor of human immunodeficiency virus, from the surfaces of target cells and thereby enhances resistance to superinfection. *J Virol*. 2006;80(22):11141-11152. doi:10.1128/JVI.01556-06
78. Jacob RA, Edgar CR, Prévost J, et al. The HIV-1 accessory protein Nef increases surface expression of the checkpoint receptor Tim-3 in infected CD4<sup>+</sup> T cells. *J Biol Chem*. 2021;297(3):101042. doi:10.1016/j.jbc.2021.101042
79. Tarafdar S, Poe JA, Smithgall TE. The accessory factor Nef links HIV-1 to Tec/Btk kinases in an Src homology 3 domain-dependent manner. *J Biol Chem*. 2014;289(22):15718-15728. doi:10.1074/jbc.M114.572099
80. Li WF, Aryal M, Shu ST, Smithgall TE. HIV-1 Nef dimers short-circuit immune receptor signaling by activating Tec-family kinases at the host cell membrane. *J Biol Chem*. 2020;295(15):5163-5174. doi:10.1074/jbc.RA120.012536
81. Renkema GH, Manninen A, Mann DA, Harris M, Saksela K. Identification of the Nef-associated kinase as p21-activated kinase 2. *Curr Biol*. 1999;9(23):1407-1411. doi:10.1016/S0960-9822(00)80086-X
82. Haller C, Rauch S, Fackler OT. HIV-1 Nef employs two distinct mechanisms to modulate Lck subcellular localization and TCR induced actin remodeling. *PLoS One*. 2007;2(11):e1212. doi:10.1371/journal.pone.0001212
83. Smith BL, Krushelnycky BW, Mochly-Rosen D, Berg P. The HIV Nef protein associates with protein kinase C theta. *J Biol Chem*. 1996;271(28):16753-16757. doi:10.1074/jbc.271.28.16753
84. Swingler S, Mann A, Jacqué JM, et al. HIV-1 Nef mediates lymphocyte chemotaxis and activation by infected macrophages. *Nat Med*. 1999;5(9):997-1003. doi:10.1038/12433

85. Lee JH, Schierer S, Blume K, et al. HIV-Nef and ADAM17-containing plasma extracellular vesicles induce and correlate with immune pathogenesis in chronic HIV infection. *EBioMedicine*. 2016;6:103-113. doi:10.1016/j.ebiom.2016.03.004
86. Jacob RA, Johnson AL, Pawlak EN, et al. The interaction between HIV-1 Nef and adaptor protein-2 reduces Nef-mediated CD4<sup>+</sup> T cell apoptosis. *Virology*. 2017;509:1-10. doi:10.1016/j.virol.2017.05.018
87. Finzi D. Identification of a reservoir for HIV-1 in patients on highly active antiretroviral therapy. *Science*. 1997;278(5341):1295-1300. doi:10.1126/science.278.5341.1295
88. Finzi D, Blankson J, Siliciano JD, et al. Latent infection of CD4<sup>+</sup> T cells provides a mechanism for lifelong persistence of HIV-1, even in patients on effective combination therapy. *Nat Med*. 1999;5(5):512-517. doi:10.1038/8394
89. Spina CA, Kwoh TJ, Chowes MY, Guatelli JC, Richman DD. The importance of nef in the induction of human immunodeficiency virus type 1 replication from primary quiescent CD4 lymphocytes. *J Exp Med*. 1994;179(1):115-123. doi:10.1084/jem.179.1.115
90. Miller MD, Warmerdam MT, Gaston I, Greene WC, Feinberg MB. The human immunodeficiency virus-1 nef gene product: a positive factor for viral infection and replication in primary lymphocytes and macrophages. *J Exp Med*. 1994;179(1):101-113. doi:10.1084/jem.179.1.101
91. Fujinaga K, Zhong Q, Nakaya T, et al. Extracellular Nef protein regulates productive HIV-1 infection from latency. *J Immunol*. 1995;155(11):5289-5298.
92. Kuang XT, Brockman MA. Implications of HIV-1 Nef for “shock and kill” strategies to eliminate latent viral reservoirs. *Viruses*. 2018;10(12):677. doi:10.3390/v10120677
93. Arenaccio C, Anticoli S, Manfredi F, Chiozzini C, Olivetta E, Federico M. Latent HIV-1 is activated by exosomes from cells infected with either replication-competent or defective HIV-1. *Retrovirology*. 2015;12:87. doi:10.1186/s12977-015-0216-y
94. Deng K, Perteu M, Rongvaux A, et al. Broad CTL response is required to clear latent HIV-1 due to dominance of escape mutations. *Nature*. 2015;517(7534):381-385. doi:10.1038/nature14053
95. Huang SH, Ren Y, Thomas AS, et al. Latent HIV reservoirs exhibit inherent resistance to elimination by CD8<sup>+</sup> T cells. *J Clin Invest*. 2018;128(2):876-889. doi:10.1172/JCI97555

96. Duette G, Hiener B, Morgan H, et al. The HIV-1 proviral landscape reveals that Nef contributes to HIV-1 persistence in effector memory CD4<sup>+</sup> T cells. *J Clin Invest.* 2022;132(7):e154422. doi:10.1172/JCI154422
97. Zhou D, Hayashi T, Jean M, et al. Inhibition of Polo-like kinase 1 (PLK1) facilitates the elimination of HIV-1 viral reservoirs in CD4<sup>+</sup> T cells ex vivo. *Sci Adv.* 2020;6(29):eaba1941. doi:10.1126/sciadv.aba1941
98. Lenassi M, Cagney G, Liao M, et al. HIV Nef is secreted in exosomes and triggers apoptosis in bystander CD4<sup>+</sup> T cells. *Traffic.* 2010;11(1):110-122. doi:10.1111/j.1600-0854.2009.01006.x
99. Kaw S, Ananth S, Tsopoulidis N, et al. HIV-1 infection of CD4 T cells impairs antigen-specific B cell function. *EMBO J.* 2020;39(24). doi:10.15252/embj.2020105594
100. Murakami Y, Fukazawa H, Kobatake T, et al. A mammalian two-hybrid screening system for inhibitors of interaction between HIV Nef and the cellular tyrosine kinase Hck. *Antiviral Res.* 2002;55(1):161-168. doi:10.1016/s0166-3542(02)00017-7
101. Betzi S, Restouin A, Opi S, et al. Protein protein interaction inhibition (2P2I) combining high throughput and virtual screening: application to the HIV-1 Nef protein. *Proc Natl Acad Sci U S A.* 2007;104(49):19256-19261. doi:10.1073/pnas.0707130104
102. Lugari A, Breuer S, Coursindel T, et al. A specific protein disorder catalyzer of HIV-1 Nef. *Bioorg Med Chem.* 2011;19(24):7401-7406. doi:10.1016/j.bmc.2011.10.051
103. Tribble RP, Narute P, Emert-Sedlak LA, et al. Discovery of a diaminoquinoxaline benzenesulfonamide antagonist of HIV-1 Nef function using a yeast-based phenotypic screen. *Retrovirology.* 2013;10:135. doi:10.1186/1742-4690-10-135
104. Emert-Sedlak L, Kodama T, Lerner EC, et al. Chemical library screens targeting an HIV-1 accessory factor/host cell kinase complex identify novel antiretroviral compounds. *ACS Chem Biol.* 2009;4(11):939-947. doi:10.1021/cb900195c
105. Narute PS, Smithgall TE. Nef alleles from all major HIV-1 clades activate Src-family kinases and enhance HIV-1 replication in an inhibitor-sensitive manner. *PloS One.* 2012;7(2):e32561. doi:10.1371/journal.pone.0032561
106. Pene-Dumitrescu T, Shu ST, Wales TE, et al. HIV-1 Nef interaction influences the ATP-binding site of the Src-family kinase, Hck. *BMC Chem Biol.* 2012;12:1. doi:10.1186/1472-6769-12-1
107. Wales TE, Hochrein JM, Morgan CR, Emert-Sedlak LA, Smithgall TE, Engen JR. Subtle dynamic changes accompany Hck activation by HIV-1 Nef and are reversed

- by an antiretroviral kinase inhibitor. *Biochemistry*. 2015;54(41):6382-6391. doi:10.1021/acs.biochem.5b00875
108. Emert-Sedlak LA, Narute P, Shu ST, et al. Effector kinase coupling enables high-throughput screens for direct HIV-1 Nef antagonists with antiretroviral activity. *Chem Biol*. 2013;20(1):82-91. doi:10.1016/j.chembiol.2012.11.005
  109. Shu ST, Emert-Sedlak LA, Smithgall TE. Cell-based fluorescence complementation reveals a role for HIV-1 Nef protein dimerization in AP-2 adaptor recruitment and CD4 co-receptor down-regulation. *J Biol Chem*. 2017;292(7):2670-2678. doi:10.1074/jbc.M116.770016
  110. Iyer PC, Zhao J, Emert-Sedlak LA, Moore KK, Smithgall TE, Day BW. Synthesis and structure-activity analysis of diphenylpyrazolodiazene inhibitors of the HIV-1 Nef virulence factor. *Bioorg Med Chem Lett*. 2014;24(7):1702-1706. doi:10.1016/j.bmcl.2014.02.045
  111. Emert-Sedlak LA, Loughran HM, Shi H, et al. Synthesis and evaluation of orally active small molecule HIV-1 Nef antagonists. *Bioorg Med Chem Lett*. 2016;26(5):1480-1484. doi:10.1016/j.bmcl.2016.01.043
  112. Shi H, Tice CM, Emert-Sedlak L, et al. Tight-binding hydroxypyrazole HIV-1 Nef inhibitors suppress viral replication in donor mononuclear cells and reverse Nef-mediated MHC-I downregulation. *ACS Infect Dis*. 2020;6(2):302-312. doi:10.1021/acsinfecdis.9b00382
  113. Mujib S, Saiyed A, Fadel S, et al. Pharmacologic HIV-1 Nef blockade promotes CD8 T cell-mediated elimination of latently HIV-1-infected cells in vitro. *JCI Insight*. 2017;2(17):e93684. doi:10.1172/jci.insight.93684
  114. Emert-Sedlak LA, Moukha-Chafiq O, Shi H, et al. Inhibitors of HIV-1 Nef-Mediated Activation of the Myeloid Src-Family Kinase Hck Block HIV-1 Replication in Macrophages and Disrupt MHC-I Downregulation. *ACS Infect Dis*. 2022;8(1):91-105. doi:10.1021/acsinfecdis.1c00288
  115. Poe JA, Vollmer L, Vogt A, Smithgall TE. Development and validation of a high-content bimolecular fluorescence complementation assay for small-molecule inhibitors of HIV-1 Nef dimerization. *J Biomol Screen*. 2014;19(4):556-565. doi:10.1177/1087057113513640
  116. Chutiwitoonchai N, Hiyoshi M, Mwimanzi P, et al. The identification of a small molecule compound that reduces HIV-1 Nef-mediated viral infectivity enhancement. *PloS One*. 2011;6(11):e27696. doi:10.1371/journal.pone.0027696
  117. Liu B, Zhang X, Zhang W, et al. Lovastatin inhibits HIV-1-induced MHC-I downregulation by targeting Nef-AP-1 complex formation: a new strategy to boost immune eradication of HIV-1 infected cells. *Front Immunol*. 2019;10:2151. doi:10.3389/fimmu.2019.02151

118. Painter MM, Zimmerman GE, Merlino MS, et al. Concanamycin A counteracts HIV-1 Nef to enhance immune clearance of infected primary cells by cytotoxic T lymphocytes. *Proc Natl Acad Sci U S A*. 2020;117(38):23835-23846. doi:10.1073/pnas.2008615117
119. Olszewski A, Sato K, Aron ZD, et al. Guanidine alkaloid analogs as inhibitors of HIV-1 Nef interactions with p53, actin, and p56<sup>lck</sup>. *Proc Natl Acad Sci U S A*. 2004;101(39):14079-14084. doi:10.1073/pnas.0406040101
120. Hunegnaw R, Vassilyeva M, Dubrovsky L, et al. Interaction between HIV-1 Nef and calnexin: from modeling to small molecule inhibitors reversing HIV-induced lipid accumulation. *Arterioscler Thromb Vasc Biol*. 2016;36(9):1758-1771. doi:10.1161/ATVBAHA.116.307997
121. Adzhubei AA, Anashkina AA, Tkachev YV, et al. Modelling interaction between HIV-1 Nef and calnexin. *AIDS*. 2018;32(15):2103-2111. doi:10.1097/QAD.0000000000001951
122. Ptak RG, Gentry BG, Hartman TL, et al. Inhibition of human immunodeficiency virus type 1 by tricyridine involves the accessory protein nef. *Antimicrob Agents Chemother*. 2010;54(4):1512-1519. doi:10.1128/AAC.01443-09
123. Bouchet J, Basmaciogullari SE, Chrobak P, et al. Inhibition of the Nef regulatory protein of HIV-1 by a single-domain antibody. *Blood*. 2011;117(13):3559-3568. doi:10.1182/blood-2010-07-296749
124. Lülfi S, Matz J, Rouyez MC, et al. Structural basis for the inhibition of HIV-1 Nef by a high-affinity binding single-domain antibody. *Retrovirology*. 2014;11(1):24. doi:10.1186/1742-4690-11-24
125. Breuer S, Schievink SI, Schulte A, Blankenfeldt W, Fackler OT, Geyer M. Molecular design, functional characterization and structural basis of a protein inhibitor against the HIV-1 pathogenicity factor Nef. *PLoS One*. 2011;6(5):e20033. doi:10.1371/journal.pone.0020033
126. Bouchet J, Herate C, Guenzel CA, et al. Single-domain antibody-SH3 fusions for efficient neutralization of HIV-1 Nef functions. *J Virol*. 2012;86(9):4856-4867. doi:10.1128/JVI.06329-11
127. Järviluoma A, Strandin T, Lülfi S, et al. High-affinity target binding engineered via fusion of a single-domain antibody fragment with a ligand-tailored SH3 domain. Dübel S, ed. *PLoS ONE*. 2012;7(7):e40331. doi:10.1371/journal.pone.0040331
128. Tribble RP, Emert-Sedlak L, Smithgall TE. HIV-1 Nef selectively activates Src family kinases Hck, Lyn, and c-Src through direct SH3 domain interaction. *J Biol Chem*. 2006;281(37):27029-27038. doi:10.1074/jbc.M601128200

129. Saksela K, Cheng G, Baltimore D. Proline-rich (PxxP) motifs in HIV-1 Nef bind to SH3 domains of a subset of Src kinases and are required for the enhanced growth of Nef<sup>+</sup> viruses but not for down-regulation of CD4. *EMBO J*. 1995;14(3):484-491.
130. Lee CH, Saksela K, Mirza UA, Chait BT, Kuriyan J. Crystal structure of the conserved core of HIV-1 Nef complexed with a Src family SH3 domain. *Cell*. 1996;85(6):931-942. doi:10.1016/s0092-8674(00)81276-3
131. Moarefi I, LaFevre-Bernt M, Sicheri F, et al. Activation of the Src-family tyrosine kinase Hck by SH3 domain displacement. *Nature*. 1997;385(6617):650-653. doi:10.1038/385650a0
132. Goddard TD, Huang CC, Meng EC, et al. UCSF ChimeraX: meeting modern challenges in visualization and analysis. *Protein Sci*. 2018;27(1):14-25. doi:10.1002/pro.3235
133. Oneyama C, Agatsuma T, Kanda Y, et al. Synthetic inhibitors of proline-rich ligand-mediated protein-protein interaction: potent analogs of UCS15A. *Chem Biol*. 2003;10(5):443-451. doi:10.1016/S1074-5521(03)00101-7
134. Alberts AW. Discovery, biochemistry and biology of lovastatin. *Am J Cardiol*. 1988;62(15):10J-15J. doi:10.1016/0002-9149(88)90002-1
135. Huss M, Ingenhorst G, König S, et al. Concanamycin A, the specific inhibitor of V-ATPases, binds to the V<sub>o</sub> subunit c. *J Biol Chem*. 2002;277(43):40544-40548. doi:10.1074/jbc.M207345200
136. Jia X, Singh R, Homann S, Yang H, Guatelli J, Xiong Y. Structural basis of evasion of cellular adaptive immunity by HIV-1 Nef. *Nat Struct Mol Biol*. 2012;19(7):701-706. doi:10.1038/nsmb.2328
137. Sviridov D, Mukhamedova N, Makarov AA, Adzhubei A, Bukrinsky M. Comorbidities of HIV infection: role of Nef-induced impairment of cholesterol metabolism and lipid raft functionality. *AIDS*. 2020;34(1):1-13. doi:10.1097/QAD.0000000000002385
138. Mujawar Z, Rose H, Morrow MP, et al. Human immunodeficiency virus impairs reverse cholesterol transport from macrophages. Carr A, ed. *PLoS Biol*. 2006;4(11):e365. doi:10.1371/journal.pbio.0040365
139. Jennelle L, Hunegnaw R, Dubrovsky L, et al. HIV-1 protein Nef inhibits activity of ATP-binding cassette transporter A1 by targeting endoplasmic reticulum chaperone calnexin. *J Biol Chem*. 2014;289(42):28870-28884. doi:10.1074/jbc.M114.583591
140. Adzhubei AA, Kulkarni A, Tolstova AP, et al. Direct interaction between ABCA1 and HIV-1 Nef: molecular modeling and virtual screening for inhibitors. *Comput Struct Biotechnol J*. 2021;19:3876-3884. doi:10.1016/j.csbj.2021.06.050

141. Kucera LS, Iyer NP, Puckett SH, et al. Activity of triciribine and triciribine-5' - monophosphate against human immunodeficiency virus types 1 and 2. *AIDS Res Hum Retroviruses*. 1993;9(4):307-314. doi:10.1089/aid.1993.9.307
142. Yang L, Dan HC, Sun M, et al. Akt/protein kinase B signaling inhibitor-2, a selective small molecule inhibitor of Akt signaling with antitumor activity in cancer cells overexpressing Akt. *Cancer Res*. 2004;64(13):4394-4399. doi:10.1158/0008-5472.CAN-04-0343
143. Xue M, Yao S, Hu M, et al. HIV-1 Nef and KSHV oncogene K1 synergistically promote angiogenesis by inducing cellular miR-718 to regulate the PTEN/AKT/mTOR signaling pathway. *Nucleic Acids Res*. 2014;42(15):9862-9879. doi:10.1093/nar/gku583
144. Kumar A, Abbas W, Colin L, et al. Tuning of AKT-pathway by Nef and its blockade by protease inhibitors results in limited recovery in latently HIV infected T-cell line. *Sci Rep*. 2016;6(1):24090. doi:10.1038/srep24090
145. Chang AH, O'Shaughnessy MV, Jirik FR, Hck SH3 domain-dependent abrogation of Nef-induced class I MHC down-regulation. *Eur J Immunol*. 2001;31(8):2382-2387. doi:10.1002/1521-4141(200108)31:8<2382::aid-immu2382>3.0.co;2-k
146. Hiipakka M, Poikonen K, Saksela K. SH3 domains with high affinity and engineered ligand specificities targeted to HIV-1 Nef. *J Mol Biol*. 1999;293(5):1097-1106. doi:10.1006/jmbi.1999.3225
147. Hiipakka M, Huotari P, Manninen A, Renkema GH, Saksela K. Inhibition of cellular functions of HIV-1 Nef by artificial SH3 domains. *Virology*. 2001;286(1):152-159. doi:10.1006/viro.2001.0973
148. Stangler T, Tran T, Hoffmann S, Schmidt H, Jonas E, Willbold D. Competitive displacement of full-length HIV-1 Nef from the Hck SH3 domain by a high-affinity artificial peptide. *Biol Chem*. 2007;388(6):611-615. doi:10.1515/BC.2007.075
149. Fan X, Wei J, Xiong H, et al. A homogeneous time-resolved fluorescence-based high-throughput screening for discovery of inhibitors of Nef-sdAb19 interaction. *Int J Oncol*. 2015;47(4):1485-1493. doi:10.3892/ijo.2015.3132
150. Breuer S, Espinola S, Morelli X, Torbett BE, Arold ST, Engels IH. A biochemical/biophysical assay dyad for HTS-compatible triaging of inhibitors of the HIV-1 Nef/Hck SH3 interaction. *Curr Chem Genomics Transl Med*. 2013;7:16-20. doi:10.2174/2213988501307010016
151. Craik DJ, Fairlie DP, Liras S, Price D. The Future of Peptide-based Drugs: Peptides in Drug Development. *Chem Biol Drug Des*. 2013;81(1):136-147. doi:10.1111/cbdd.12055

152. Henninot A, Collins JC, Nuss JM. The Current State of Peptide Drug Discovery: Back to the Future? *J Med Chem*. 2018;61(4):1382-1414. doi:10.1021/acs.jmedchem.7b00318
153. Diao L, Meibohm B. Pharmacokinetics and Pharmacokinetic–Pharmacodynamic Correlations of Therapeutic Peptides. *Clin Pharmacokinet*. 2013;52(10):855-868. doi:10.1007/s40262-013-0079-0
154. Vagner J, Qu H, Hraby VJ. Peptidomimetics, a synthetic tool of drug discovery. *Curr Opin Chem Biol*. 2008;12(3):292-296. doi:10.1016/j.cbpa.2008.03.009
155. Lenci E, Trabocchi A. Peptidomimetic toolbox for drug discovery. *Chem Soc Rev*. 2020;49(11):3262-3277. doi:10.1039/D0CS00102C
156. Mcgregor D. Discovering and improving novel peptide therapeutics. *Curr Opin Pharmacol*. 2008;8(5):616-619. doi:10.1016/j.coph.2008.06.002
157. Choudhary A, Raines RT. An Evaluation of Peptide-Bond Isosteres. *ChemBioChem*. 2011;12(12):1801-1807. doi:10.1002/cbic.201100272
158. Mahanta N, Szantai-Kis DM, Petersson EJ, Mitchell DA. Biosynthesis and Chemical Applications of Thioamides. *ACS Chem Biol*. 2019;14(2):142-163. doi:10.1021/acscchembio.8b01022
159. Glendening ED, Hrabal JA. Resonance in Formamide and Its Chalcogen Replacement Analogues: A Natural Population Analysis/Natural Resonance Theory Viewpoint. *J Am Chem Soc*. 1997;119(52):12940-12946. doi:10.1021/ja970074j
160. Truter MR. An accurate determination of the crystal structure of thioacetamide. *J Chem Soc*. 1960:997-1007. doi:10.1039/jr9600000997
161. Dudek EP, Dudek GO. Proton magnetic resonance spectra of thiocarboxamides. *J Org Chem*. 1967;32(3):823-824. doi:10.1021/jo01278a074
162. Hollósi M, Zewdu M, Kollát E, et al. Intramolecular H-bonds and thioamide rotational isomerism in thiopeptides. *Int J Pept Protein Res*. 2009;36(2):173-181. doi:10.1111/j.1399-3011.1990.tb00963.x
163. Wiberg KB, Rush DJ. Solvent Effects on the Thioamide Rotational Barrier: An Experimental and Theoretical Study. *J Am Chem Soc*. 2001;123(9):2038-2046. doi:10.1021/ja003586y
164. Verma H, Khatri B, Chakraborti S, Chatterjee J. Increasing the bioactive space of peptide macrocycles by thioamide substitution. *Chem Sci*. 2018;9(9):2443-2451. doi:10.1039/C7SC04671E



165. Zhang W, Li J, Liu LW, et al. A novel analog of antimicrobial peptide Polybia-MPI, with thioamide bond substitution, exhibits increased therapeutic efficacy against cancer and diminished toxicity in mice. *Peptides*. 2010;31(10):1832-1838. doi:10.1016/j.peptides.2010.06.019
166. Bartlett PA, Spear KL, Jacobsen NE. A thioamide substrate of carboxypeptidase A. *Biochemistry*. 1982;21(7):1608-1611. doi:10.1021/bi00536a022
167. Foje KL, Hanzlik RP. Peptidyl thioamides as substrates and inhibitors of papain, and as probes of the kinetic significance of the oxyanion hole. *Biochim Biophys Acta Gen Subj*. 1994;1201(3):447-453. doi:10.1016/0304-4165(94)90075-2
168. Zacharie B, Lagraoui M, Dimarco M, Penney CL, Gagnon L. Thioamides: Synthesis, Stability, and Immunological Activities of Thioanalogues of Imreg. Preparation of New Thioacylating Agents Using Fluorobenzimidazolone Derivatives. *J Med Chem*. 1999;42(11):2046-2052. doi:10.1021/jm9900467
169. Bach A, Eildal JNN, Stuhr-Hansen N, et al. Cell-Permeable and Plasma-Stable Peptidomimetic Inhibitors of the Postsynaptic Density-95/ N -Methyl- D -Aspartate Receptor Interaction. *J Med Chem*. 2011;54(5):1333-1346. doi:10.1021/jm1013924
170. Chen X, Mietlicki-Baase EG, Barrett TM, et al. Thioamide Substitution Selectively Modulates Proteolysis and Receptor Activity of Therapeutic Peptide Hormones. *J Am Chem Soc*. 2017;139(46):16688-16695. doi:10.1021/jacs.7b08417
171. Schutkowski M, Neubert K, Fischer G. Influence on proline-specific enzymes of a substrate containing the thioxoaminoacyl-prolyl peptide bond. *Eur J Biochem*. 1994;221(1):455-461. doi:10.1111/j.1432-1033.1994.tb18758.x
172. Campbell P, Nashed NT. Carboxypeptidase A catalyzed hydrolysis of thiopeptide and thioester analogs of specific substrates. An effect on kcat for peptide, but not ester, substrates. *J Am Chem Soc*. 1982;104(19):5221-5226. doi:10.1021/ja00383a038
173. Jagodziński TS. Thioamides as Useful Synthons in the Synthesis of Heterocycles. *Chem Rev*. 2003;103(1):197-228. doi:10.1021/cr0200015
174. Miller M, Schneider J, Sathyanarayana BK, et al. Structure of Complex of Synthetic HIV-1 Protease with a Substrate-Based Inhibitor at 2.3 Å Resolution. *Science*. 1989;246(4934):1149-1152. doi:10.1126/science.2686029
175. Coburn CA, Stachel SJ, Jones KG, et al. BACE-1 inhibition by a series of  $\psi$ [CH<sub>2</sub>NH] reduced amide isosteres. *Bioorg Med Chem Lett*. 2006;16(14):3635-3638. doi:10.1016/j.bmcl.2006.04.076
176. Szelke M, Leckie B, Hallett A, et al. Potent new inhibitors of human renin. *Nature*. 1982;299(5883):555-557. doi:10.1038/299555a0

177. Zivec M, Jakopin Z, Gobec S. Recent Advances in the Synthesis and Applications of Reduced Amide Pseudopeptides. *Curr Med Chem*. 2009;16(18):2289-2304. doi:10.2174/092986709788453113
178. Rautio J, Kumpulainen H, Heimbach T, et al. Prodrugs: design and clinical applications. *Nat Rev Drug Discov*. 2008;7(3):255-270. doi:10.1038/nrd2468
179. Brinckerhoff LH, Kalashnikov VV, Thompson LW, et al. Terminal modifications inhibit proteolytic degradation of an immunogenic mart-127-35 peptide: Implications for peptide vaccines. *Int J Cancer*. 1999;83(3):326-334. doi:10.1002/(SICI)1097-0215(19991029)83:3<326::AID-IJC7>3.0.CO;2-X
180. Fleming FF, Yao L, Ravikumar PC, Funk L, Shook BC. Nitrile-Containing Pharmaceuticals: Efficacious Roles of the Nitrile Pharmacophore. *J Med Chem*. 2010;53(22):7902-7917. doi:10.1021/jm100762r
181. Owen DR, Allerton CMN, Anderson AS, et al. An oral SARS-CoV-2 M<sup>pro</sup> inhibitor clinical candidate for the treatment of COVID-19. *Science*. 2021;374(6575):1586-1593. doi:10.1126/science.abl4784
182. Lassalas P, Gay B, Lasfargeas C, et al. Structure Property Relationships of Carboxylic Acid Isosteres. *J Med Chem*. 2016;59(7):3183-3203. doi:10.1021/acs.jmedchem.5b01963
183. Herr RJ. 5-Substituted-1H-tetrazoles as carboxylic acid isosteres: medicinal chemistry and synthetic methods. *Bioorg Med Chem*. 2002;10(11):3379-3393. doi:10.1016/S0968-0896(02)00239-0
184. Holland GF, Pereira JN. Heterocyclic Tetrazoles, a New Class of Lipolysis Inhibitors. *J Med Chem*. 1967;10(2):149-154. doi:10.1021/jm00314a004
185. Figdor SK, von Wittenau MSchach. Metabolism of 5-(3-Pyridyl)tetrazole. *J Med Chem*. 1967;10(6):1158-1159. doi:10.1021/jm00318a038
186. Beaudreau JL, Blais V, Holleran BJ, et al. N-Guanidyl and C-Tetrazole Leu-Enkephalin Derivatives: Efficient Mu and Delta Opioid Receptor Agonists with Improved Pharmacological Properties. *ACS Chem Neurosci*. 2019;10(3):1615-1626. doi:10.1021/acschemneuro.8b00550
187. Liljebris C, Larsen SD, Ogg D, Palazuk BJ, Bleasdale JE. Investigation of Potential Bioisosteric Replacements for the Carboxyl Groups of Peptidomimetic Inhibitors of Protein Tyrosine Phosphatase 1B: Identification of a Tetrazole-Containing Inhibitor with Cellular Activity. *J Med Chem*. 2002;45(9):1785-1798. doi:10.1021/jm011100y
188. Subirós-Funosas R, Prohens R, Barbas R, El-Faham A, Albericio F. Oxyma: An Efficient Additive for Peptide Synthesis to Replace the Benzotriazole-Based HOBT

- and HOAt with a Lower Risk of Explosion. *Chemistry*. 2009;15(37):9394-9403. doi:10.1002/chem.200900614
189. Subirós-Funosas R, El-Faham A, Albericio F. Low-epimerization Peptide Bond Formation with Oxyma Pure: Preparation of Z-L-Phg-Val-OMe. *Org Synth*. 2013;90:306. doi:10.15227/orgsyn.090.0306
190. Carpino LA. Methyl ester nonequivalence in the <sup>1</sup>H NMR spectra of diastereomeric dipeptide esters incorporating N-terminal .alpha.-phenylglycine units. *J Org Chem*. 1988;53(4):875-878. doi:10.1021/jo00239a037
191. Yabuuchi T, Kusumi T. Phenylglycine Methyl Ester, a Useful Tool for Absolute Configuration Determination of Various Chiral Carboxylic Acids. *J Org Chem*. 2000;65(2):397-404. doi:10.1021/jo991218a
192. Campagna F, Carotti A, Casini G. A convenient synthesis of nitriles from primary amides under mild conditions. *Tetrahedron Lett*. 1977;18(21):1813-1815. doi:10.1016/S0040-4039(01)83612-1
193. Cianni L, Lemke C, Gilberg E, et al. Mapping the S1 and S1' subsites of cysteine proteases with new dipeptidyl nitrile inhibitors as trypanocidal agents. Almeida IC, ed. *PLoS Negl Trop Dis*. 2020;14(3):e0007755. doi:10.1371/journal.pntd.0007755
194. Roh J, Vávrová K, Hrabálek A. Synthesis and Functionalization of 5-Substituted Tetrazoles. *Eur J Org Chem*. 2012;2012(31):6101-6118. doi:10.1002/ejoc.201200469
195. Demko ZP, Sharpless KB. Preparation of 5-Substituted 1H-Tetrazoles from Nitriles in Water. *J Org Chem*. 2001;66(24):7945-7950. doi:10.1021/jo010635w
196. Demko ZP, Sharpless KB. An Expedient Route to the Tetrazole Analogues of  $\alpha$ -Amino Acids. *Org Lett*. 2002;4(15):2525-2527. doi:10.1021/ol020096x
197. Finnegan WG, Henry RA, Lofquist R. An Improved Synthesis of 5-Substituted Tetrazoles. *J Am Chem Soc*. 1958;80(15):3908-3911. doi:10.1021/ja01548a028
198. Treitler DS, Leung S, Lindrud M. Development and Demonstration of a Safer Protocol for the Synthesis of 5-Aryltetrazoles from Aryl Nitriles. *Org Process Res Dev*. 2017;21(3):460-467. doi:10.1021/acs.oprd.7b00016
199. Koguro K, Oga T, Mitsui S, Orita R. Novel Synthesis of 5-Substituted Tetrazoles from Nitriles. *Synthesis*. 1998;1998(06):910-914. doi:10.1055/s-1998-2081
200. Manzor K, Kelleher F. Synthesis of orthogonally protected thioamide dipeptides for use in solid-phase peptide synthesis. *Tetrahedron Lett*. 2016;57(47):5237-5239. doi:10.1016/j.tetlet.2016.10.036

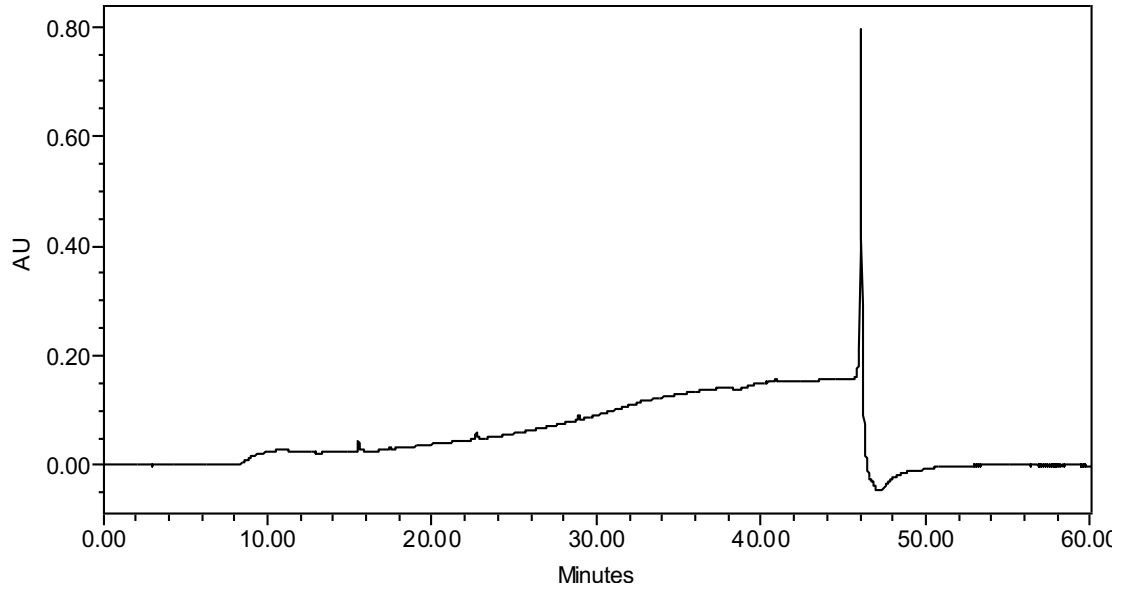
201. Panduranga V, Prabhu G, Kumar L. R, Krishnamurthy M, Sureshababu VV. Thionation of di and tripeptides employing thiourea as a sulphur transfer reagent. *RSC Adv.* 2016;6(100):98141-98146. doi:10.1039/C6RA18639D
202. Curphey TJ. Thionation with the Reagent Combination of Phosphorus Pentasulfide and Hexamethyldisiloxane. *J Org Chem.* 2002;67(18):6461-6473. doi:10.1021/jo0256742
203. Ozturk T, Ertas E, Mert O. A Berzelius Reagent, Phosphorus Decasulfide (P<sub>4</sub>S<sub>10</sub>), in Organic Syntheses. *Chem Rev.* 2010;110(6):3419-3478. doi:10.1021/cr900243d
204. Ozturk T, Ertas E, Mert O. Use of Lawesson's Reagent in Organic Syntheses. *Chem Rev.* 2007;107(11):5210-5278. doi:10.1021/cr040650b
205. Bergman J, Pettersson B, Hasimbegovic V, Svensson PH. Thionations Using a P<sub>4</sub>S<sub>10</sub>-Pyridine Complex in Solvents Such as Acetonitrile and Dimethyl Sulfone. *J Org Chem.* 2011;76(6):1546-1553. doi:10.1021/jo101865y
206. Brillon D. *In Situ* Reagents For Thionation of Amides, Peptides and Lactams. *Synth Commun.* 1990;20(19):3085-3095. doi:10.1080/00397919008051529
207. Guzic FS, Wasmund LM. An improved method for the preparation of desoxopeptides—reductions of endotheiopeptides. *Tetrahedron Lett.* 1990;31(1):23-26. doi:10.1016/S0040-4039(00)94324-7
208. Morreale FE, Testa A, Chaugule VK, Bortoluzzi A, Ciulli A, Walden H. Mind the Metal: A Fragment Library-Derived Zinc Impurity Binds the E2 Ubiquitin-Conjugating Enzyme Ube2T and Induces Structural Rearrangements. *J Med Chem.* 2017;60(19):8183-8191. doi:10.1021/acs.jmedchem.7b01071
209. Hermann JC, Chen Y, Wartchow C, et al. Metal Impurities Cause False Positives in High-Throughput Screening Campaigns. *ACS Med Chem Lett.* 2013;4(2):197-200. doi:10.1021/ml3003296
210. Weirath NA, Hurben AK, Chao C, et al. Small Molecule Inhibitors of TET Dioxygenases: Bobcat339 Activity Is Mediated by Contaminating Copper(II). *ACS Med Chem Lett.* 2022;13(5):792-798. doi:10.1021/acsmchemlett.1c00677
211. Sureshababu VV, Venkataramanarao R, Naik SA, Chennakrishnareddy G. Synthesis of tetrazole analogues of amino acids using Fmoc chemistry: isolation of amino free tetrazoles and their incorporation into peptides. *Tetrahedron Lett.* 2007;48(39):7038-7041. doi:10.1016/j.tetlet.2007.07.129
212. Shibahara F, Sugiura R, Murai T. Direct Thionation and Selenation of Amides Using Elemental Sulfur and Selenium and Hydrochlorosilanes in the Presence of Amines. *Org Lett.* 2009;11(14):3064-3067. doi:10.1021/o19010882

213. Poupaert J, Carato P, McCurdy C. A Simple and Effective Method for the Thionation of Amides to Thioamides Using Al<sub>2</sub>O<sub>3</sub>-Supported P<sub>4</sub>S<sub>10</sub>. *Lett Org Chem*. 2005;2(4):330-333. doi:10.2174/1570178054038957
214. Lajoie G, Lépine F, Maziak L, Belleau B. Facile regioselective formation of thiopeptide linkages from oligopeptides with new thionation reagents. *Tetrahedron Lett*. 1983;24(36):3815-3818. doi:10.1016/S0040-4039(00)94282-5
215. Khatri B, Bhat P, Chatterjee J. Convenient synthesis of thioamidated peptides and proteins. *J Pept Sci*. 2020;26(4-5). doi:10.1002/psc.3248
216. Shalaby MA, Grote CW, Rapoport H. Thiopeptide Synthesis.  $\alpha$ -Amino Thionoacid Derivatives of Nitrobenzotriazole as Thioacylating Agents. *J Org Chem*. 1996;61(25):9045-9048. doi:10.1021/jo961245q
217. Kingi N, Bergman J. Thionation of Tryptanthrin, Rutaecarpine, and Related Molecules with a Reagent Prepared from P<sub>4</sub>S<sub>10</sub> and Pyridine. *J Org Chem*. 2016;81(17):7711-7716. doi:10.1021/acs.joc.6b01346
218. Mukherjee S, Chatterjee J. Suppressing the epimerization of endothioamide peptides during Fmoc/*t*-Bu-based solid phase peptide synthesis: Suppressing the Epimerization of Endothioamide Peptides. *J Pept Sci*. 2016;22(11-12):664-672. doi:10.1002/psc.2929
219. Camacho LA, Lampkin BJ, VanVeller B. A Bottom-Up Approach To Preserve Thioamide Residue Stereochemistry during Fmoc Solid-Phase Peptide Synthesis. *Org Lett*. 2019;21(17):7015-7018. doi:10.1021/acs.orglett.9b02598
220. Kornfeld EC. Raney Nickel Hydrogenolysis of Thioamides: A New Amine Synthesis. *J Org Chem*. 1951;16(1):131-138. doi:10.1021/jo01141a020
221. Roeske RW, Weitzl FL, Prasad KU, Thompson RM. Selective reduction of the amide carbonyl group in dipeptides by borane. *J Org Chem*. 1976;41(7):1260-1261. doi:10.1021/jo00869a041
222. Sharma A, Kumar A, Abdel Monaim SAH, et al. *N*-methylation in amino acids and peptides: Scope and limitations. *Biopolymers*. 2018;109(10):e23110. doi:10.1002/bip.23110
223. Ghosh AK, Brindisi M. Organic Carbamates in Drug Design and Medicinal Chemistry. *J Med Chem*. 2015;58(7):2895-2940. doi:10.1021/jm501371s
224. Varma MVS, Feng B, Obach RS, et al. Physicochemical Determinants of Human Renal Clearance. *J Med Chem*. 2009;52(15):4844-4852. doi:10.1021/jm900403j
225. Naylor MR, Ly AM, Handford MJ, et al. Lipophilic Permeability Efficiency Reconciles the Opposing Roles of Lipophilicity in Membrane Permeability and

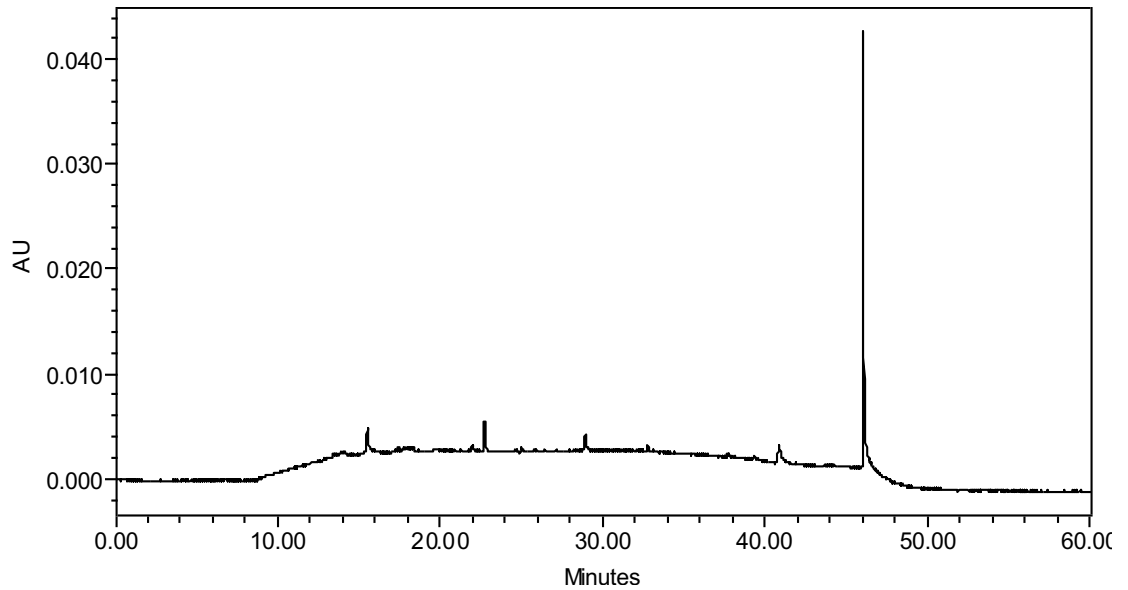
- Aqueous Solubility. *J Med Chem.* 2018;61(24):11169-11182.  
doi:10.1021/acs.jmedchem.8b01259
226. Subbaiah MAM, Meanwell NA. Bioisosteres of the Phenyl Ring: Recent Strategic Applications in Lead Optimization and Drug Design. *J Med Chem.* 2021;64(19):14046-14128. doi:10.1021/acs.jmedchem.1c01215
227. Fang Z, Song Y, Zhan P, Zhang Q, Liu X. Conformational restriction: an effective tactic in 'follow-on'-based drug discovery. *Future Med Chem.* 2014;6(8):885-901. doi:10.4155/fmc.14.50
228. Dixon AS, Schwinn MK, Hall MP, et al. NanoLuc Complementation Reporter Optimized for Accurate Measurement of Protein Interactions in Cells. *ACS Chem Biol.* 2016;11(2):400-408. doi:10.1021/acscchembio.5b00753
229. Di L, Kerns EH, Hong Y, Chen H. Development and application of high throughput plasma stability assay for drug discovery. *Int J Pharm.* 2005;297(1-2):110-119. doi:10.1016/j.ijpharm.2005.03.022

# Appendices

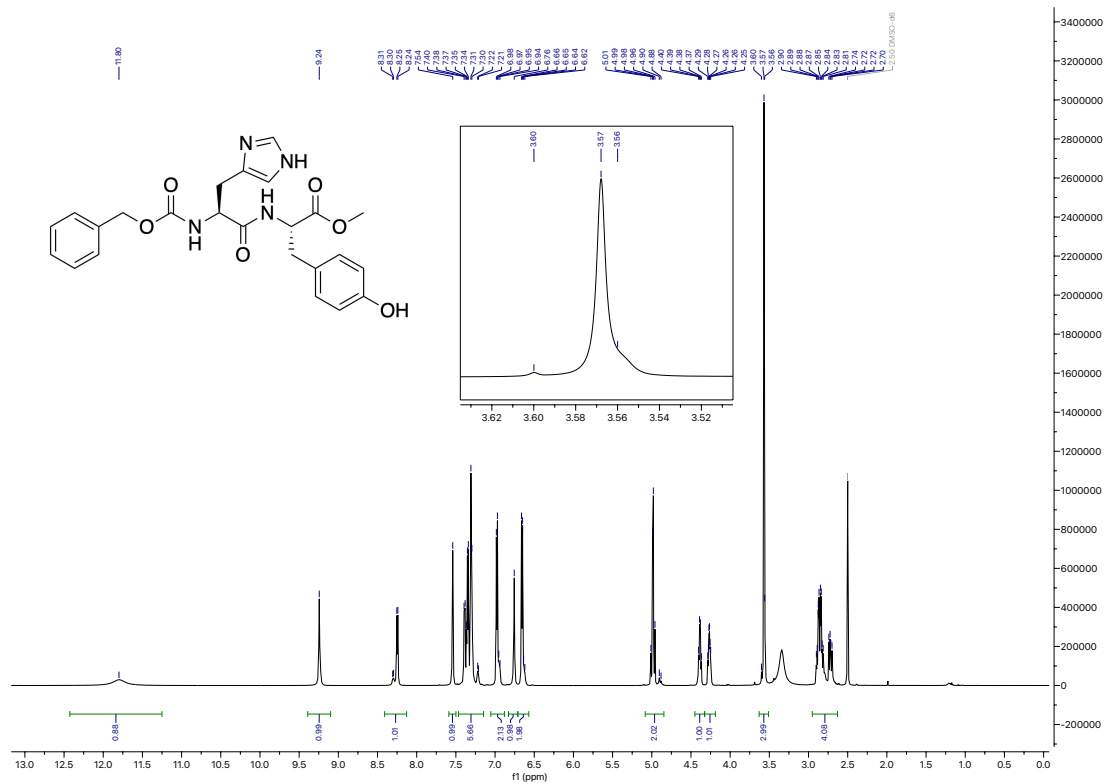
## A



## B

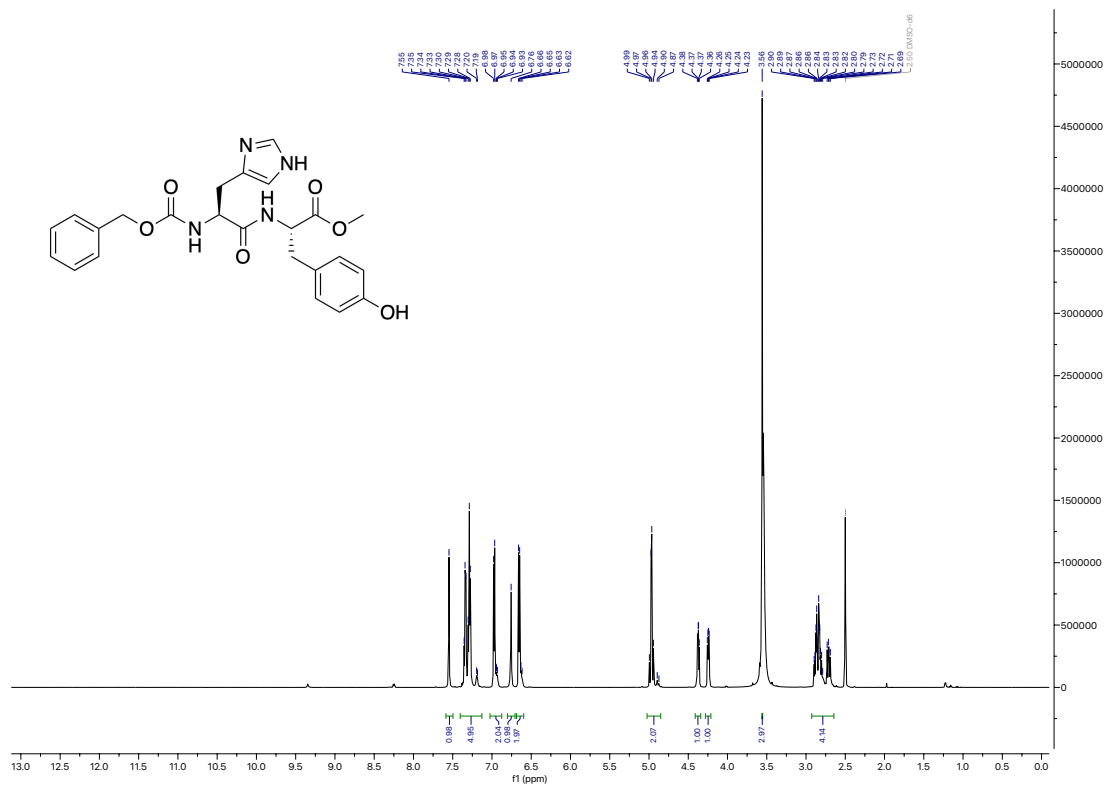


**Appendix 1. Baseline RP-HPLC chromatograms.** Chromatograms are representative of three independent injections ( $N = 3$ ). **A)** Monitoring at  $\lambda = 220$  nm. **B)** Monitoring at  $\lambda = 275$  nm.

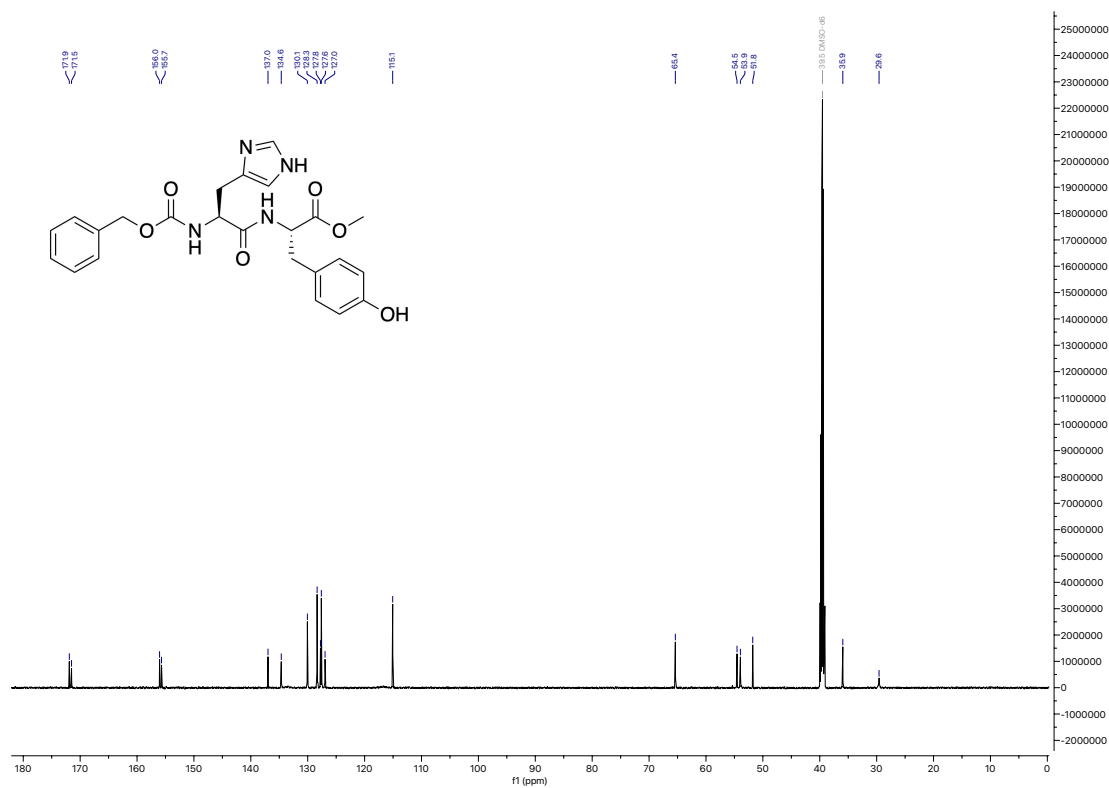


**Appendix 2.** <sup>1</sup>H NMR spectrum of H3-1 methyl ester (H3-1M) in DMSO-*d*<sub>6</sub>. Inset: magnification of the methyl ester proton peak ( $\delta$  3.57), highlighting a trace presence of the *D,L* diastereomer ( $\delta$  3.60, 1.9%).





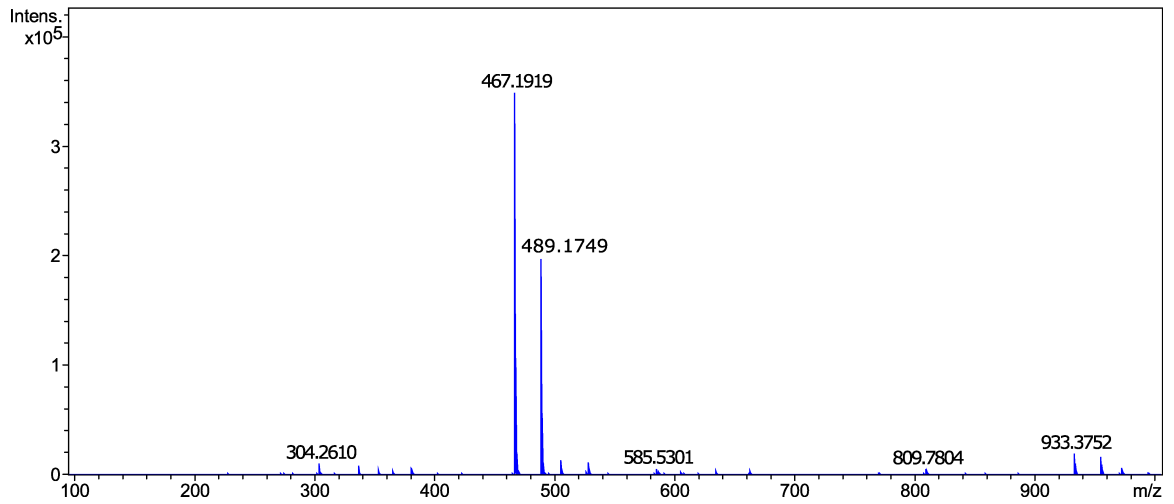
**Appendix 3. <sup>1</sup>H NMR spectrum of H3-1 methyl ester (H3-1M) in DMSO-*d*<sub>6</sub> with the addition of D<sub>2</sub>O.**



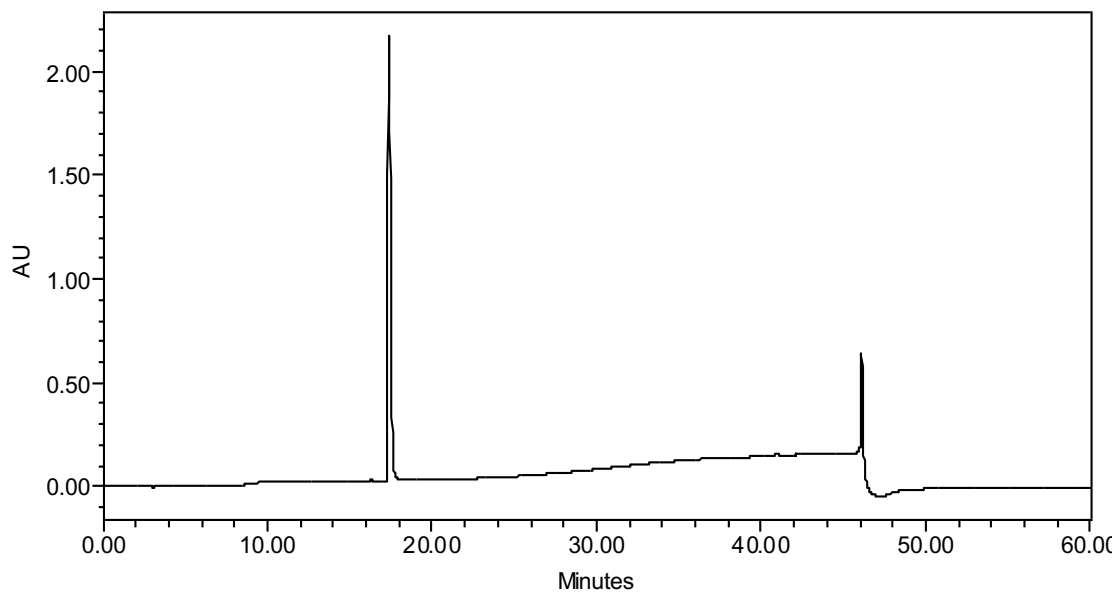
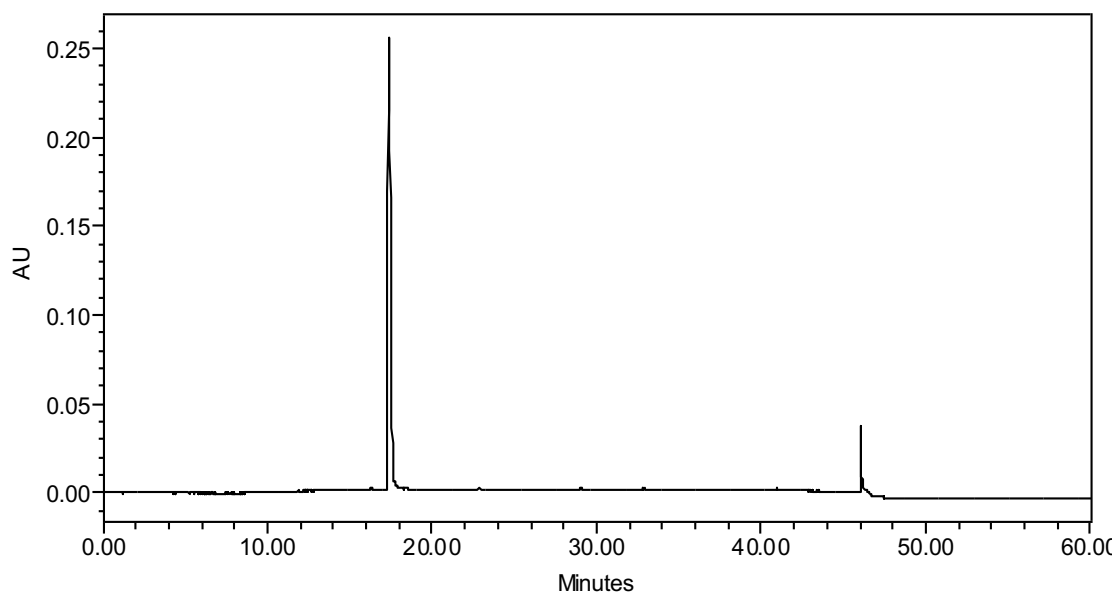
Appendix 4.  $^{13}\text{C}\{^1\text{H}\}$  NMR spectrum of H3-1 methyl ester (H3-1M) in  $\text{DMSO-}d_6$ .

**Acquisition Parameter**

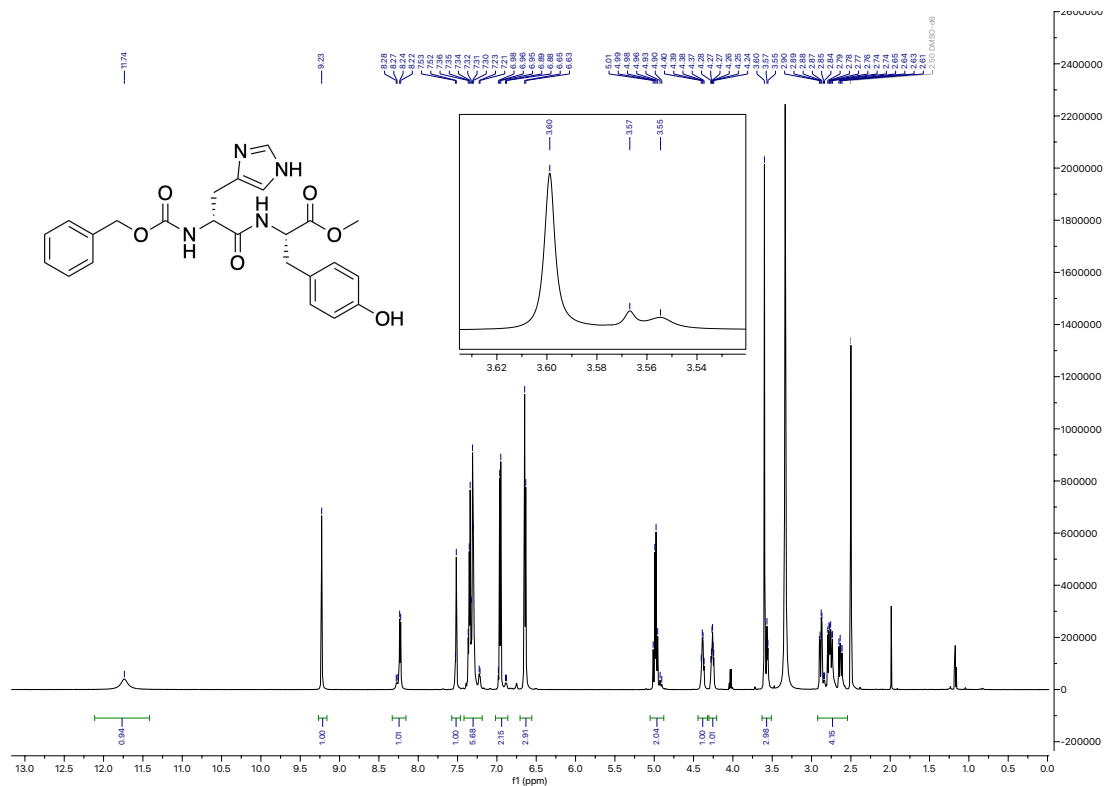
Source Type	ESI	Ion Polarity	Positive	Set Nebulizer	2.0 Bar
Focus	Active			Set Dry Heater	100 °C
Scan Begin	100 m/z	Set Capillary	5000 V	Set Dry Gas	6.0 l/min
Scan End	1000 m/z	Set End Plate Offset	-500 V	Set Divert Valve	Source



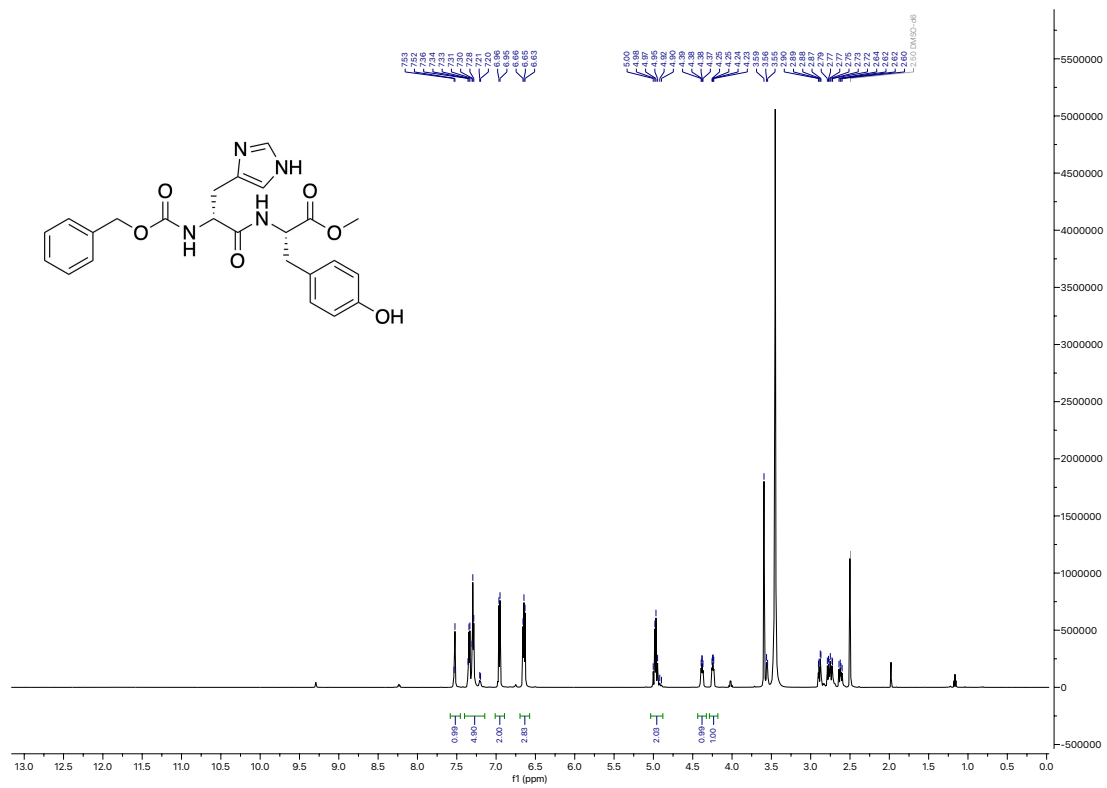
**Appendix 5. ESI-TOF MS of H3-1 methyl ester (H3-1M).**

**A****B**

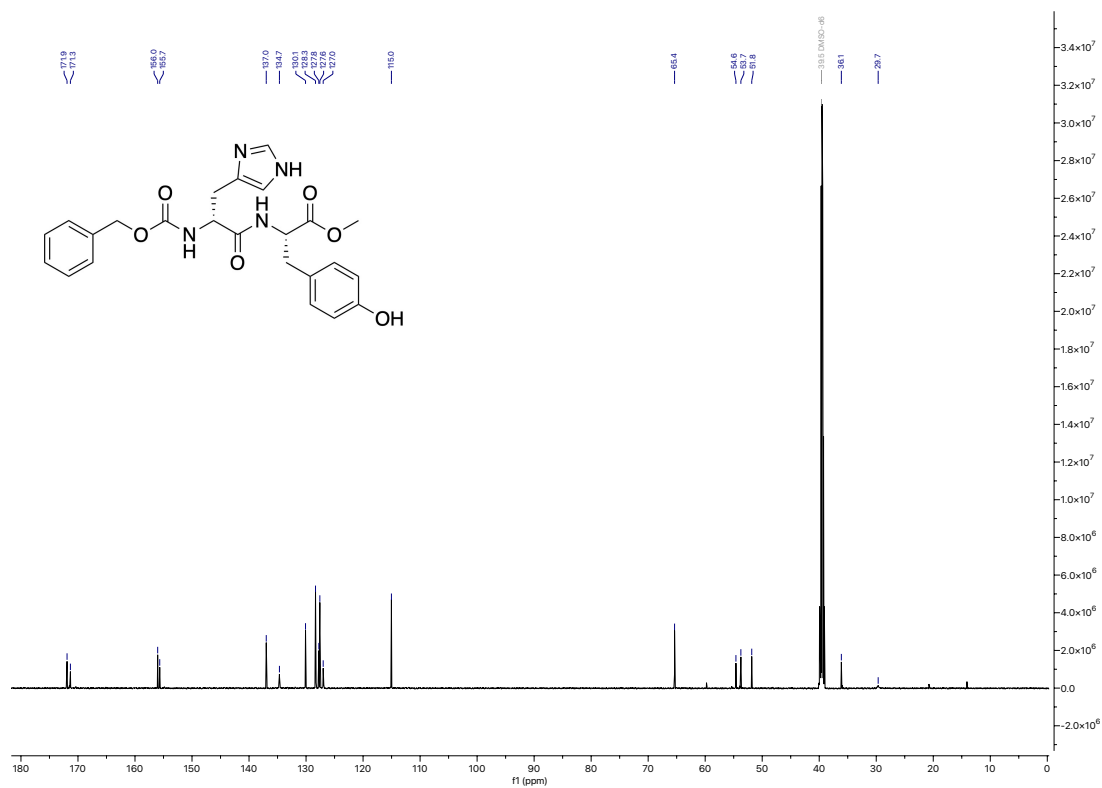
**Appendix 6. RP-HPLC chromatograms of H3-1 methyl ester (H3-1M).** Chromatograms are representative of three independent injections (N = 3). **A)** Monitoring at  $\lambda = 220$  nm. **B)** Monitoring at  $\lambda = 275$  nm.



**Appendix 7. <sup>1</sup>H NMR spectrum of *D,L*-H3-1 methyl ester (*D,L*-H3-1M) in DMSO-*d*<sub>6</sub>.**  
 Inset: magnification of the methyl ester proton peak (δ 3.60), highlighting a presence of the *L,L* diastereomer (δ 3.57, 9.8%).



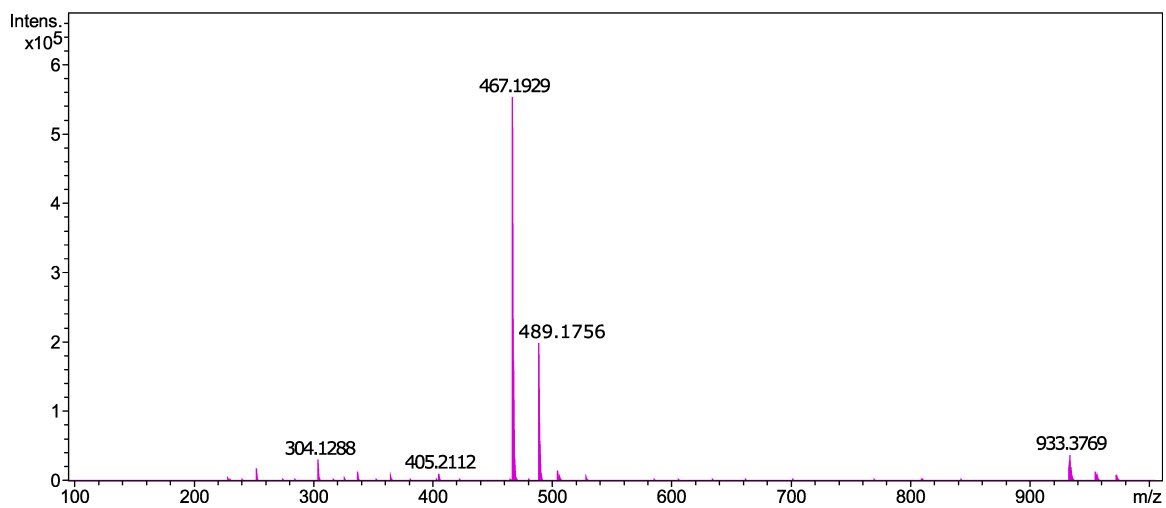
Appendix 8. <sup>1</sup>H NMR spectrum of *D,L*-H3-1 methyl ester (*D,L*-H3-1M) in DMSO-*d*<sub>6</sub> with the addition of D<sub>2</sub>O.



**Appendix 9.**  $^{13}\text{C}\{^1\text{H}\}$  NMR spectrum of *D,L*-H3-1 methyl ester (*D,L*-H3-1M) in  $\text{DMSO-}d_6$ .

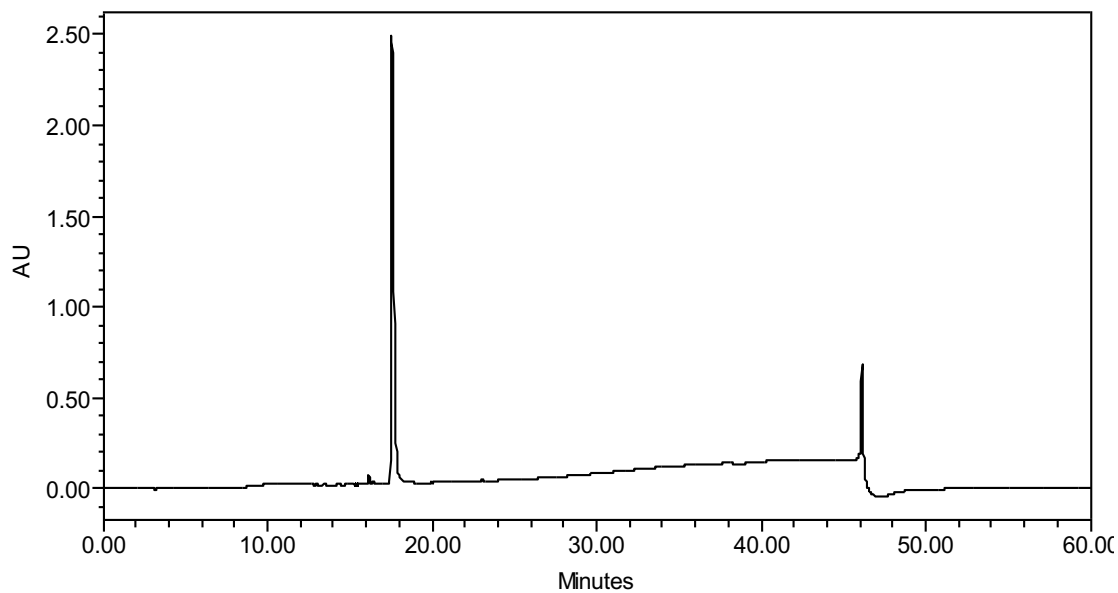
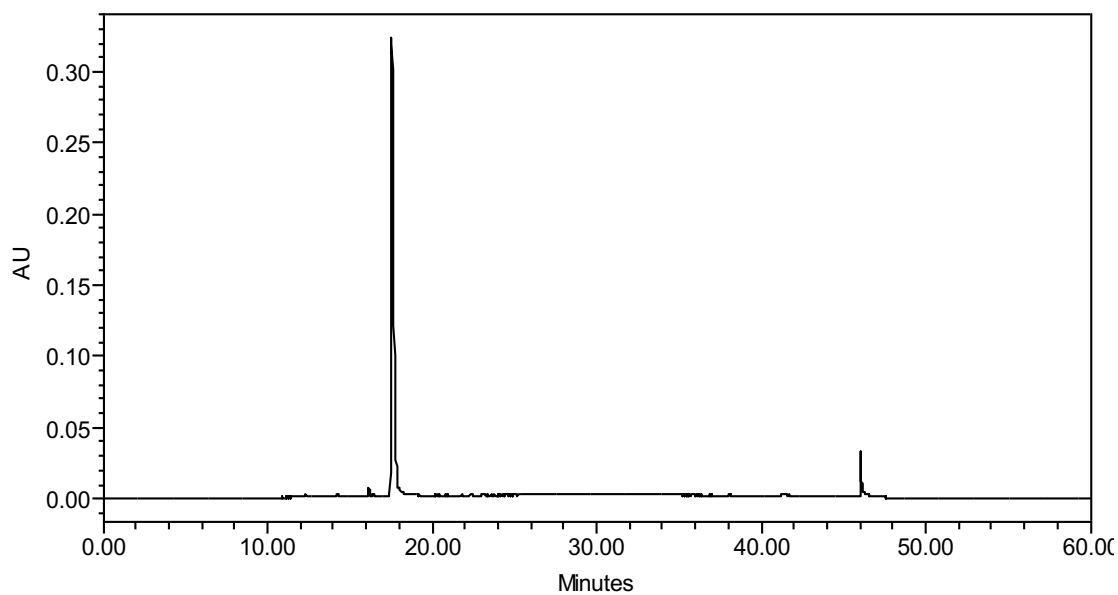
**Acquisition Parameter**

Source Type	ESI	Ion Polarity	Positive	Set Nebulizer	2.0 Bar
Focus	Active			Set Dry Heater	100 °C
Scan Begin	100 m/z	Set Capillary	5000 V	Set Dry Gas	6.0 l/min
Scan End	1000 m/z	Set End Plate Offset	-500 V	Set Divert Valve	Source

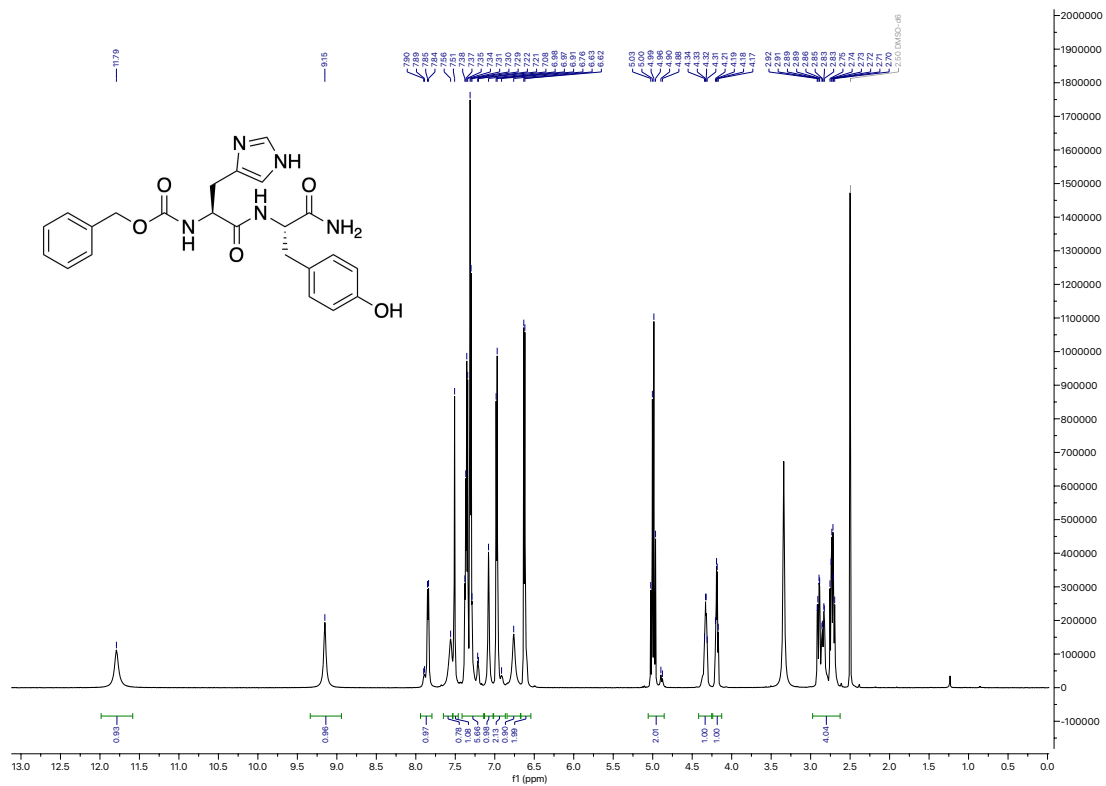


**Appendix 10. ESI-TOF MS of *D,L*-H3-1 methyl ester (*D,L*-H3-1M).**

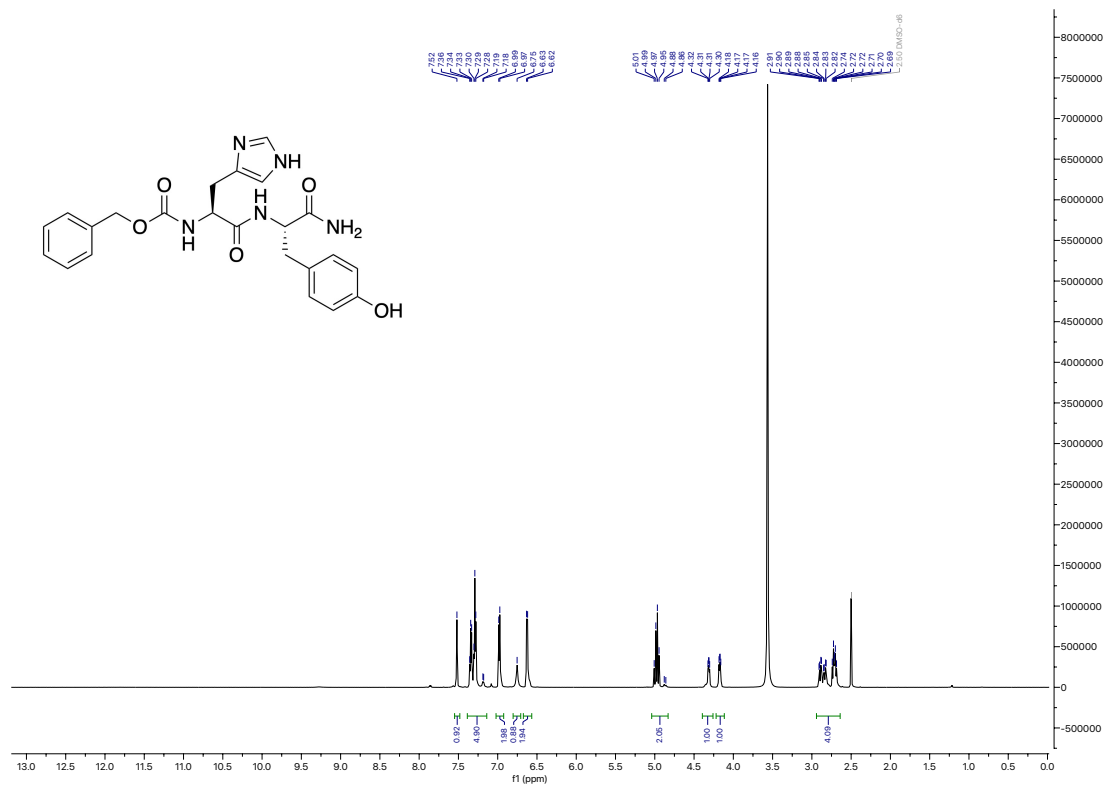


**A****B**

**Appendix 11. RP-HPLC chromatograms of *D,L*-H3-1 methyl ester (*D,L*-H3-1M).** Chromatograms are representative of three independent injections (N = 3). **A)** Monitoring at  $\lambda = 220$  nm. **B)** Monitoring at  $\lambda = 275$  nm.



Appendix 12. <sup>1</sup>H NMR spectrum of H3-1 C-terminal amide (H3-1A) in DMSO-d<sub>6</sub>.



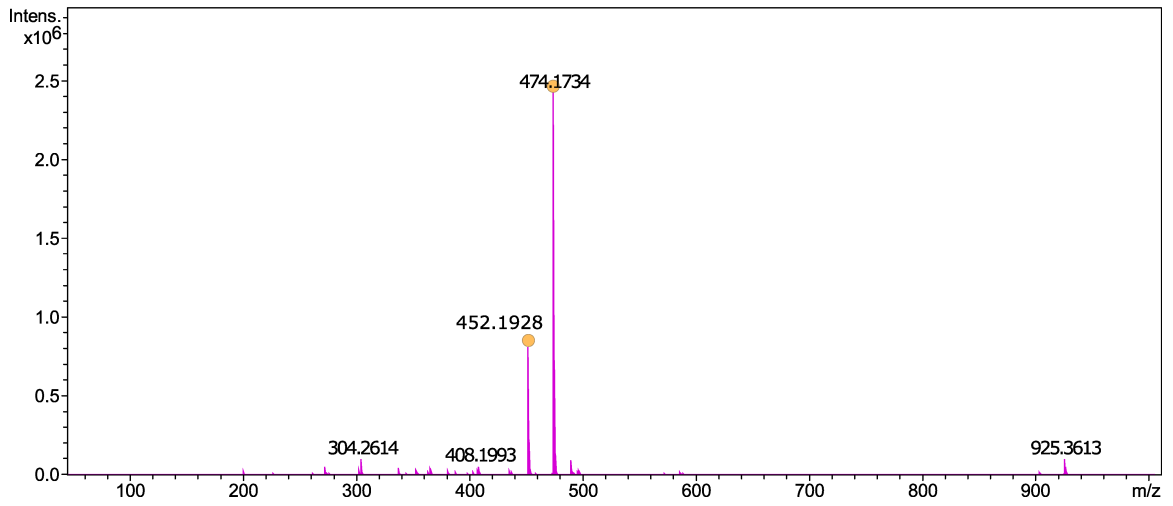
**Appendix 13. <sup>1</sup>H NMR spectrum of H3-1 C-terminal amide (H3-1A) in DMSO-*d*<sub>6</sub> with the addition of D<sub>2</sub>O.**



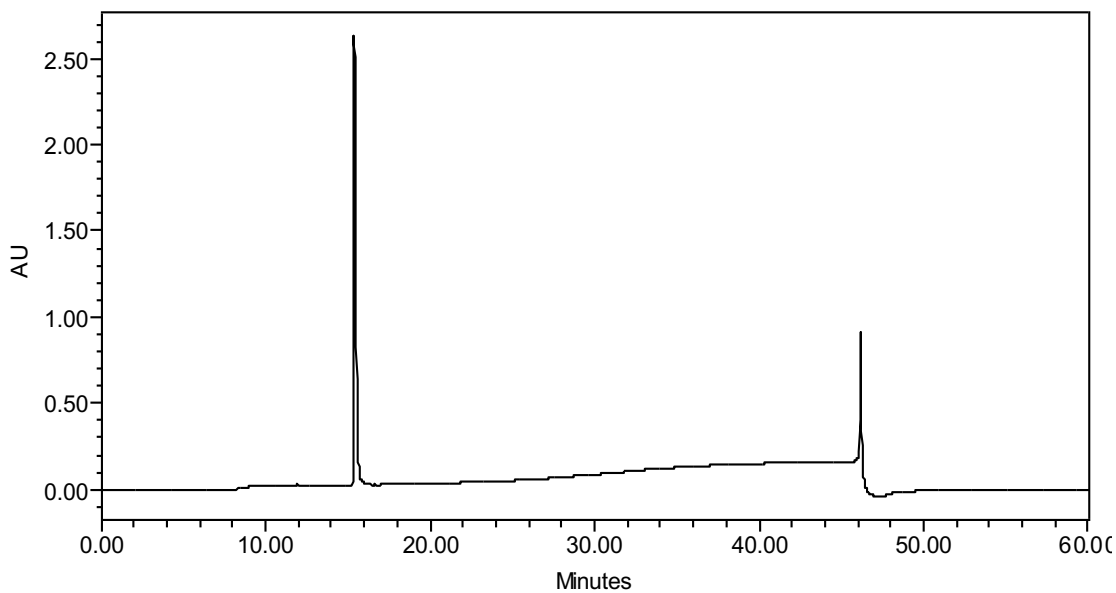
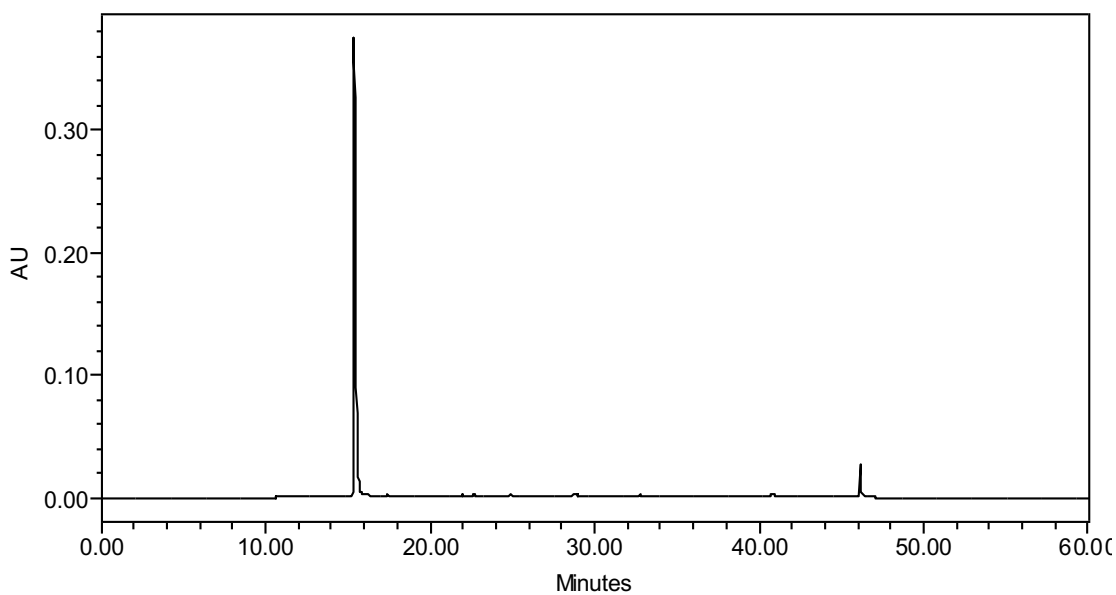
**Appendix 14.  $^{13}\text{C}\{^1\text{H}\}$  NMR spectrum of H3-1 C-terminal amide (H3-1A) in  $\text{DMSO-}d_6$ .**

**Acquisition Parameter**

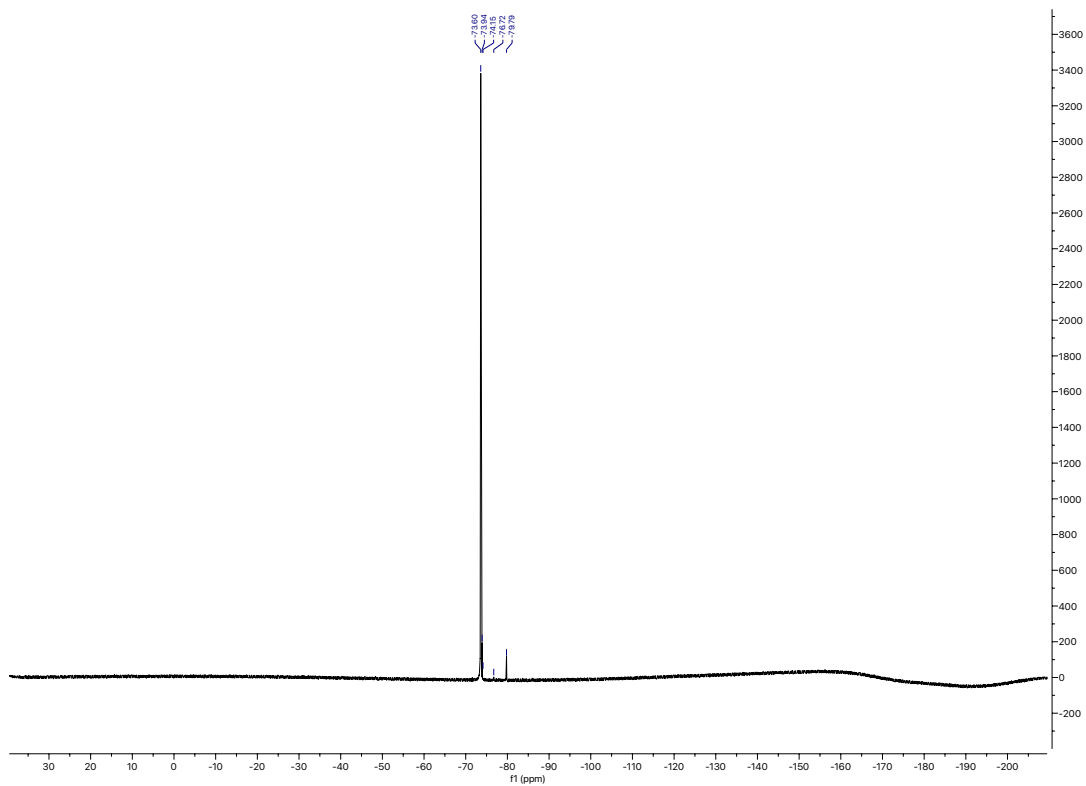
Source Type	ESI	Ion Polarity	Positive	Set Nebulizer	2.1 Bar
Focus	Active			Set Dry Heater	200 °C
Scan Begin	50 m/z	Set Capillary	3000 V	Set Dry Gas	5.0 l/min
Scan End	1000 m/z	Set End Plate Offset	-500 V	Set Divert Valve	Source



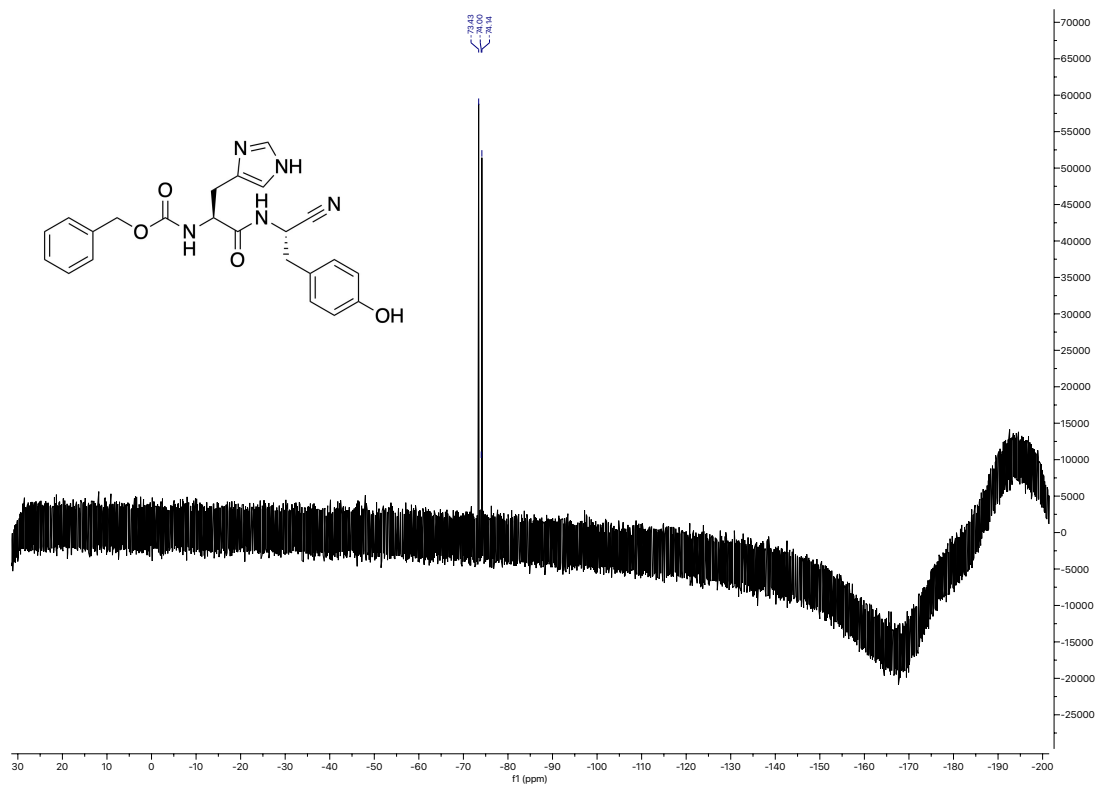
**Appendix 15. ESI-TOF MS of H3-1 C-terminal amide (H3-1A).**

**A****B**

**Appendix 16. RP-HPLC chromatograms of H3-1 C-terminal amide (H3-1A).** Chromatograms are representative of three independent injections (N = 3). **A)** Chromatogram monitoring at  $\lambda = 220$  nm. **B)** Chromatogram monitoring at  $\lambda = 275$  nm.

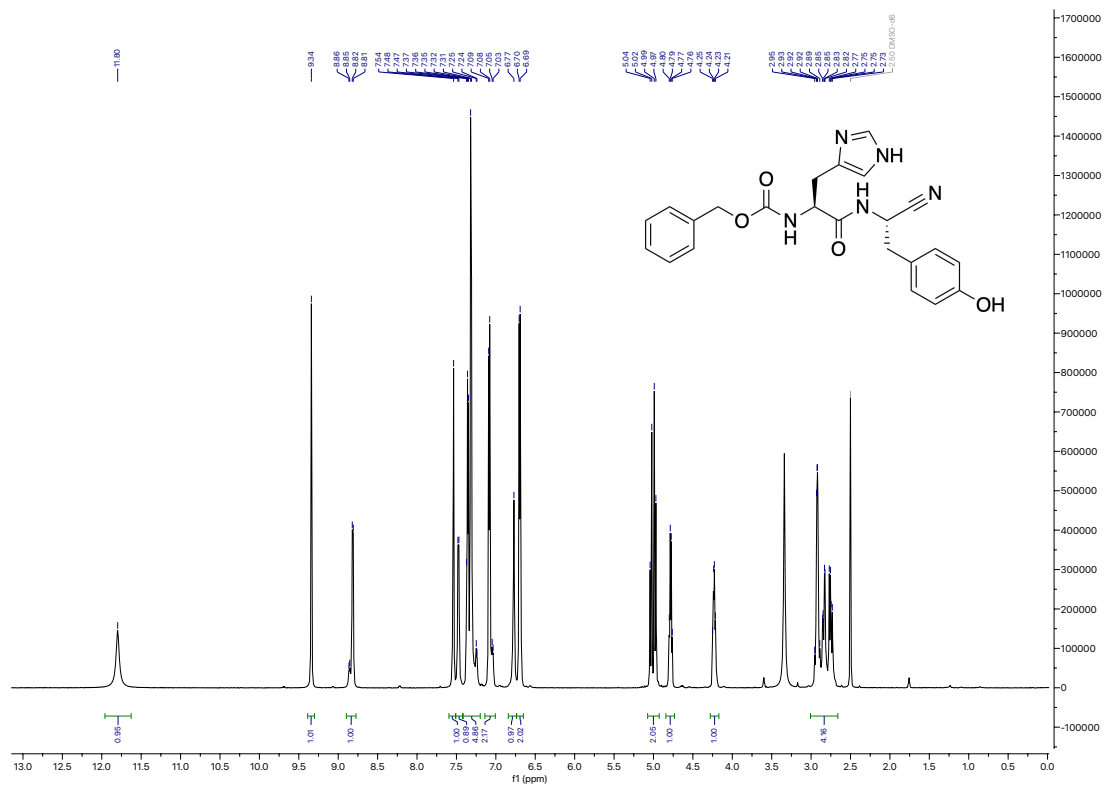


**Appendix 17.  $^{19}\text{F}$  NMR spectrum of H3-1 nitrile (H3-1N) in  $\text{DMSO-}d_6$  without treatment with base.**

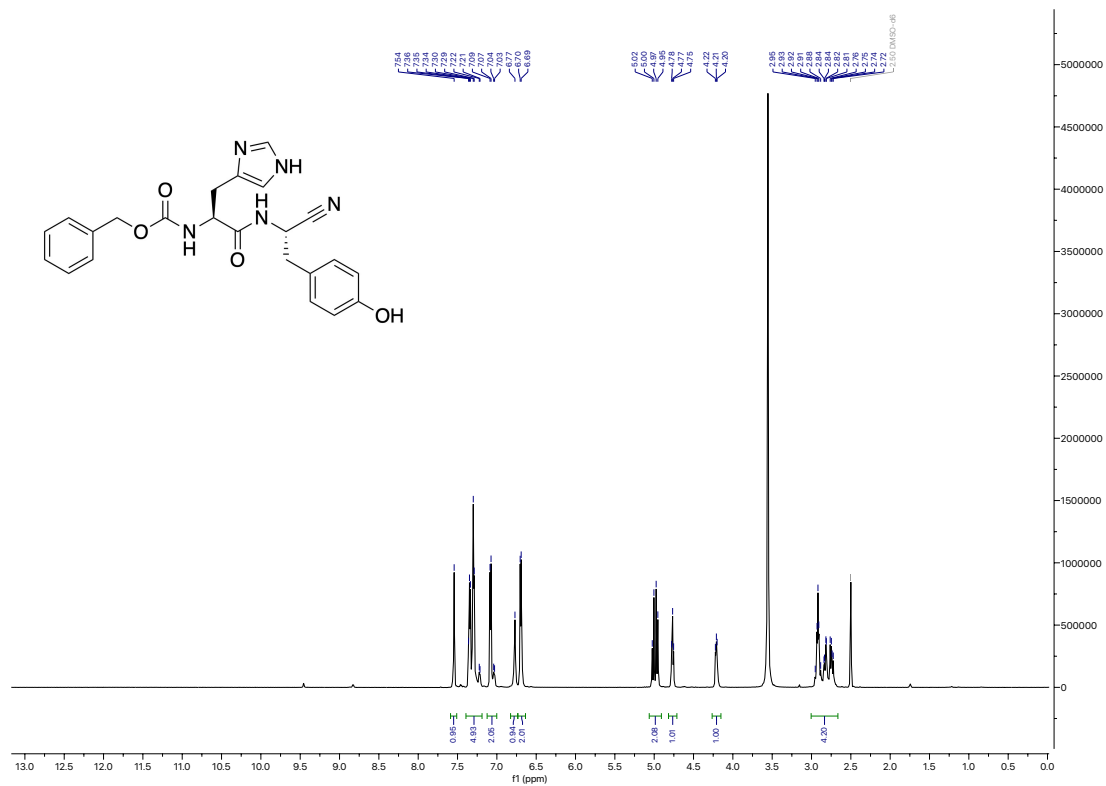


**Appendix 18.  $^{19}\text{F}$  NMR spectrum of H3-1 nitrile (H3-1N) in  $\text{DMSO-}d_6$  following treatment with base.**

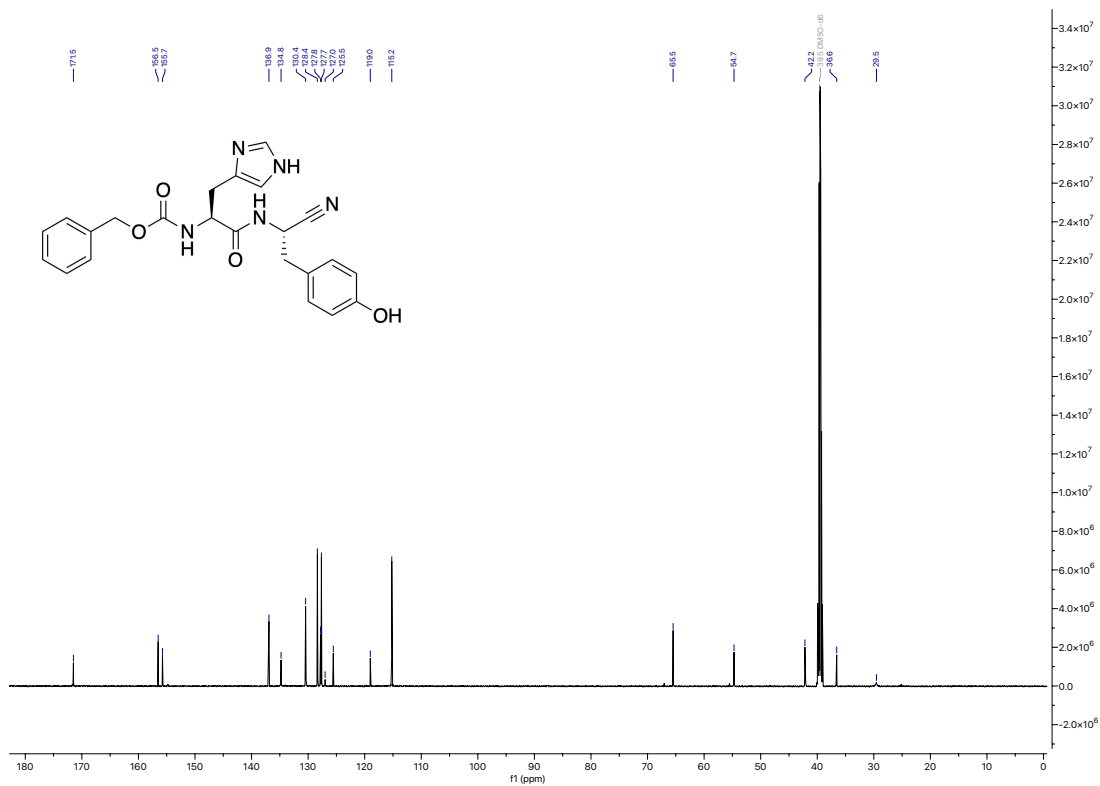




**Appendix 19.  $^1\text{H}$  NMR spectrum of H3-1 nitrile (H3-1N) in  $\text{DMSO-}d_6$ .**



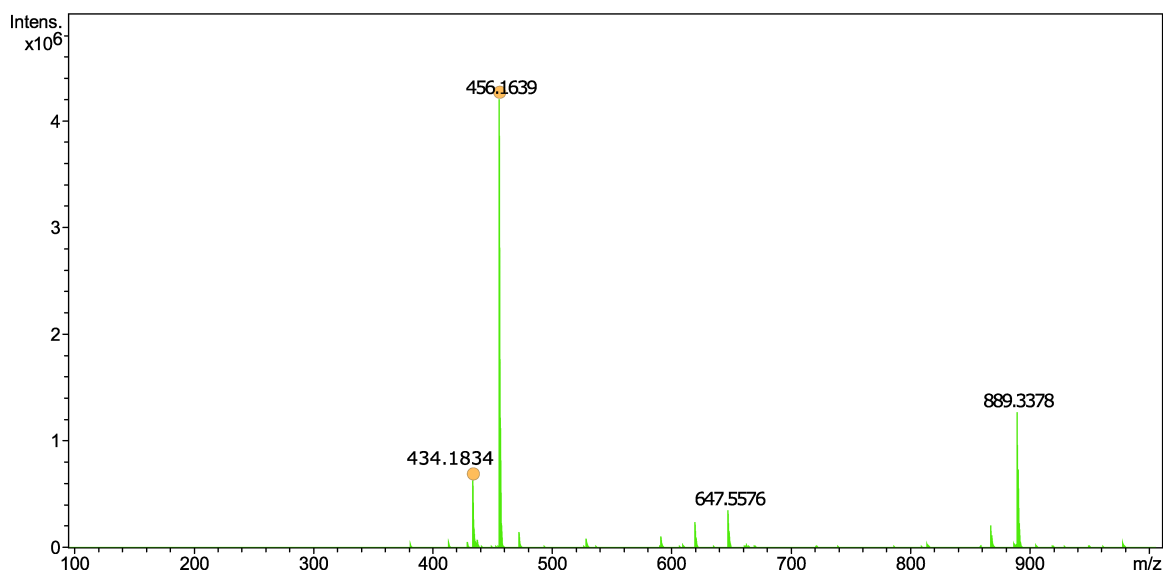
**Appendix 20. <sup>1</sup>H NMR spectrum of H3-1 nitrile (H3-1N) in DMSO-*d*<sub>6</sub> with the addition of D<sub>2</sub>O.**



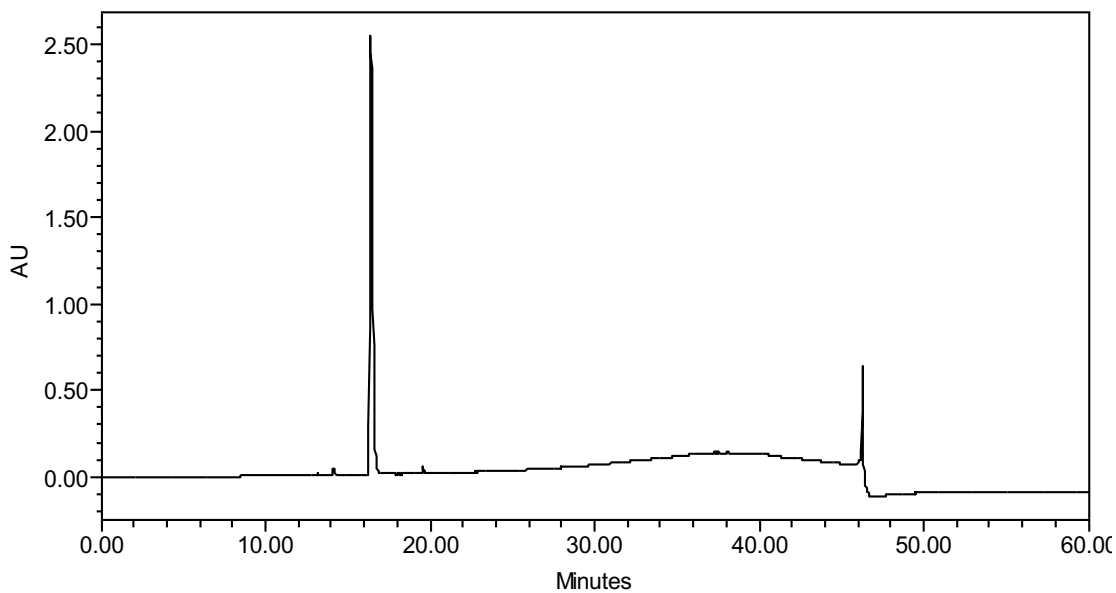
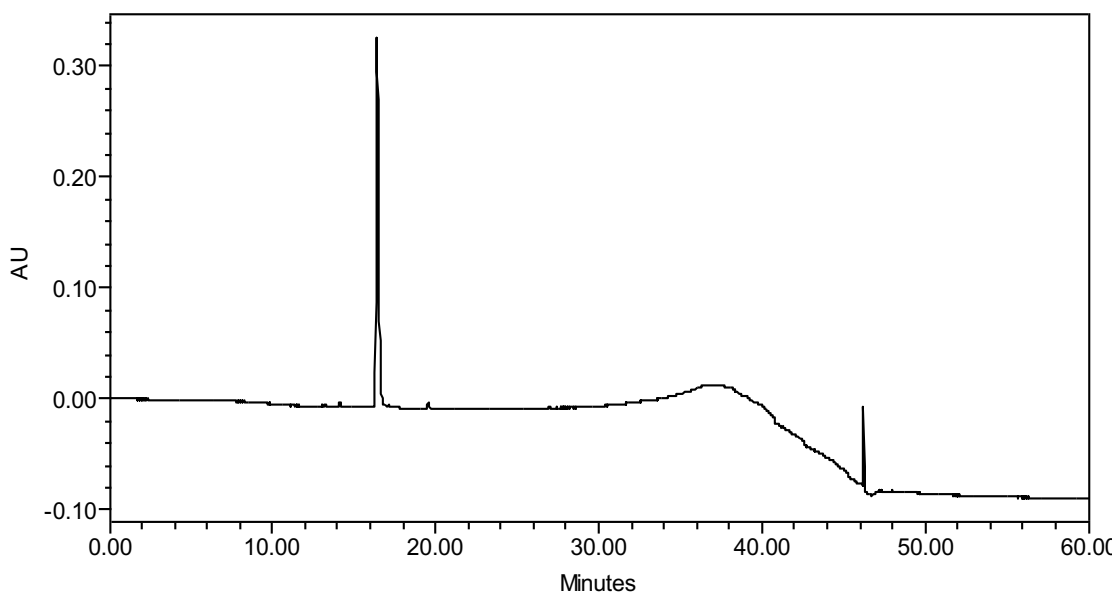
**Appendix 21.  $^{13}\text{C}\{^1\text{H}\}$  NMR spectrum of H3-1 nitrile (H3-1N) in  $\text{DMSO}-d_6$ .**

**Acquisition Parameter**

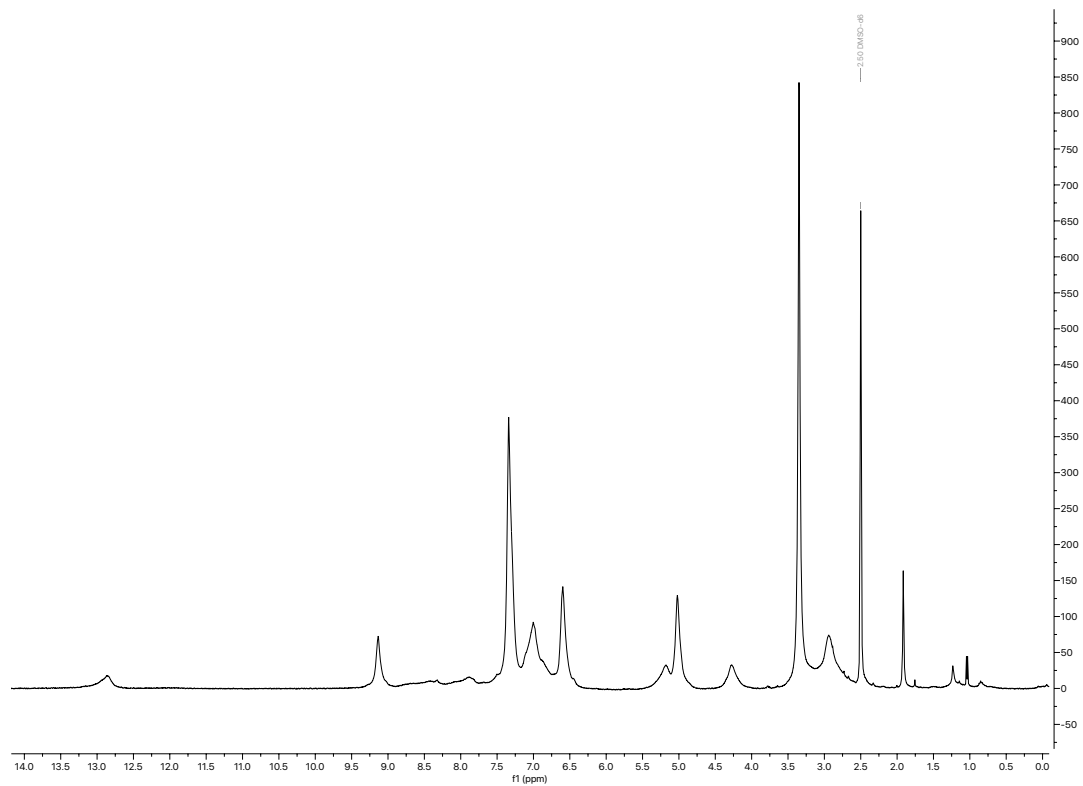
Source Type	ESI	Ion Polarity	Positive	Set Nebulizer	1.7 Bar
Focus	Active			Set Dry Heater	180 °C
Scan Begin	100 m/z	Set Capillary	4000 V	Set Dry Gas	6.0 l/min
Scan End	1000 m/z	Set End Plate Offset	-500 V	Set Divert Valve	Source



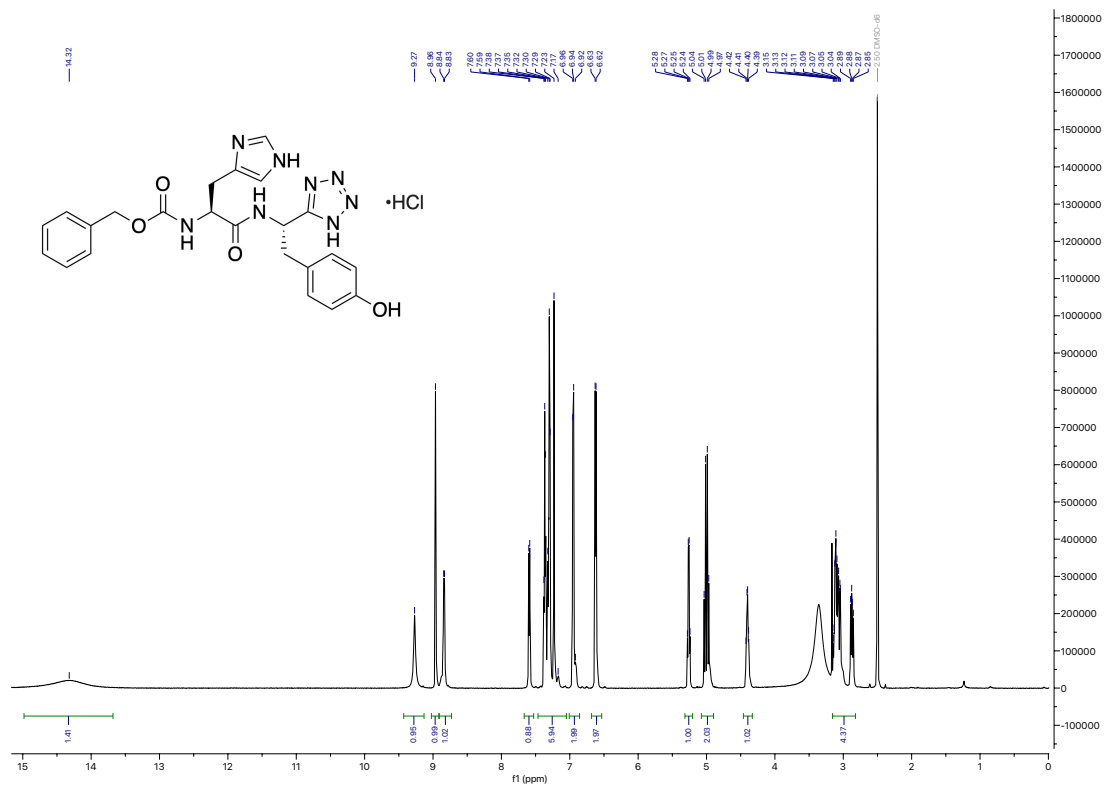
**Appendix 22. ESI-TOF MS of H3-1 nitrile (H3-1N).**

**A****B**

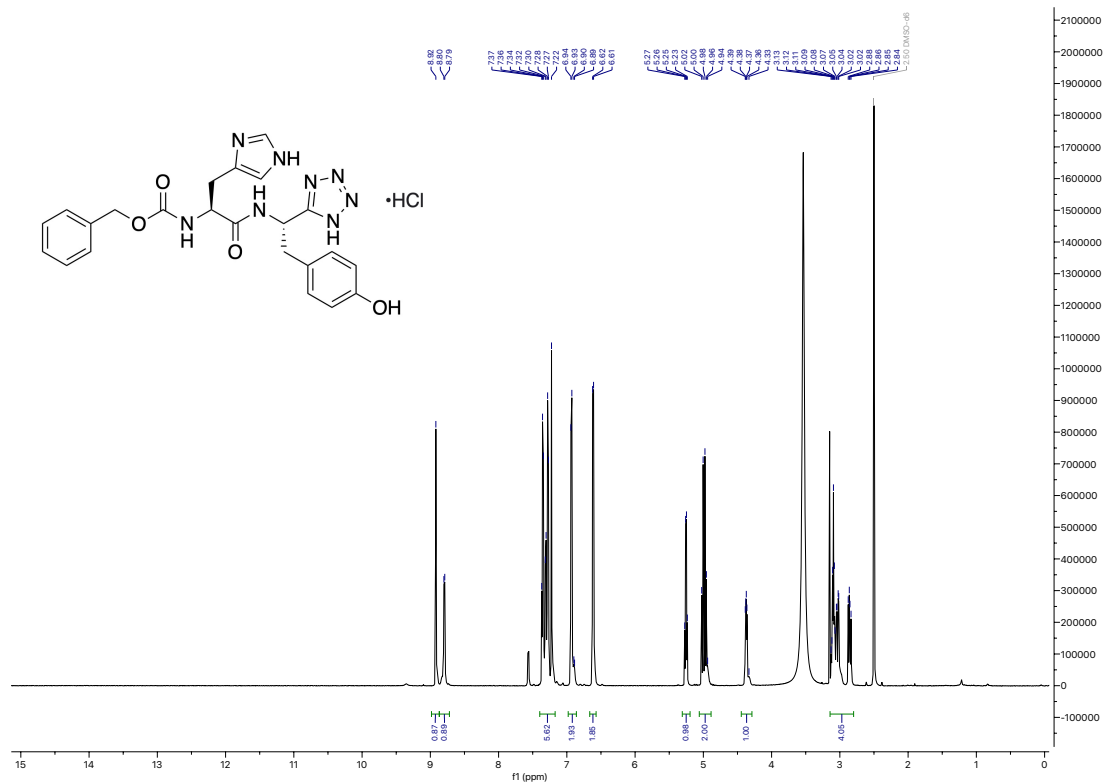
**Appendix 23. RP-HPLC chromatograms of H3-1 nitrile (H3-1N).** Chromatograms are representative of three independent injections (N = 3). **A)** Chromatogram monitoring at  $\lambda = 220$  nm. **B)** Chromatogram monitoring at  $\lambda = 275$  nm.



**Appendix 24.  $^1\text{H}$  NMR spectrum of the complex between H3-1 tetrazole and zinc (H3-1T:Zn) in  $\text{DMSO-}d_6$ .**

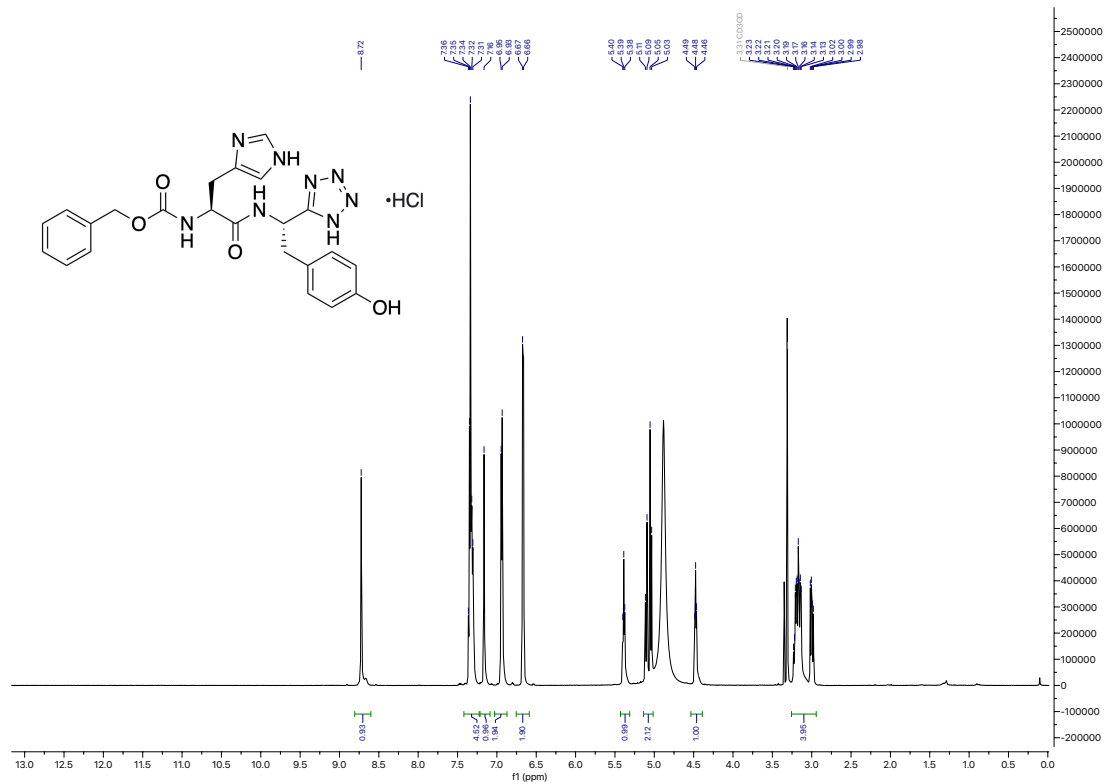


**Appendix 25. <sup>1</sup>H NMR spectrum of H3-1 tetrazole hydrochloride (H3-1T•HCl) in DMSO-*d*<sub>6</sub>.**

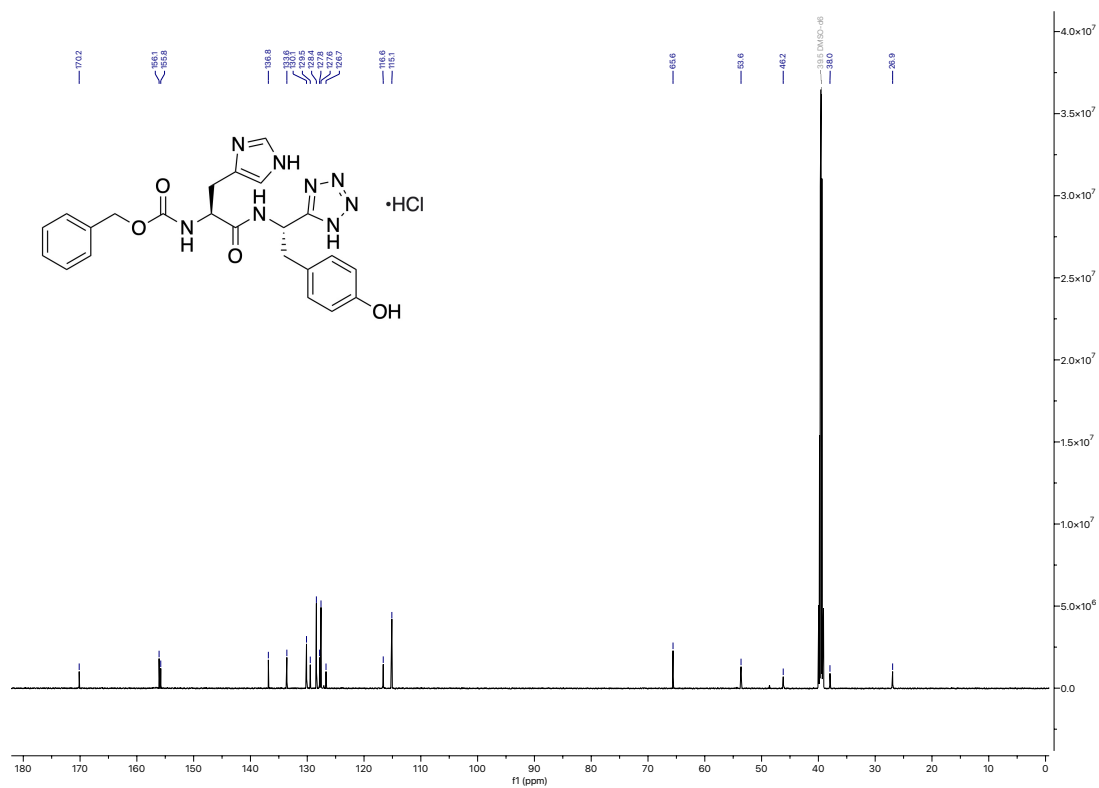


**Appendix 26. <sup>1</sup>H NMR spectrum of H3-1 tetrazole hydrochloride (H3-1T·HCl) in DMSO-*d*<sub>6</sub> with the addition of D<sub>2</sub>O.**





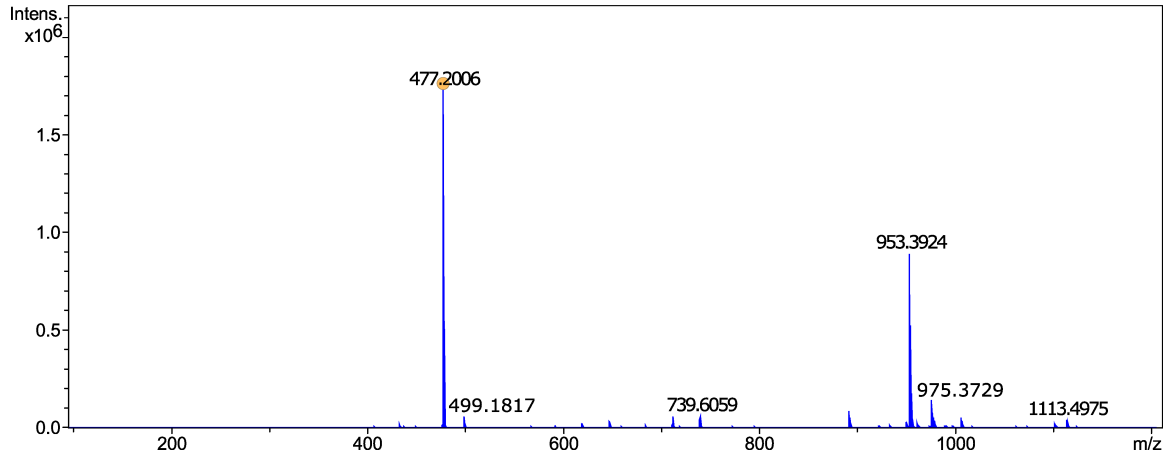
**Appendix 27.  $^1\text{H}$  NMR spectrum of H3-1 tetrazole hydrochloride (H3-1T•HCl) in  $\text{MeOH-}d_4$ .**



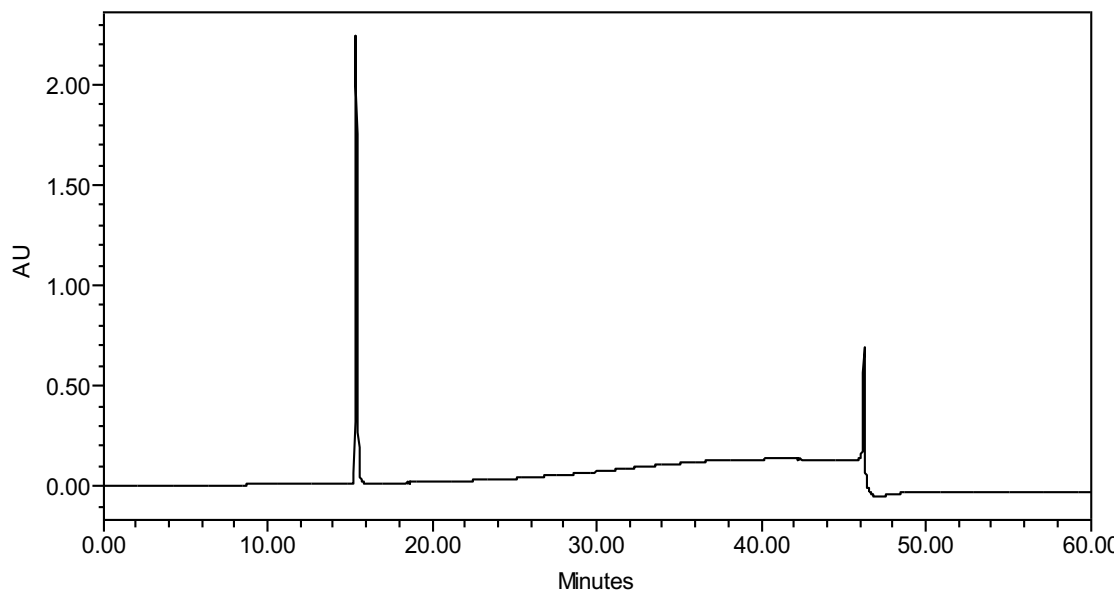
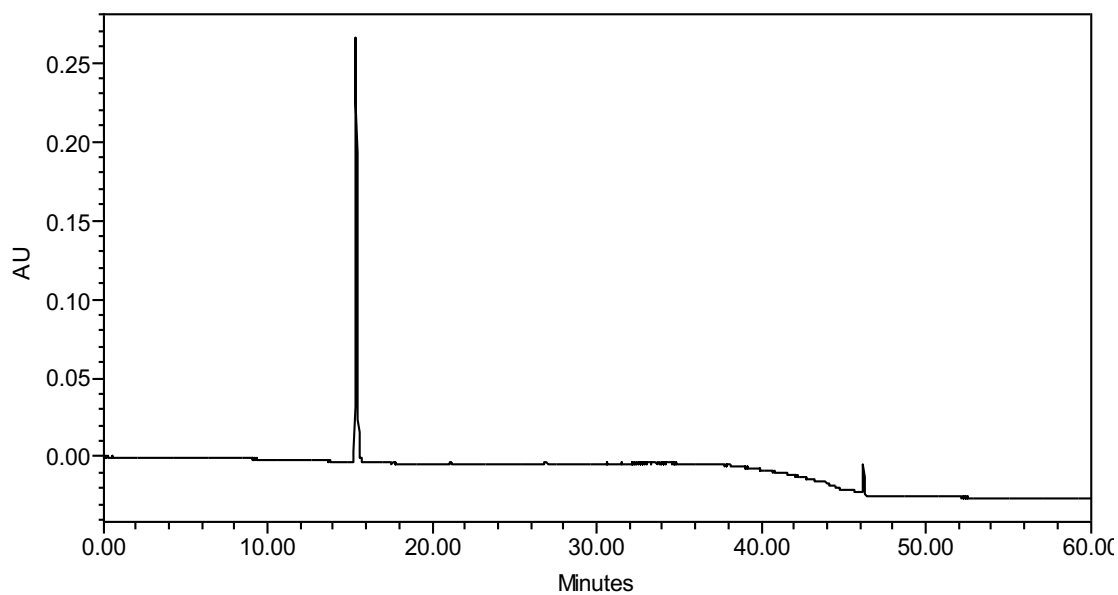
**Appendix 28.  $^{13}\text{C}\{^1\text{H}\}$  NMR spectrum of H3-1 tetrazole hydrochloride (H3-1T·HCl) in  $\text{DMSO-}d_6$ .**

**Acquisition Parameter**

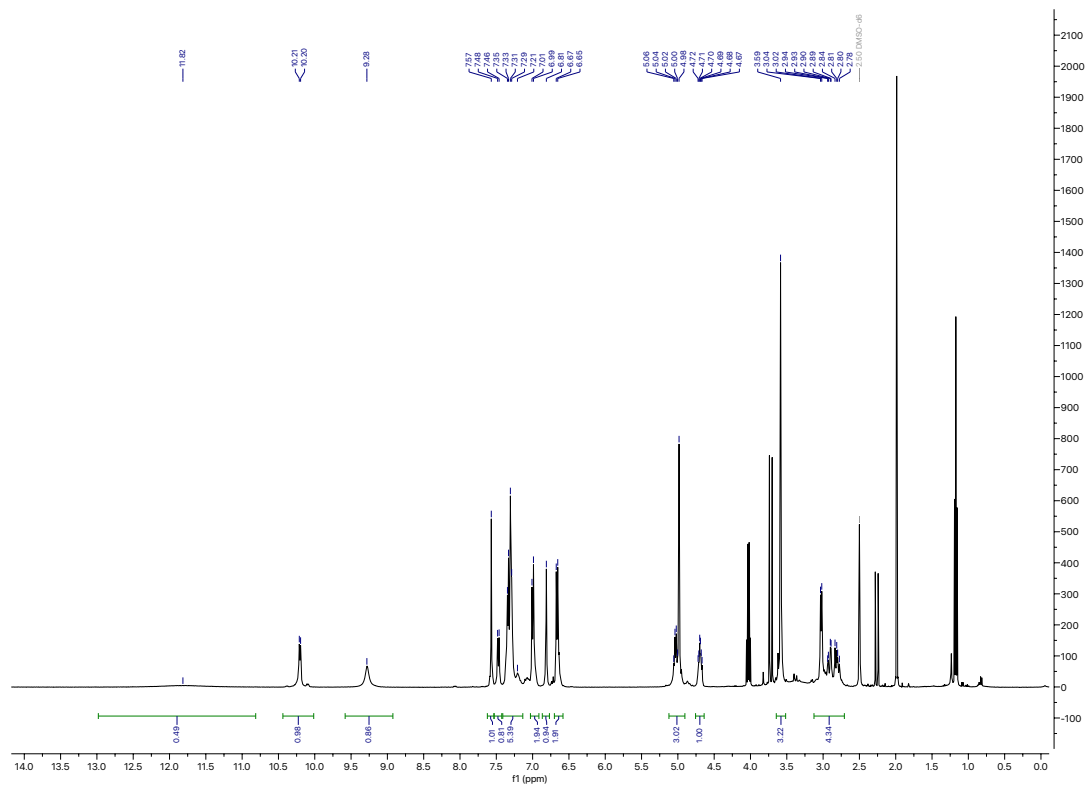
Source Type	ESI	Ion Polarity	Positive	Set Nebulizer	1.7 Bar
Focus	Active			Set Dry Heater	200 °C
Scan Begin	100 m/z	Set Capillary	4000 V	Set Dry Gas	6.0 l/min
Scan End	1200 m/z	Set End Plate Offset	-500 V	Set Divert Valve	Source



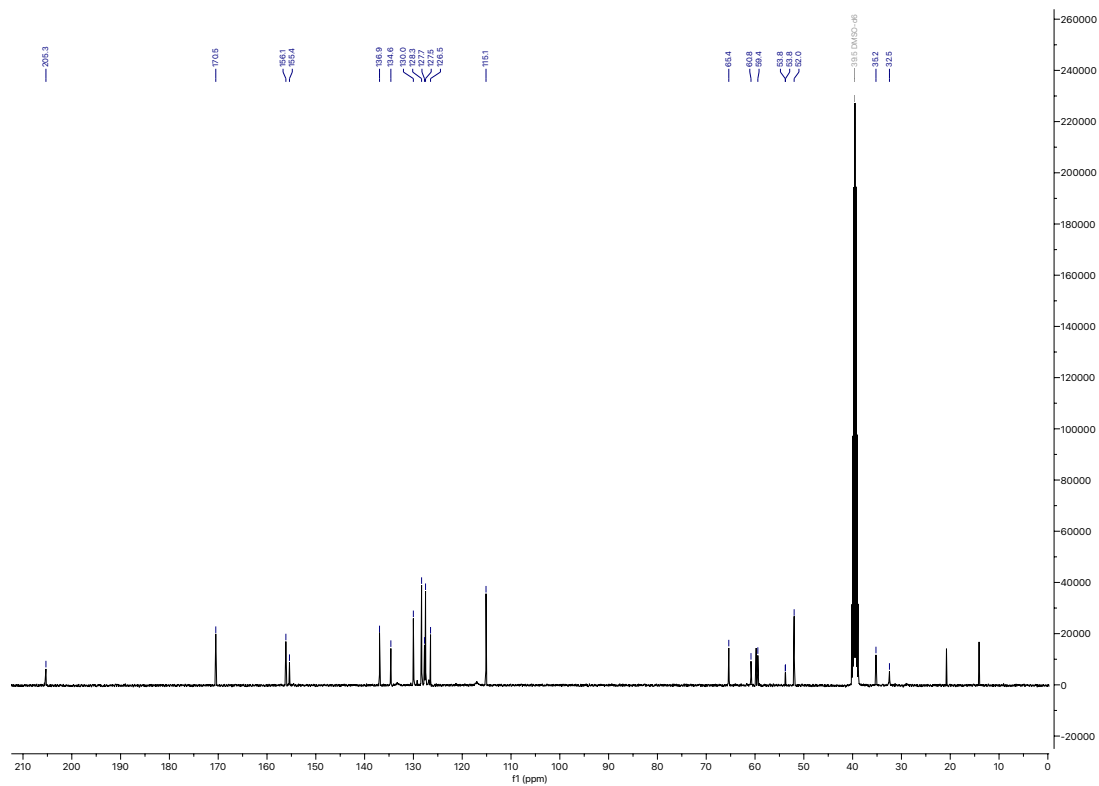
**Appendix 29. ESI-TOF MS of H3-1 tetrazole hydrochloride (H3-1T•HCl).**

**A****B**

**Appendix 30. RP-HPLC chromatograms of H3-1 tetrazole hydrochloride (H3-1T•HCl).** Chromatograms are representative of three independent injections ( $N = 3$ ). **A)** Chromatogram monitoring at  $\lambda = 220$  nm. **B)** Chromatogram monitoring at  $\lambda = 275$  nm.



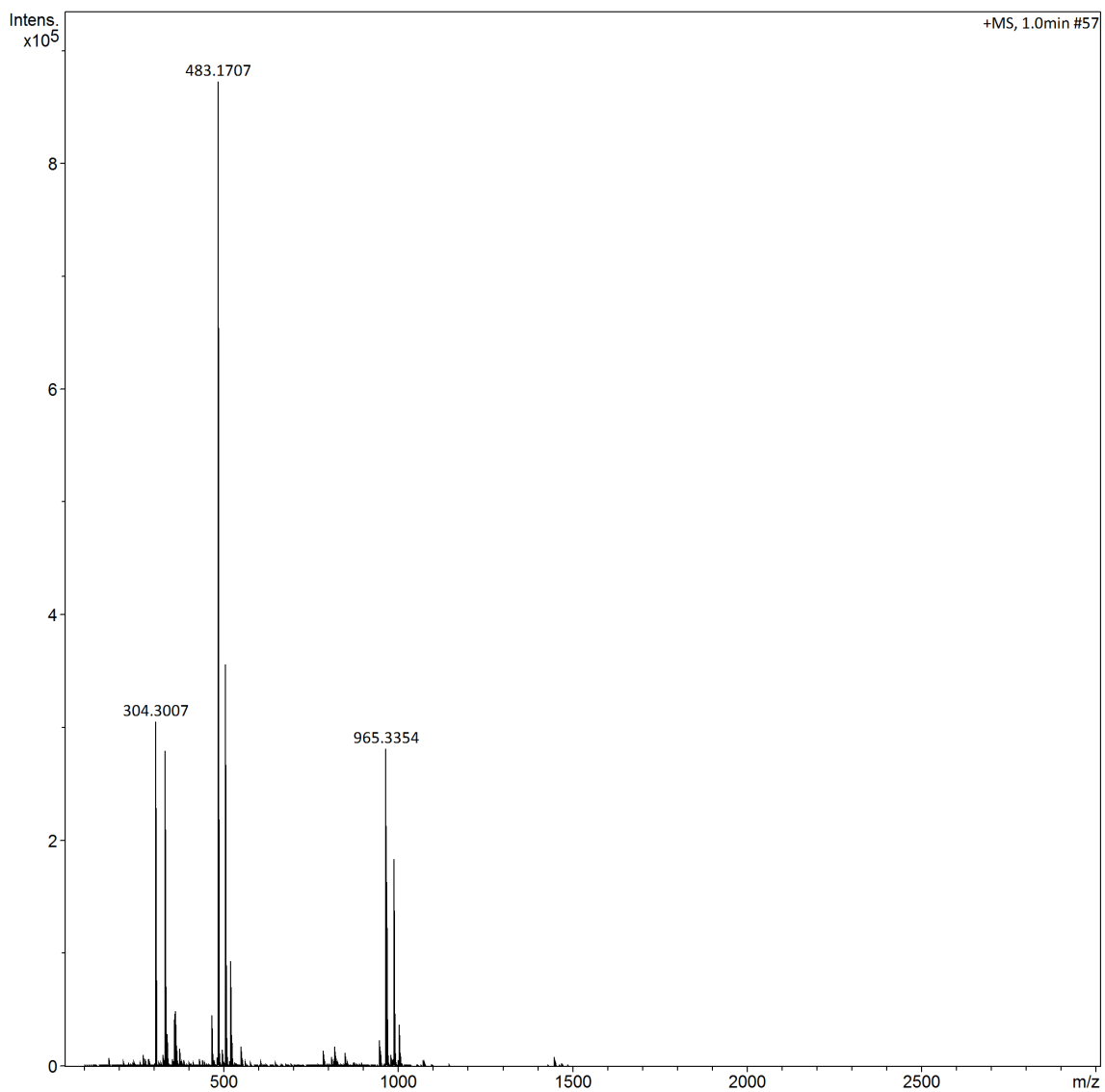
**Appendix 31.  $^1\text{H}$  NMR spectrum of crude thioamide H3-1 methyl ester (TH3-1M) in  $\text{DMSO-}d_6$ .**



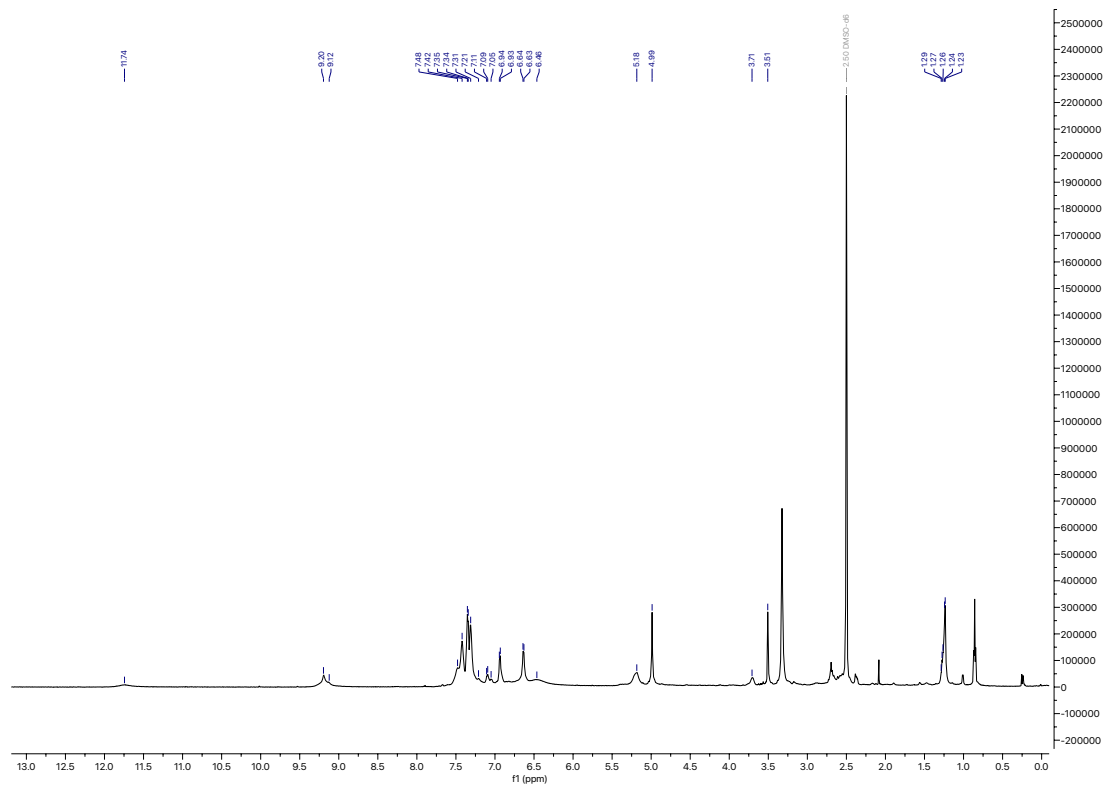
**Appendix 32.  $^{13}\text{C}\{^1\text{H}\}$  NMR spectrum of crude thioamide H3-1 methyl ester (TH3-1M) in  $\text{DMSO-}d_6$ .**

**Acquisition Parameter**

Source Type	ESI	Ion Polarity	Positive	Set Nebulizer	1.5 Bar
Focus	Not active			Set Dry Heater	180 °C
Scan Begin	50 m/z	Set Capillary	4500 V	Set Dry Gas	4.0 l/min
Scan End	3000 m/z	Set End Plate Offset	-400 V	Set Divert Valve	Source



**Appendix 33. ESI-TOF MS of crude thioamide H3-1 methyl ester (TH3-1M).**

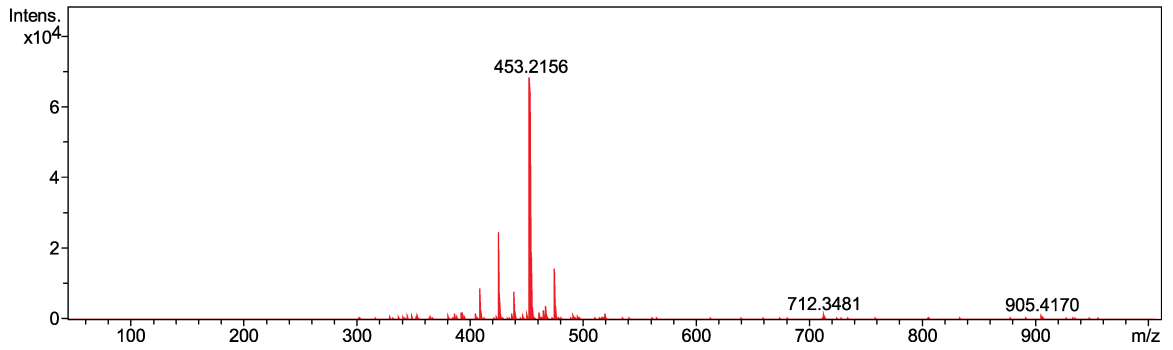


**Appendix 34.  $^1\text{H}$  NMR spectrum of crude methyleneamino H3-1 methyl ester (MH3-1M) in  $\text{DMSO-}d_6$ .**



**Acquisition Parameter**

Source Type	ESI	Ion Polarity	Positive	Set Nebulizer	2.0 Bar
Focus	Active			Set Dry Heater	100 °C
Scan Begin	50 m/z	Set Capillary	5000 V	Set Dry Gas	6.0 l/min
Scan End	1000 m/z	Set End Plate Offset	-500 V	Set Divert Valve	Source



**Appendix 35. ESI-TOF MS of crude methyleneamino H3-1 methyl ester (MH3-1M).**

# Curriculum Vitae

## EDUCATION

---

- 2020 – 2022                    **MSc, Microbiology and Immunology**  
University of Western Ontario, London, Ontario, Canada
- 2016 – 2020                    **BMSc (Honours), Biochemistry of Infection and Immunity**  
University of Western Ontario, London, Ontario, Canada

## PUBLICATIONS

---

### Refereed Journal Articles

1. **Lurie, A.**, Fink, C., Gosselin, G., Dekaban, G.A., Dikeakos, J.D. (2022). Inhibitors of HIV-1 Nef: applications and developments for a practical cure. *Virologie (Montrouge)*, 26(1), 17–33. <https://doi.org/10.1684/vir.2022.0940>
2. Trothen, S.M., Zang, R., **Lurie, A.**, Dikeakos, J.D. (2022). PACS-1 contains distinct motifs for nuclear-cytoplasmic transport and interacts with the RNA-binding protein PTBP1 in the nucleus and cytosol. *FEBS Letters*, 596(2), 232–248. <https://doi.org/10.1002/1873-3468.14243>
3. Jacob, R.A., Edgar, C.R., Prévost, J., Trothen, S.M., **Lurie, A.**, Mumby, M.J., Galbraith, A., Kirchhoff, F., Haeryfar, S.M.M., Finzi, A., Dikeakos, J.D. (2021). The HIV-1 accessory protein Nef increases surface expression of the checkpoint receptor Tim-3 in infected CD4<sup>+</sup> T cells. *Journal of Biological Chemistry*, 297(3), 101042. <https://doi.org/10.1016/j.jbc.2021.101042>
4. **Lurie, A.**, Wang, J., Hinnegan, K.J., McIntyre, W.F., Belley-Côté, E.P., Amit, G., Healey, J.S., Connolly, S.J., Wong, J.A. (2021). Prevalence of left atrial thrombus in anticoagulated patients with atrial fibrillation. *Journal of the American College of Cardiology*, 77(23), 2875–2886. <https://doi.org/10.1016/j.jacc.2021.04.036>
5. **Lurie, A.**, Amit, G., Divakaramenon, S., Acosta, J.G., Healey, J.S., Wong, J.A. (2021). Outcomes and safety of fluoroless catheter ablation for atrial fibrillation. *Canadian Journal of Cardiology Open*, 3(3), 303–310. <https://doi.org/10.1016/j.cjco.2020.11.002>
6. Hutson, J.R., **Lurie, A.**, Eastabrook, G., de Vrijer, B., Garcia-Bournissen, F. (2021). Acetaminophen in late pregnancy and potential for in utero closure of the ductus arteriosus – a pharmacokinetic evaluation and critical review of the literature. *American Journal of Obstetrics and Gynecology MFM*, 3(1), 100288. <https://doi.org/10.1016/j.ajogmf.2020.100288>

### Letters

1. **Lurie, A.**, Wang, J., Healey, J.S., Wong, J.A. (2021). Reply: effects of cardiac amyloidosis and screening approach on left atrial thrombus prevalence in atrial fibrillation. *Journal of the American College of Cardiology*, 78(13), e91–e92. <https://doi.org/10.1016/j.jacc.2021.07.037>

## Conference Proceedings

1. **Lurie, A.**, Amit, G., Divakaramenon, S., Acosta, J.G., Healey, J.S., Wong, J.A. (2020). Outcomes and safety of fluoroless radiofrequency catheter ablation for atrial fibrillation. *Canadian Journal of Cardiology*, 36(10), S49.  
<https://doi.org/10.1016/j.cjca.2020.07.105>

## CONFERENCE PRESENTATIONS

---

\* Presenting author is underlined.

1. Fink, C., **Lurie, A.**, Hudson, R.H.E., Dekaban, G.A., Dikeakos, J.D. (June 5<sup>th</sup>–7<sup>th</sup>, 2022). The adjuvant role of Nef inhibitors towards a cure for HIV/AIDS. Oral presentation at the 4<sup>th</sup> Symposium of the Canadian Society for Virology (CSV), Edmonton, Alberta, Canada.
2. Lurie, A., Fink, C., Hudson, R.H.E., Dekaban, G.A., Dikeakos, J.D. (April 27<sup>th</sup>–29<sup>th</sup>, 2022). Peptidomimetic inhibitors of the Nef–Src family kinase interaction as adjuvants in an immune-directed HIV-1 cure. Poster presentation at the 31<sup>st</sup> Canadian Conference on HIV/AIDS Research (CAHR), London, Ontario, Canada.
3. Fink, C., **Lurie, A.**, Dekaban, G.A., Dikeakos, J.D. (April 27<sup>th</sup>–29<sup>th</sup>, 2022). The adjuvant role of Nef inhibitors towards a cure for HIV/AIDS. Oral presentation at the 31<sup>st</sup> Canadian Conference on HIV/AIDS Research (CAHR), London, Ontario, Canada.
4. Lurie, A., Fink, C., Hudson, R.H.E., Dekaban, G.A., Dikeakos, J.D. (August 10<sup>th</sup>, 2021). HIV-1 Nef-mediated immune evasion: why and how should we block it? Three-minute thesis presentation at the 3<sup>rd</sup> Virtual Workshop of the Canadian Society for Virology (CSV).
5. Lurie, A., Fink, C., Hudson, R.H.E., Dekaban, G.A., Dikeakos, J.D. (July 19<sup>th</sup>–23<sup>rd</sup>, 2021). Small molecule inhibitors of the Nef–Src family kinase interaction to enable an HIV-1 cure. Oral presentation at the 40<sup>th</sup> Annual Meeting of the American Society for Virology (ASV).
6. Fink, C., **Lurie, A.**, Urquhart B.L., Wortman, M.D., Thomas, G., Dekaban, G.A., Dikeakos, J.D. (May 25<sup>th</sup>–28<sup>th</sup>, 2021). Nef inhibitors as adjuvants towards a cure for HIV/AIDS. Poster presentation at the Cold Spring Harbor Laboratory (CSHL) 2021 Retroviruses Meeting, Laurel Hollow, New York, United States.
7. Lurie, A., Fink, C., Hudson, R.H.E., Dekaban, G.A., Dikeakos, J.D. (October 27<sup>th</sup>, 2020). Inhibitors of the Nef–kinase interaction: small molecules to enable an HIV-1 cure. Five-minute thesis presentation at the Infection and Immunity Research Forum (IIRF) 2020, University of Western Ontario, London, Ontario, Canada.
8. Lurie, A., Amit, G., Divakaramenon, S., Acosta, J.G., Healey, J.S., Wong, J.A. (October 21<sup>st</sup>–24<sup>th</sup>, 2020). Outcomes and safety of fluoroless radiofrequency catheter ablation for atrial fibrillation. Poster presentation at the Canadian Cardiovascular Congress (CCC) 2020.
9. Lurie, A., Hudson, R.H.E. (September 13<sup>th</sup>, 2018). Synthesis of an azo-based nucleobase quencher. Oral presentation at the Department of Chemistry Summer Undergraduate Student Presentation Day, University of Western Ontario, London, Ontario, Canada.

10. Hutson, J.R., Lurie, A., Gratton, R.J., de Vrijer, B. (April 18<sup>th</sup>, 2018). A systematic review and pharmacokinetic analysis of acetaminophen use in pregnancy and in utero closure of the ductus arteriosus. Oral presentation at the 16<sup>th</sup> Annual Paul Harding Research Awards Day, University of Western Ontario, London, Ontario, Canada.

#### **AWARDS, HONOURS, AND SCHOLARSHIPS**

---

- |             |  |
|-------------|--|
| 2022        | <b>Dr. FW Luney Graduate Travel Award in Microbiology and Immunology</b><br>Department of Microbiology and Immunology, University of Western Ontario |
| 2021        | <b>Third Place, Three-Minute Thesis Oral Presentation</b><br>Canadian Society for Virology   |
| 2021        | <b>Canada Graduate Scholarship – Master’s (CGSM) Award</b><br>Canadian Institutes of Health Research   |
| 2021        | <b>Queen Elizabeth II Graduate Scholarship in Science and Technology (Declined for CGSM)</b><br>Province of Ontario                                  |
| 2021        | <b>Student Registration Award</b><br>American Society for Virology   |
| 2020        | <b>First Place, Five-Minute Thesis Oral Presentation</b><br>Infection and Immunity Research Forum, University of Western Ontario                     |
| 2020        | <b>Queen Elizabeth II Graduate Scholarship in Science and Technology</b><br>Province of Ontario  |
| 2020        | <b>Dr. FW Luney Graduate Entrance Scholarship</b><br>Department of Microbiology and Immunology, University of Western Ontario                        |
| 2016 – 2020 | <b>Undergraduate Dean’s Honour List</b><br>University of Western Ontario   |
| 2019        | <b>Summer Studentship Award</b><br>Population Health Research Institute, McMaster University   |
| 2016        | <b>Western Entrance Scholarship of Excellence</b><br>University of Western Ontario   |

#### **RELEVANT WORK EXPERIENCE**

---

- |             |  |
|-------------|--|
| 2021 – 2022 | <b>Graduate Teaching Assistant</b><br>Department of Microbiology and Immunology, University of Western Ontario |
|-------------|--|